ISSN 1916-9698 (Print)
ISSN 1916-9701 (Online)

INTERNATIONAL JOURNAL OF CHEMISTRY

Vol. 14, No. 1, May 2022

CANADIAN CENTER OF SCIENCE AND EDUCATION

International Journal of Chemistry

An International Peer-reviewed and Open Access Journal for Chemistry

International Journal of Chemistry (IJC) is an international, peer-reviewed, open-access journal, published by Canadian Center of Science and Education. The journal is published Semiannually (May and November) in both print and online versions. IJC aims to promote excellence through dissemination of high-quality research findings, specialist knowledge, and discussion of professional issues that reflect the diversity of this field.

The scopes of the journal include:

- Analytical
- Biochemistry
- Inorganic
- Materials
- Neurochemistry
- Nuclear Chemistry
- Organic Physical
- Chemistry

The journal is included in:

- CABI
- CAS (Chemical Abstracts Service, ACS)
- COPAC
- ERA
- Google Scholar
- Infotrieve
- MIAR
- ResearchGate

Open-Access Policy

We follow the Gold Open Access way in journal publishing. This means that our journals provide immediate open access for readers to all articles on the publisher's website. The readers, therefore, are allowed to read, download, copy, distribute, print, search, link to the full texts or use them for any other lawful purpose. The operations of the journals are alternatively financed by article processing charge paid by authors or by their institutions or funding agencies.

Copyright Policy

Copyrights for articles are retained by the authors, with first publication rights granted to the journal/publisher. Authors have rights to reuse, republish, archive, and distribute their own articles after publication. The journal/publisher is not responsible for subsequent uses of the work.

Submission Policy

Submission of an article implies that the work described has not been published previously (except in the form of an abstract or as part of a published lecture or academic thesis), that it is not under consideration for publication elsewhere, that its publication is approved by all authors and tacitly or explicitly by the authorities responsible where the work was carried out. However, we accept submissions that have previously appeared on preprint servers (for example: arXiv, bioRxiv, Nature Precedings, Philica, Social Science Research Network, and Vixra); have previously been presented at conferences; or have previously appeared in other "non-journal" venues (for example: blogs or posters). Authors are responsible for updating the archived preprint with the journal reference (including DOI) and a link to the published articles on the appropriate journal website upon publication.

The publisher and journals have a zero-tolerance plagiarism policy. We check the issue using the plagiarism prevention tool and a reviewer check. All submissions will be checked by iThenticate before being sent to reviewers.

IJC accepts both Online and Email submission. The online system makes readers to submit and track the status of their manuscripts conveniently. For any questions, please contact ijc@ccsenet.org.

International Journal of Chemistry; Vol. 14, No. 1; 2022
ISSN 1916-9698 E-ISSN 1916-9701
Published by Canadian Center of Science and Education

EDITORIAL TEAM

International Journal of Chemistry; Vol. 14, No. 1; 2022
ISSN 1916-9698 E-ISSN 1916-9701
Published by Canadian Center of Science and Education

Contents

International Journal of Chemistry; Vol. 14, No. 1; 2022
ISSN 1916-9698 E-ISSN 1916-9701
Published by Canadian Center of Science and Education

Ionic Disorders in Malaria and Dengue Co-Infection

Fabienne M. Soudre[1,7], Arnaud Kouraogo[3], Alice T.C.R. Kiba[4,7], Raoul Karfo[3,7], Thierry Guiguemde[2,7], Bibata Kabore[7], Elie Kabre[6,7], Jean Sakande[3,7]

[1]Biochemistry Unit, Pediatric University Teaching Hospital Charles de Gaulle, Ouagadougou, Burkina Faso

[2]Parasitology Unit, Pediatric University Teaching Hospital Charles de Gaulle, Ouagadougou, Burkina Faso

[3]Biochemistry Department, University Teaching Hospital Yalgado Ouédraogo, Ouagadougou, Burkina Faso

[4]Biochemistry Service, University Teaching Hospital of Tengandogo, Ouagadougou, Burkina Faso

[5]Immunology-Serology Unit, Pediatric University Teaching Hospital Charles de Gaulle, Ouagadougou, Burkina Faso

[6]National Laboratory of Public Health, Ouagadougou, Burkina Faso

[7]Training and Research Unit in Health Sciences, University Joseph Ki-Zerbo, Ouagadougou, Burkina Faso

Correspondence: Fabienne M. Soudre, Pediatric University Teaching Hospital Charles de Gaulle, Ouagadougou, Burkina Faso.

Received: October 3, 2021 Accepted: November 1, 2021 Online Published: November 3, 2021

doi:10.5539/ijc.v14n1p1 URL: https://doi.org/10.5539/ijc.v14n1p1

Abstract

Introduction: The aim of this study was to investigate ionic disorders in malaria and dengue co-infection at Ouagadougou, Burkina Faso.

Material and methods: This is a descriptive cross-sectional study with retrospective data collection, carried out in the laboratory of the Pediatric University Hospital Charles de Gaulle in Ouagadougou, Burkina Faso, from January 1st, 2017 to December 31st, 2019. The study was on patients who performed a thick blood drop/smear, dengue serology and blood ionogram.

Results: On 1405 cases included in the study, 102 patients (7.26%) were confirmed of malaria. Dengue serology was positive in 235 patients (16.72%). The frequency of co-infection was 1.14% (n=16). The mean age of the patients was 9.93 years and the age group of 0 to 15 years represented 78.93% of the cases. There was a male predominance with a sex ratio (M/F) of 2.58. Hyponatremia (40%), hypocalcemia (40%), hypokalemia (30%) and hypophosphatemia (30%) were the main blood ionogram disturbances in malaria and dengue co-infection. The statistically significant disturbances in case of malaria and dengue co-infection were the absence of hypobicarbonatemia (p=0.036).

Conclusion: Malaria and dengue are responsible for significant morbidity and mortality in Burkina Faso. Although co-infection was rare in the study (1.14%), it was associated with several blood ionogram disturbances. Evaluation and consideration of these disturbances during treatment would contribute to a better care of patients.

Keywords: pediatric university hospital, co-infection, dengue, blood ionogram, malaria

1. Introduction

Malaria and dengue are vector-borne diseases, which are public health problems worldwide and particularly in Burkina Faso. According to the World Health Organization (WHO), malaria was responsible for 228 million cases in 2018 with 405 000 deaths, mostly among children under five years old (World Health Organization [WHO], 2019). Similarly, more than 390 million dengue virus infections occur worldwide each year, with 5.2 million cases reported to WHO in 2019 (WHO, 2021). Both diseases are found in common geographical areas, especially in the tropics and subtropics, and cases of co-infection are increasingly reported (Epelboin et al., 2012; Faruque et al., 2012; Mohapatra et al., 2012; Baba et al., 2013; Mendonça et al., 2015). In Burkina Faso, a survey on 264 children revealed 18 positive cases of dengue, including 10 cases associated with malaria (Ministry of Health, 2014). In 2017, out of 51 cases of dengue observed in the infectious disease department of the University Hospital Yalgado Ouedraogo at Ouagadougou, a co-infection with malaria was observed in 7 patients (Savadogo et al., 2017). These diseases are related to high morbidity, and in endemic areas, complications are responsible for a high number of deaths. The main complications arise from changes in certain haematological and biochemical characteristics, which can aggravate the clinical picture, but also from the immune response against the parasitized red blood cells or against the dengue virus. Thus, some biological complications may be

life-threatening, such as severe thrombocytopenia, severe hepatitis, renal failure and potentially serious ionic disorders. These complications must be detected in the laboratory and treated appropriately to ensure patient survival.

In Burkina-Faso, few studies focused on the biological complications of malaria and dengue co-infection, particularly hydro-electrolytic disorders, making this study necessary. Thus, we studied the disturbances of blood ionogram in malaria and dengue co-infection at the pediatric university hospital Charles de Gaulle in order to allow a better care of the patients.

2. Material and Methods

The study was conducted in the medical analysis laboratory of the University Hospital Charles de Gaulle at Ouagadougou, Burkina Faso. It was a descriptive cross-sectional study, with retrospective data collection on a period of three (03) years, from January 1st, 2017 to December 31st, 2019. The population studied consisted of all patients (all ages) who had a thick blood drop/screen, dengue serology and biochemical examinations including blood ionogram. Sampling was systematic and exhaustive during the study.

The thick blood drop and the blood smear were performed on a slide from a capillary blood sample, stained with Giemsa and May-Grünwald Giemsa respectively. The thick drop was used to make a positive diagnosis of malaria; the blood smear was used to diagnose the species and to evaluate the parasite density. Dengue serology and biochemical assays were performed on venous blood samples collected in dry tubes, centrifuged at 3500 rpm for 5 minutes with serum collection. The SD Bioline Dengue Duo kit (Standard Diagnostics) was used for the diagnosis of dengue and was considered as a probable case of dengue, any patient with a positive serology for NS1 antigen and/or immunoglobulin M. Blood ionogram parameters were represented by the serum determination of sodium, potassium, chlorine, calcium, magnesium, phosphate and proteins, using the Indiko Plus automaton (Thermo Fisher Scientific). The values obtained were interpreted according to the patient's age.

Data collected on a questionnaire were entered from Microsoft Office Excel 2013 software and analyzed with Epi-Info™ 7 software in its version 7.2.0. Univariate and bivariate regression analyses were performed to establish a statistical relationship between the variables. For univariate analysis, Chi-2 or Fischer tests were used and for bivariate analysis, measures of association such as Odds Ratio and p-value were performed. The significance level was $p < 0.05$. Before the beginning of the study, a request for authorization to collect data was obtained from the management of the Pediatric University Hospital Charles de Gaulle. Data confidentiality was maintained throughout the study.

3. Results

A total of 1405 subjects were included in the study.

3.1 Socio-Demographic Characteristics

The mean age of the patients of the study was 9.93 ± 10.26 years with extremes from 1 day to 80 years. The age range of 0 to 15 years was the majority with 1109 patients, representing a frequency of 78.93%. Male sex was the most represented with a sex ratio of 1.15. The sociodemographic characteristics are presented in Table 1.

Table 1. Distribution of patients according to socio-demographic characteristics

Characteristic		Number	Percentage (%)
Age (years)	≤ 15	1109	78.93
	] 15-30]	138	9.82
	] 30-45]	121	8.61
	> 45	37	2.63
Gender	Male	752	53.52
	Female	653	46.48

3.2 Prevalence of Malaria, Dengue and Co-infection

Thick blood tests were positive in 102 patients, i.e. a prevalence of malaria of 7.26%. The mean parasite density was 30 163.93 ± 67 741.85 trophozoites/µL, ranging from 110 to 520 909 trophozoites/µL. Dengue serology was positive in 235 patients (16.72%). Out of the 1405 patients, the frequency of malaria-dengue co-infection was 1.14% with n=16 (Figure 1).

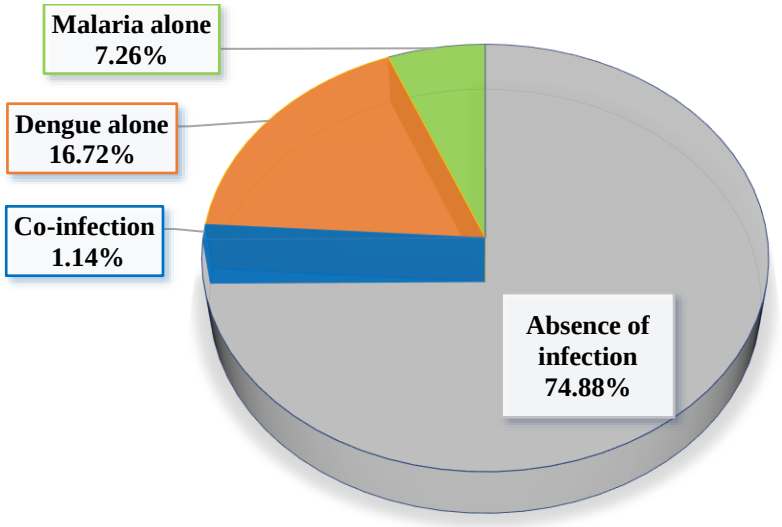

Figure 1. Frequency of malaria, dengue and co-infection

3.3 Blood Ionogram Results

3.3.1 Mean Values of Blood Ionogram Parameters

Table 2 presents the mean values obtained after the determination of the different parameters of the blood ionogram, according to the cases of co-infection, dengue or malaria.

Table 2. Mean values of blood ionogram parameters

Parameters	Co-infection	Dengue	Malaria
Natremia (mmol/L)	135.44 ± 08.09	134.71 ± 05.57	134.94 ± 05.90
Kalemia (mmol/L)	3.65 ± 0.44	4.35 ± 0.80	4.30 ± 0.66
Calcemia (mmol/L)	2.26 ± 0.29	2.35 ± 0.35	2.33 ± 0.48
Chloremia (mmol/L)	104.02 ± 04.71	99.87 ± 11.74	104.61 ± 4.54
Phosphatemia (mmol/L)	1.22 ± 0.41	1.55 ± 0.46	1.32 ± 0.73
Magnesemia (mmol/L)	0.80 ± 0.40	0.76 ± 0.31	0.71 ± 0.24
Bicarbonate (mmol/L)	23.89 ± 3.48	21.74 ± 4.21	19.69 ± 4.26
Protidemia (g/L)	72.64 ±11.65	72.21 ±11.58	66.4 ± 11.75

3.3.2 Frequency of disturbances

The frequencies of blood ionogram disturbances are presented in Figure 2. In case of malaria-dengue co-infection, the main disturbances were hyponatremia (40%), hypokalemia (30%), hypocalcemia (40%) and hypophosphatemia (30%).

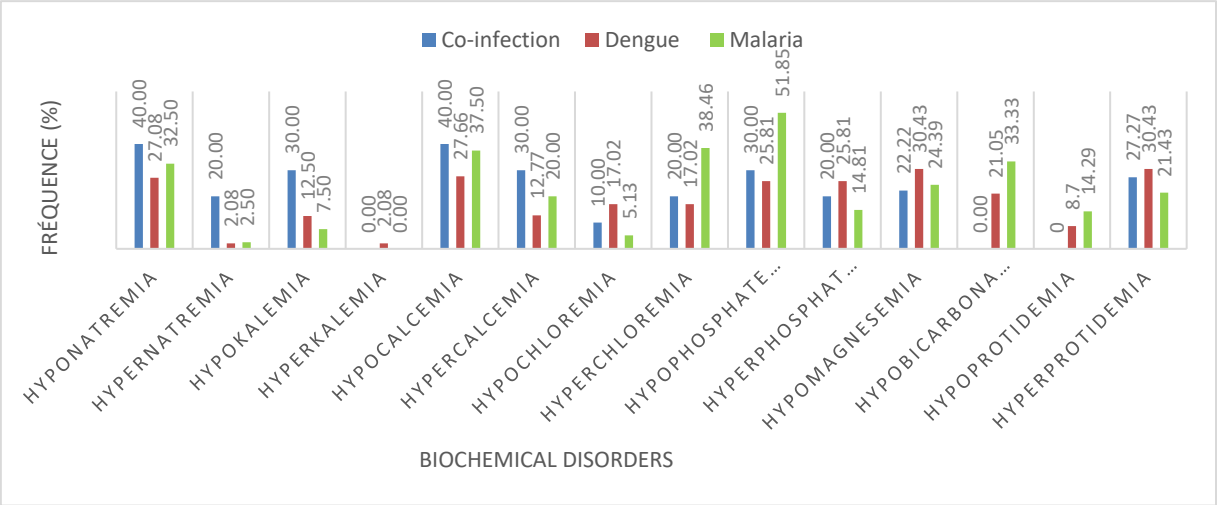

Figure 2. Frequency of blood ionogram disturbances

3.3.3 Univariate Analysis

In univariate analyses, the absence of hypobicarbonatemia (p=0.036) was significantly associated with malaria-dengue co-infection.

No abnormality was associated with the presence of dengue alone. Hypobicarbonatemia (p=0.048), hyperchloremia (p=0.013) and hypophosphatemia (p=0.043) were present in malaria infection alone (Table 3).

Table 3. Univariate analysis of blood ionogram disturbances between co-infection, dengue and malaria

Disturbances	Co-infection	Dengue	Malaria
Hypobicarbonatemia	**0.036**	0.280	**0.048**
Hyponatremia	0.250	0.230	0.370
Hyperchloremia	0.350	0.060	**0.013**
Hypercalcemia	0.150	0.290	0.590
Hypomagnesemia	0.770	0.500	0.650
Hypophosphatemia	0.330	0.130	**0.043**
Hypokalemia	0.440	0.450	0.340
Hyperprotidemia	0.450	0.490	0.360

3.3.4 Bivariate Analysis

Among biological disturbances, hypophosphatemia was less frequent in the co-infection group than in the malaria-only group (OR= 0.24; CI95%: 0.06-0.99; p-value = 0.044). On the contrary, hypophosphatemia was more common in the co-infection group than in the dengue-only group (OR = 7.04; CI95%: 1.52-32.63; p-value = 0.009).

4. Discussion

The aim of the present study was to investigate blood ionogram disturbances in malaria and dengue co-infection at the Pediatric University Hospital Charles de Gaulle. Despite the retrospective nature of the study with the fact that some clinical records were not complete, 1405 patients were included.

4.1 Prevalence of Malaria And Dengue Co-Infection

The prevalence of the co-infection in this study was 1.14% (Figure 1), thus relatively low. In a study at Thaïlande, on 194 dengue patients, no association with malaria has been found(Singhsilarak et al., 2006). Even if the phenomenon of co-infection seems to be rare in terms of frequency (Abdul-Ghani et al., 2021), it is often described in the literature. Thus, Im et al. identified in their study 39 cases of co-infection in 2762 patients, i.e. a frequency of 1.4%; thus similar to our results (Im et al., 2020). The low frequency (1.14%) could be explained by the fact that the study was limited to results recorded only in the laboratory. It could also be due to low recording of the results of thick blood drop in the registers of

the parasitology department, but this remains to be confirmed with further studies. In addition, the study period did not coincide with dengue outbreak as the one which occurred in the city of Ouagadougou in October 2016; this epidemic being considered as the biggest of its history (Im et al., 2020; Lim et al., 2021). On the other hand, Mohapatra et al. reported a higher frequency of 7.4% in 2012 in India (Mohapatra et al., 2012). In Burkina Faso, few data are available on malaria and dengue co-infection (Ministry of Health, 2014; Savadogo et al., 2017; Im et al., 2020), except for some doctoral theses which found co-infection frequencies of 20.4% in 2017 (Ly, 2017) and 55.24% in 2020 (Kane, 2020). The high prevalence of these studies may be explained by the methodology used, which included patients with only Ig G positivity in dengue cases. However, the presence of Ig G is most often a sign of old dengue and only titration could distinguish it from secondary dengue. All cases of positive Ig G alone were excluded from this present study, as titration was not available.

4.2 Ionic Disorders

Many studies focused on the biological aspects of malaria and dengue co-infection (Epelboin et al., 2012; Mohapatra et al., 2012; S. Ahmad et al., 2016; Shah & Mehta, 2017; Kotepui & Kotepui, 2019; A. Ahmad et al., 2019; Kotepui et al., 2020; Galani et al., 2021), but very few noted ionic disturbances. The present study highlighted numerous blood ionogram disturbances during the concomitant presence of malaria with dengue (Figure 2). However, the lack of evidence in the literature on the hydroelectrolytic disorders encountered during coinfection considerably limits discussion.

Hyponatremia was found in 40% of co-infected patients, in 27.08% of dengue cases alone and 32.5% of malaria cases. Regarding the results of dengue, Vachvanichsanong and McNeil found 46.7% of hyponatremia (Vachvanichsanong & McNeil, 2015). Epelboin noted that 7.1% of patients co-infected with dengue and malaria had hyponatremia (Epelboin et al., 2012). In the literature, hyponatremia is the most common biochemical disturbance in dengue or malaria (Karnad et al., 2018; Rehman et al., 2020; Ng & Cheong, 2021) ; but insufficiently documented in co-infection. However, on the one hand, this may be explained by an excess of water due to an increase in metabolism, an inappropriate transient secretion of antidiuretic hormone leading to an increased tubular reabsorption, an influx of sodium into the cells due to a dysfunction of the sodium-potassium pump, or a combination of these factors; and on the other hand by digestive losses of sodium (diarrhea, vomiting). Indeed, Kane noted 38% of patients presenting digestive signs as vomiting and diarrhea, responsible for extracellular dehydration leading to a significant hyponatremia (Kane, 2020).

Hypokalemia was present in 30% of patients with co-infection (Figure 2). It could be attributed to activation of the renin-angiotensin-aldosterone system resulting in loss of potassium in the urine. In contrast, hyperkalemia was absent in co-infection but only found in one patient (2.08%) infected with dengue alone. These results are similar to those of Epelboin who recorded 1.5% in his study (Epelboin et al., 2012). Vachvanichsanong and McNeil reported an hyperkalemia of 5.95% (Vachvanichsanong & McNeil, 2015). This hyperkalemia could be explained on the one hand by the presence of metabolic acidosis and on the other hand by the altered renal function of some patients.

Hypocalcemia was present in 40% of patients with co-infection, 27.66% and 37.50% in isolated dengue and isolated malaria respectively (Figure 2). Hypocalcemia, although insufficiently reported in co-infection, is particularly well documented in dengue (Bunnag & Kalayanarooj, 2011; Kapoor & Singh, 2012; Constantine et al., 2014) and malaria (Ayoola et al., 2005; Aijazi et al., 2020). Hypocalcemia is observed in severe dengue and is thought to be associated with increased mortality. Hypercalcemia was found in 30% of co-infected patients, compared to 37.50% for malaria mono-infection and 27.66% for isolated dengue. Hypercalcemia could be explained by an excess of intravenous calcium intake or by the altered renal function of some of the patients. Calcium remains an important parameter to avoid cardiac complications.

Hyperchloremia was observed in 38.46% of malaria cases, 17.02% for dengue and 20% in case of co-infection (Figure 2). The results are similar to those of Syed et al. who demonstrated that serum chloride levels in dengue patients significantly increase (Syed et al., 2014). This observed hyperchloremia could be due to the extracellular dehydration of the patients due to vomiting, but also to the decrease of bicarbonates.

We reported hypophosphatemia in 30%, 25.81% and 51.85% of patients respectively with co-infection, dengue and malaria. Likewise, hypomagnesemia was found in 22.22% of co-infected patients, 24.39% with malaria and 30.43% of those suffering from dengue. Hypophosphatemia and hypomagnesemia could be explained by the presence of hypercalcemia and the renal dysfunction of some of our patients.

No cases of decreased bicarbonate ions or hypoprotidemia were noted during the study. However, 27.27% of cases of hyperprotidemia were present in case of co-infection, versus 21.43% for malaria and 30.43% for dengue. It could be explained by the presence of hemoconcentration due to digestive losses (vomiting, diarrhea).

5. Conclusion

Malaria and dengue are the two major stars of tropical infectious diseases and are endemic in Burkina Faso. Both diseases

can be diagnosed in the same patient and the present study found a co-infection frequency of 1.14%. It was found that the ionogram disturbances were dominated by hyponatremia, hypocalcemia, hypokalemia and hypophosphatemia. It seems appropriate that further studies be carried out to assess the correlation of these ionic disorders with the evolution of patients with malaria-dengue co-infection.

Conflicts of interest

The authors declare that they have no conflicts of interest.

Acknowledgements

We are grateful to all the staff of the laboratory of the Pediatric University Hospital Charles de Gaulle at Ouagadougou (Burkina Faso).

References

Abdul-Ghani, R., Mahdy, M. A. K., Alkubati, S., Al-Mikhlafy, A. A., Alhariri, A., Das, M., Dave, K., & Gil-Cuesta, J. (2021). Malaria and dengue in Hodeidah city, Yemen: High proportion of febrile outpatients with dengue or malaria, but low proportion co-infected. *PloS One*, *16*(6), e0253556. https://doi.org/10.1371/journal.pone.0253556

Ahmad, A., Khan, I. A., & Raza, M. (2019). *Clinico-hematological profile of children with Dengue and co-infection with Malaria: A hospital based study*. https://doi.org/10.18203/2349-3291.ijcp20193687

Ahmad, S., Dhar, M., Mittal, G., Bhat, N. K., Shirazi, N., Kalra, V., Sati, H. C., & Gupta, V. (2016). A comparative hospital-based observational study of mono- and co-infections of malaria, dengue virus and scrub typhus causing acute undifferentiated fever. *European Journal of Clinical Microbiology & Infectious Diseases: Official Publication of the European Society of Clinical Microbiology*, *35*(4), 705-711. https://doi.org/10.1007/s10096-016-2590-3

Aijazi, I., Chaudary, M., Adam Mukhtar, S. H., & Abdulla Al Shama, F. M. (2020). Falciparum Malaria Presenting With Tetany: Endocrinopathies Associated With Falciparum Malaria. *Journal of Ayub Medical College, Abbottabad: JAMC*, *32*(1), 136-138.

Ayoola, O. O., Fawole, O. I., & Omotade, O. O. (2005). Calcium and phosphate levels in Nigerian children with malaria. *Annals of Tropical Paediatrics*, *25*(4), 303-306. https://doi.org/10.1179/146532805X72467

Baba, M., Logue, C. H., Oderinde, B., Abdulmaleek, H., Williams, J., Lewis, J., Laws, T. R., Hewson, R., Marcello, A., & D' Agaro, P. (2013). Evidence of arbovirus co-infection in suspected febrile malaria and typhoid patients in Nigeria. *Journal of Infection in Developing Countries*, *7*(1), 51-59. https://doi.org/10.3855/jidc.2411

Bunnag, T., & Kalayanarooj, S. (2011). Dengue shock syndrome at the emergency room of Queen Sirikit National Institute of Child Health, Bangkok, Thailand. *Journal of the Medical Association of Thailand = Chotmaihet Thangphaet*, *94 Suppl 3*, S57-63.

Constantine, G. R., Rajapakse, S., Ranasinghe, P., Parththipan, B., Wijewickrama, A., & Jayawardana, P. (2014). Hypocalcemia is associated with disease severity in patients with dengue. *The Journal of Infection in Developing Countries*, *8*(09), 1205-1209. https://doi.org/10.3855/jidc.4974

Epelboin, L., Hanf, M., Dussart, P., Ouar-Epelboin, S., Djossou, F., Nacher, M., & Carme, B. (2012). Is dengue and malaria co-infection more severe than single infections? A retrospective matched-pair study in French Guiana. *Malaria Journal*, *11*, 142. https://doi.org/10.1186/1475-2875-11-142

Faruque, L. I., Zaman, R. U., Alamgir, A. S. M., Gurley, E. S., Haque, R., Rahman, M., & Luby, S. P. (2012). Hospital-Based Prevalence of Malaria and Dengue in Febrile Patients in Bangladesh. *The American Journal of Tropical Medicine and Hygiene*, *86*(1), 58-64. https://doi.org/10.4269/ajtmh.2012.11-0190

Galani, B. R. T., Mapouokam, D. W., Simo, F. B. N., Mohamadou, H., Chuisseu, P. D. D., Njintang, N. Y., & Moundipa, P. F. (2021). Investigation of dengue-malaria coinfection among febrile patients consulting at Ngaoundere Regional Hospital, Cameroon. *Journal of Medical Virology*, *93*(6), 3350-3361. https://doi.org/10.1002/jmv.26732

Im, J., Balasubramanian, R., Ouedraogo, M., Wandji Nana, L. R., Mogeni, O. D., Jeon, H. J., van Pomeren, T., Haselbeck, A., Lim, J. K., Prifti, K., Baker, S., Meyer, C. G., Kim, J. H., Clemens, J. D., Marks, F., & Soura, A. B. (2020). The epidemiology of dengue outbreaks in 2016 and 2017 in Ouagadougou, Burkina Faso. *Heliyon*, *6*(7), e04389. https://doi.org/10.1016/j.heliyon.2020.e04389

Kane, C. (2020). *Perturbations des paramètres biochimiques au cours de la dengue au Centre Hospitalier Universitaire Pédiatrique Charles De Gaulle du 1er Janvier 2017 Au 31 Décembre 2018* [Unpublished doctoral dissertation]. Université Joseph Ki-Zerbo, Ouagadougou, Burkina Faso.

Kapoor, S., & Singh, A. (2012). Hypocalcemic tetany: An infrequently recognized association with acute dengue infection. *Indian Journal of Pediatrics*, *79*(12), 1673. https://doi.org/10.1007/s12098-012-0690-3

Karnad, D. R., Nor, M. B. M., Richards, G. A., Baker, T., Amin, P., & Council of the World Federation of Societies of Intensive and Critical Care Medicine. (2018). Intensive care in severe malaria: Report from the task force on tropical diseases by the World Federation of Societies of Intensive and Critical Care Medicine. *Journal of Critical Care*, *43*, 356-360. https://doi.org/10.1016/j.jcrc.2017.11.007

Kotepui, M., & Kotepui, K. U. (2019). Prevalence and laboratory analysis of malaria and dengue co-infection: A systematic review and meta-analysis. *BMC Public Health*, *19*(1), 1148. https://doi.org/10.1186/s12889-019-7488-4

Kotepui, M., Kotepui, K. U., Milanez, G. D. J., & Masangkay, F. R. (2020). Prevalence of and risk factors for severe malaria caused by Plasmodium and dengue virus co-infection: A systematic review and meta-analysis. *Infectious Diseases of Poverty*, *9*, 134. https://doi.org/10.1186/s40249-020-00741-z

Lim, J. K., Carabali, M., Edwards, T., Barro, A., Lee, J.-S., Dahourou, D., Lee, K. S., Nikiema, T., Shin, M. Y., Bonnet, E., Kagone, T., Kaba, L., Namkung, S., Somé, P.-A., Yang, J. S., Ridde, V., Yoon, I.-K., Alexander, N., & Seydou, Y. (2021). Estimating the Force of Infection for Dengue Virus Using Repeated Serosurveys, Ouagadougou, Burkina Faso. *Emerging Infectious Diseases*, *27*(1), 130-139. https://doi.org/10.3201/eid2701.191650

Ly, D. (2017). *La co-infection de la dengue avec le paludisme dans la ville de Ouagadougou: Aspects épidémiologiques, cliniques, biologiques et évolutifs* [Unpublished doctoral dissertation]. Université Joseph Ki-Zerbo, Ouagadougou, Burkina Faso.

Mendonça, V. R. R., Andrade, B. B., Souza, L. C. L., Magalhães, B. M. L., Mourão, M. P. G., Lacerda, M. V. G., & Barral-Netto, M. (2015). Unravelling the patterns of host immune responses in Plasmodium vivax malaria and dengue co-infection. *Malaria Journal*, *14*, 315. https://doi.org/10.1186/s12936-015-0835-8

Ministry of Health. (2014). *Directives nationales de prise en charge des cas de dengue au Burkina Faso* (p. 22). http://www.touteinfo.com/IMG/pdf/directives_pec_dengue_version_du_21_juillet.pdf

Mohapatra, M. K., Patra, P., & Agrawala, R. (2012). Manifestation and outcome of concurrent malaria and dengue infection. *Journal of Vector Borne Diseases*, *49*(4), 262-265.

Ng, W. W., & Cheong, B. M. K. (2021). Dengue Encephalitis associated with symptomatic hyponatremia due to Syndrome of Inappropriate Antidiuretic Hormone Secretion. *The Medical Journal of Malaysia*, *76*(2), 261-263.

Rehman, F. U., Omair, S. F., Memon, F., Amin, I., Rind, B. J., & Aziz, S. (2020). Electrolyte Imbalance at Admission Does Not Predict the Length of Stay or Mortality in Dengue-Infected Patients. *Cureus*, *12*(9), e10419. https://doi.org/10.7759/cureus.10419

Savadogo, M., Boushab, B. M., Fall-Malick, Z., Apoline, S., & Sow, M. (2017). Aspects epidemiologiques et cliniques des cas de dengue observes dans le Service des Maladies Infectieuses du CHU Yalgado Ouedraogo de Ouagadougou. *Annale de l'Université Ouaga 1 Pr Joseph KI-ZERBO - Série D*.

Shah, P. D., & Mehta, T. K. (2017). Evaluation of concurrent malaria and dengue infections among febrile patients. *Indian Journal of Medical Microbiology*, *35*(3), 402-405. https://doi.org/10.4103/ijmm.IJMM_15_455

Singhsilarak, T., Phongtananant, S., Jenjittikul, M., Watt, G., Tangpakdee, N., Popak, N., Chalermrut, K., & Looareesuwan, S. (2006). Possible acute coinfections in Thai malaria patients. *The Southeast Asian Journal of Tropical Medicine and Public Health*, *37*(1), 1-4.

Syed, S., Mahmood, Z., Riaz, M., Latif, S., Majeed, N., & Rashid, A. (2014). Elemental profile of blood serum of dengue fever patients from Faisalabad, Pakistan. *Int J Biol Sci*, *6*, 34-37.

Vachvanichsanong, P., & McNeil, E. (2015). Electrolyte disturbance and kidney dysfunction in dengue viral infection. *The Southeast Asian Journal of Tropical Medicine and Public Health*, *46 Suppl 1*, 108–117.

World Health Organization (WHO). (2019). *World malaria report 2019*. https://www.who.int/publications-detail-redirect/9789241565721

World Health Organization (WHO). (2021). *Dengue et dengue sévère*. https://www.who.int/fr/news-room/fact-sheets/detail/dengue-and-severe-dengue

International Journal of Chemistry; Vol. 14, No. 1; 2022
ISSN 1916-9698 E-ISSN 1916-9701
Published by Canadian Center of Science and Education

"Spatial Data Analysis for Ground Water Quality Assessment With Special Reference to Fluoride" - A Case Study of Dhar District, Madhya Pradesh, India

Dinesh Kumar Umak[1], Sandeep Kumar Rastogi[1], I. C. Das[2]

[1]M.P. Council of Science and Technology, Bhopal, India

[2]NRSC, Hyderabad, India

Correspondence: Dinesh Kumar Umak, M.P. Council of Science and Technology, Bhopal, India.

Received: December 4, 2021 Accepted: January 25, 2022 Online Published: January 31, 2022

doi:10.5539/ijc.v14n1p8 URL: https://doi.org/10.5539/ijc.v14n1p8

Abstract

Water is a prime natural resource and physiological necessity to mankind. Therefore, drinking water must not carry harmful chemicals as well as biological contaminants for the well-being and human health. Some of the chemicals like Fluoride, Iron, Arsenic, Cadmium, Chromium, Lead, selenium, and Nitrate in water may produce serious physiological changes when exist beyond permissible concentration.

The Aim of the study was to create spatial map for drinking water purpose for Dhar district, MP. The ground water quality data were collected from PHED, M.P. and IMIS (Ministry of Drinking water & Sanitation) Website,Government of India. The GWQ layers were created separately for each element for Pre-Monsoon and Post-Monsoon period from the well point layers with interpolation technique. Each element wise layer has been categorised into `three catagories (1) potable water in Desirable limits (2) Potable water in permissible limits (3) non-potable ground water, as per BIS standard, 2015. The Union of eight element layers of each pre-monsoon and post-monsoon has been done and integrated pre-monsoon and Integrated post-monsoon Ground Water Quality (GWQ) map have been prepared and after the Union of these two maps, the Final ground water quality map has been prepared. It was concluded from the study, that multiple parameters are affecting the quality of ground water in Dhar district and particularly excess Fluoride, Nitrate, Total Hardness (as Caco3), Iron, pH, and Total Dissolve solids are prevalent in the area. About 69.66% Habitation of Dhar district is severely affected mainly by excess of Fluoride, Nitrate & Total Hardness (as Caco3), pH & Iron(Fe) & It is observed that about 70.51% area of Dhar district has been affected in terms of Ground Water Quality.

Keywords: Ground Water Quality (GWQ), Geographical Information System (GIS), Bureau of Indian Standard (BIS)

1. Introduction

An adequate quantity of safe drinking water of acceptable quality is the primary necessity of every human being. India has large Human settlements in rural areas and villages which face problems of water quality and quantity, available water resources and seasonal scarcity of water. The villages mainly depend upon surface water resources, dug well water or bore well water. Surface water usually pose problem of turbidity while the bore well may pose the problems of Hardness, Fluorides and dissolved Iron. It is therefore important from the water supply point of view that critical evaluation of water treatment system need to be done on the primary factors which include raw and treated water quality, local constraints and relative cost. Simple, versatile, cost effective and innovative water treatment systems are the primary need in India for their implementation in rural areas and villages for supply of adequate quantities of safe potable water. Remote Sensing & GIS Techniques can support up to a great extent for Ground Water Quality mapping.

Dhar district situated in the south-western part of Madhya Pradesh covered area of 8145.31 sq.km. Falling in between 22°1'21.171" and 23°8'18.431"North Latitudes and 74°28'7.64" and 75°42'55.184"East Longitude and falling in survey of India degree sheets no's 46J, 46M and 46N. It is bounded by Ratlam, west nimar (Khargoan), Indore and Jhabua District of Madhya Pradesh. Dhar is the district headquarters and Badnawar, Manawar, Kukshi and Sardarpur are the important towns. The total number of settlements lying in the Dhar district are 1824. The Highest temperate in summer rises up to 46^{o}C temperature while minimum temperature during winter falls up to 5-6˚C.

2. Data and Methodology

The Ground water quality data Collected from PHED and downloaded from IMIS (India water)) website from 2009 to

2017. The Survey of India Toposheets No's 46 J/8, J/10, 11, 12, 13, 14, 15, 16; 46 M/4, 8; and 46N/1, 2, 3, 4, 5, 6, 7, 8, 10, 11, 12 were used for creating a Thematic maps like Base map, Settlement & roads etc. Indian Remote Sensing LISS III-P6 digital Satellite data of the year 2009-2010 for three seasons (January, April and October) were also used for the preparing the Geology, Geomorphology and lineament maps. District Resource Map (DRM) Published by Geological Survey of India (GSI) is also used for the reference.

The Ground Water Quality (GWQ) data were collected from IMIS & PHED and organize the ground water quality data of pre and post monsoon season. The essential eight parameters are pH, Total Hardness, Iron, chloride, Fluoride, TDS, Nitrate, & Alkalinity. Well Point layer of pre and post monsoon with their elements was generated. Element wise layers for pre monsoon and post monsoon data were created by using Inverse distance weighted analysis and classify into the desirable, permissible and non-Potable class as per Bureau of Indian Standard (BIS) 2015. By union of all Pre-monsoon layers and by union of all Post-monsoon layers, an integrated pre-monsoon and integrated post-monsoon ground water quality class map has been prepared. By union of these two maps final ground water quality class map of Dhar district has been prepared containing nine classes.

Physiography and Geomorphology

Physiographically, the district can be sub-divided into three major units viz Nothern plateau region (Malwa Plateau), central hilly region and Southern Valley (Narmada Valley). Malwa Plateau is an upland region characterised by undulating topography with elevations ranging from 350 to 550 m. Chambal, Mahi and bagh rivers flowing Northerly drain this region. The central hilly region comprises ENE-WSW trending Ridges which have steep slopes and scarp faces on the southern side. The highest elevation in the district ie,751m above MSL is located in this region. The central hilly regions forms water divide between the Northward flowing rivers of Mahi and Chambal Drainage and the southward flowing tributaries of Narmada river including Baghain, uri, man and Karam rivers. The drainage Pattern in the Northern part is sub-dendritic to sub Parallel whereas it is dendritic with local sub parallel pattern in the southern part. The southern Valley region is occupied by Narmada river flowing from East to West along a mega Lineament.

The Geomorphology was referred from National Geomorphological and Lineament Mapping (NGLM) project on 1:50000 scale. The project was sponsored by National Remote Sensing Agency, Hyderabad and Geological Survey of India. The study area Dhar district comprises of the landforms namely as Upper Plateau (above 600 m) and Lower Plateau (below 600 m) from MSL, which is Highly, Moderately and Low dissected based on drainage as well as Joint and Fractures dissections, Plateau top, Ridge, Mesa, Butte, Scarp, Plateau Remnant and Valley of Structural origin. The other landforms such as, Pediment, Pediplain, Pediment corstone tor complex, Residual Mound and Gullied Land are of Denudational origin and Gullied Tract of, fluvial origin.

Geology

In the Dhar District the oldest litho- units belong to the Aravali super group of palaeo-proterozoic age (2500 m.y.) which comprises the Udaipur, Lunavada, and champaner group. Udaipur group consist of chlorite schist exposed NNW of Kukshi. Lunavada and champaner group occurs in the southern part. Lunavada group comprises muscovite, quartzite and biotite gneisses while the champaner group comprises slate, Phyllite and dolomite which are intruded by basic igneous bodies. Bijawar group of palaeo to meso Proterozoic age (2500 to 1600 m.y.) occurs east of gandhwani and comprises shale, Slate Phyllite, Dolomite and quartzite. Narmada valley granitoids of palaeo Proterozoic age are exposed along the main river and around gandhwani and included granite gneiss and granite with enclaves of hornblende gneiss and chlorite schist. These are intruded by metabasic and quartz veins. Bagh group of lower cretaceous age (110 m.y.) unconformably overlies the rocks of Aravali super group with exposed thickness verifying from 5 to 40m. This comprises Nimar sandstone at the base followed by the calcareous units comprising nodular limestone and coralline limestone. The calcareous unit is fossiliferrous and contained echinoids, lamellibranches, gastropods, corals and brachiopods. A major part of the district is occupied by Basalt flows of Malwa group of Deccan volcanic of late cretaceous Palaeogene (68-62 m.y.) Age. This comprises 38 Basaltic fiows with a total thickness of 610m. The rock is fine to medium grain, aphyric to sparsely to moderately porphyritic containing plagioclase phenocryst. Megacrystic flow units occur at the top part of the flows. The flows have been classified into Mandleshwar, Kalisindh, Kankaria, Pirukheri, Indore and Bargonda formations in ascending order of sequence. The Deccan trap and the Bagh beds have been intruded by a large number of basic, ultra-basic and carbonate dykes. The dykes are generally trend ENE-WSW to E-W parallel to the Narmada lineament.

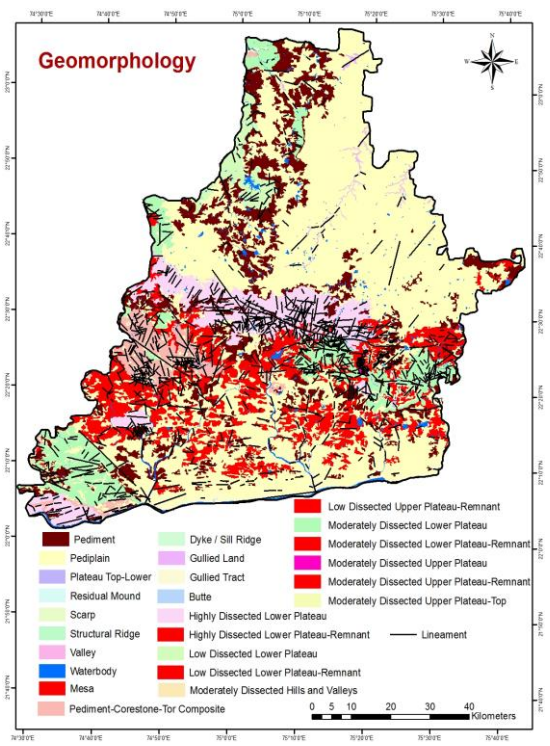
Geomorphology
Pediment
Pediplain
Plateau Top-Lower
Residual Mound
Scarp
Structural Ridge
Valley
Waterbody
Mesa
Pediment-Corestone-Tor Composite
Dyke / Sill Ridge
Gullied Land
Gullied Tract
Butte
Highly Dissected Lower Plateau
Highly Dissected Lower Plateau-Remnant
Low Dissected Lower Plateau
Low Dissected Lower Plateau-Remnant
Moderately Dissected Hills and Valleys
Low Dissected Upper Plateau-Remnant
Moderately Dissected Lower Plateau
Moderately Dissected Lower Plateau-Remnant
Moderately Dissected Upper Plateau
Moderately Dissected Upper Plateau-Remnant
Moderately Dissected Upper Plateau-Top
Lineament
0 5 10 20 30 40
Kilometers

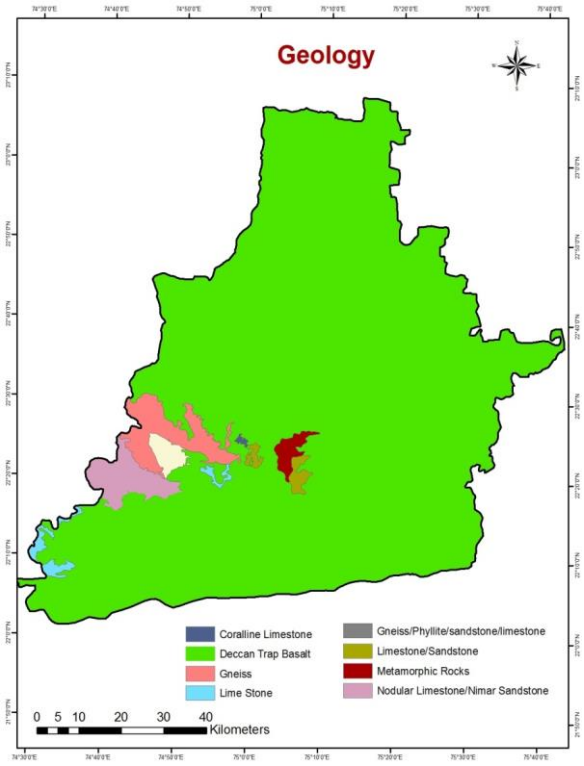
Geology
Coralline Limestone
Deccan Trap Basalt
Gneiss
Lime Stone
Gneiss/Phyllite/sandstone/limestone
Limestone/Sandstone
Metamorphic Rocks
Nodular Limestone/Nimar Sandstone
0 5 10 20 30 40
Kilometers

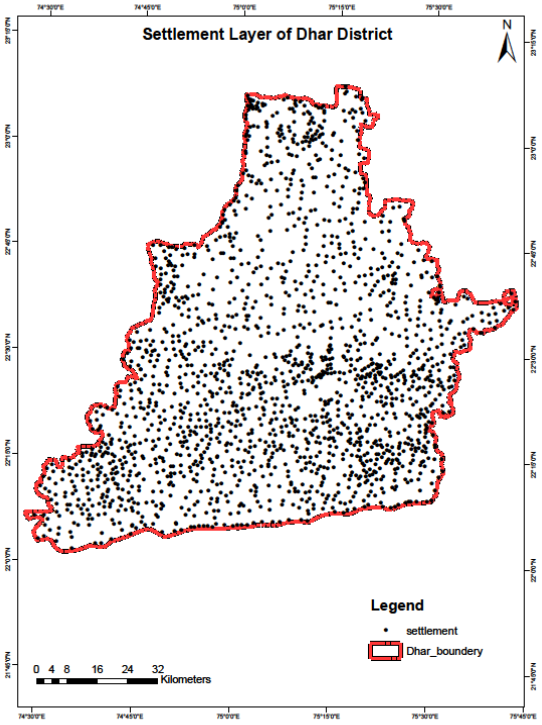
Settlement Layer of Dhar District
N
Legend
settlement
Dhar_boundery
0 4 8 16 24 32
Kilometers

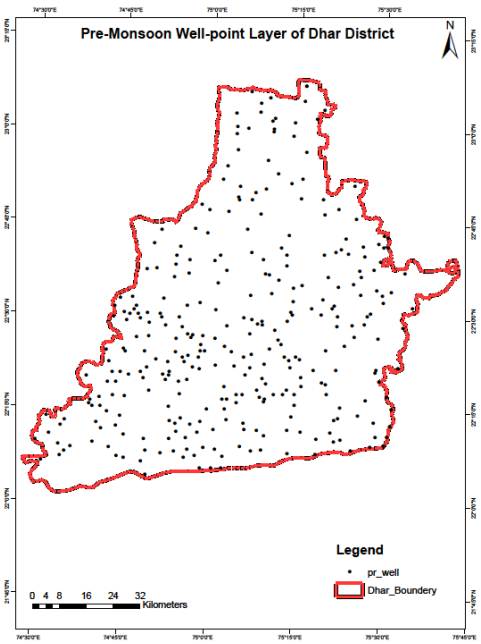
Pre-Monsoon Well-point Layer of Dhar District
N
Legend
pr_well
Dhar_Boundery
0 4 8 16 24 32
Kilometers

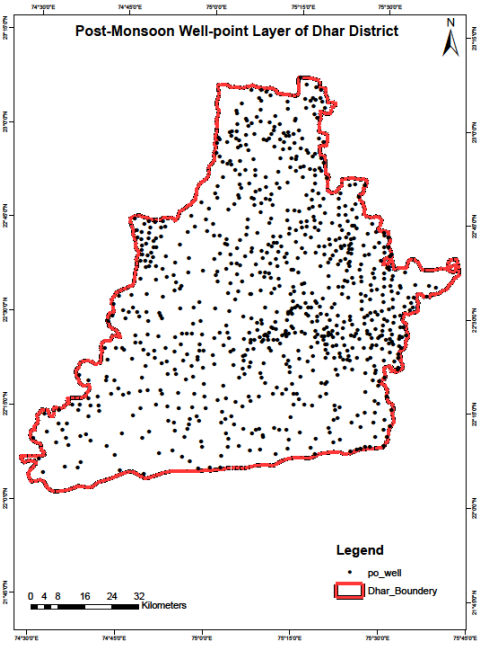
Post-Monsoon Well-point Layer of Dhar District
N
Legend
po_well
Dhar_Boundery
0 4 8 16 24 32
Kilometers

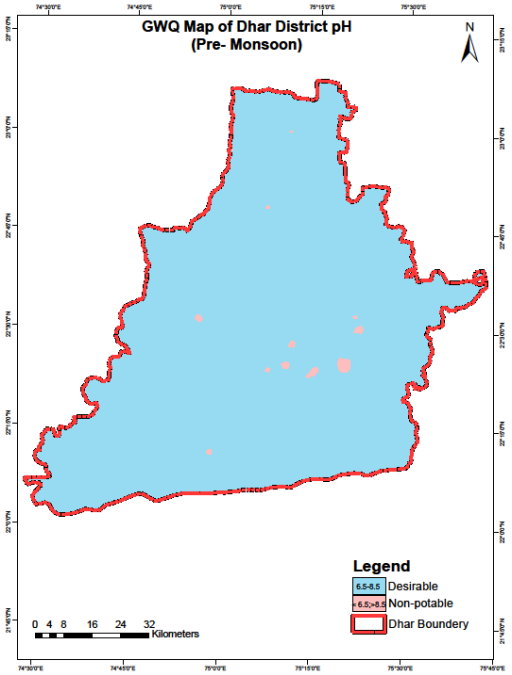
GWQ Map of Dhar District pH
(Pre- Monsoon)
N
Legend
6.5-8.5 Desirable
<6.5,>8.5 Non-potable
Dhar Boundery
0 4 8 16 24 32
Kilometers

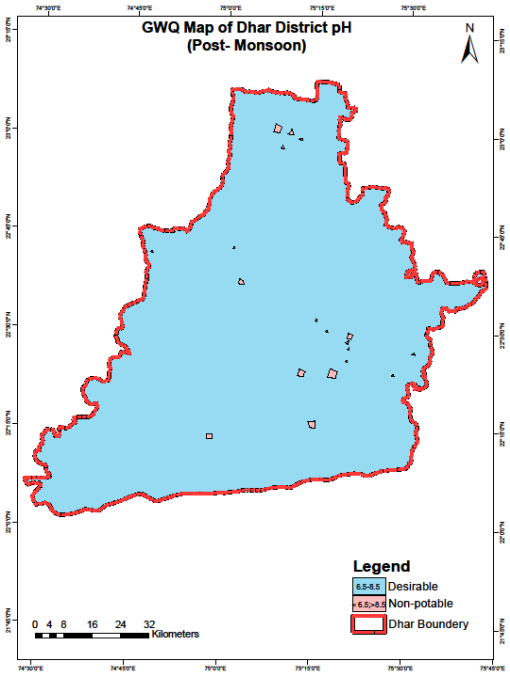
GWQ Map of Dhar District pH
(Post- Monsoon)
N
Legend
6.5-8.5 Desirable
<6.5,>8.5 Non-potable
Dhar Boundery
0 4 8 16 24 32
Kilometers

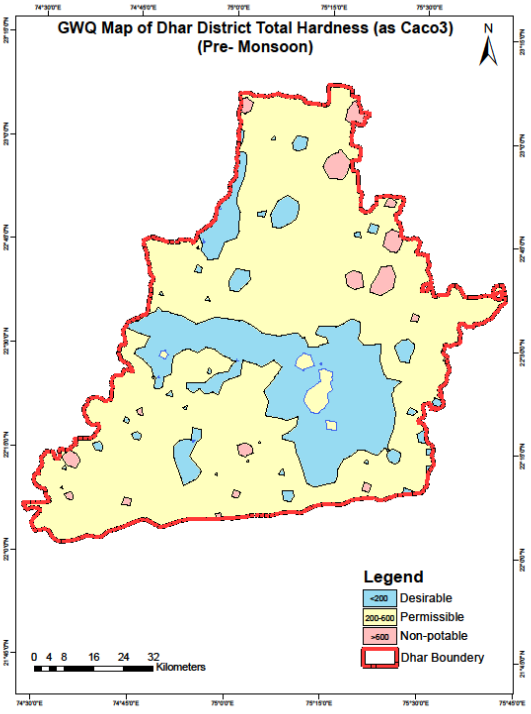
GWQ Map of Dhar District Total Hardness (as Caco3)
(Pre- Monsoon)
N
Legend
<200 Desirable
200-600 Permissible
>600 Non-potable
Dhar Boundery
0 4 8 16 24 32
Kilometers

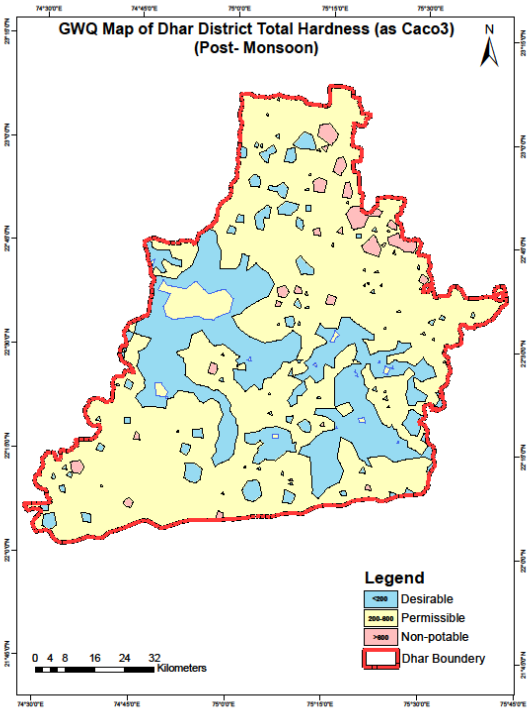
GWQ Map of Dhar District Total Hardness (as Caco3)
(Post- Monsoon)
N
Legend
Desirable
Permissible
Non-potable
Dhar Boundery
0 4 8 16 24 32
Kilometers

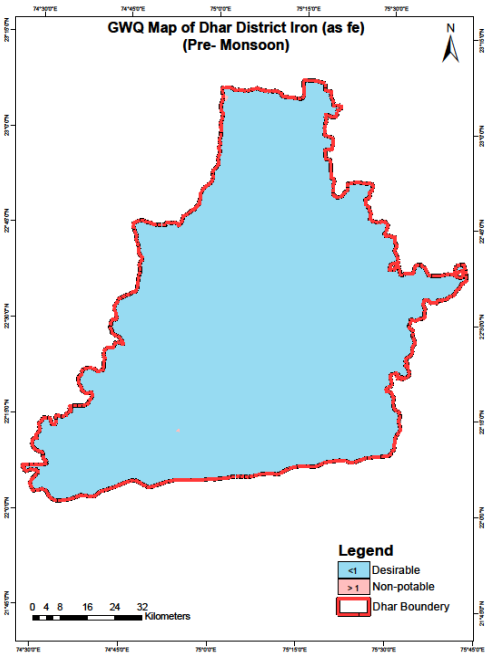
GWQ Map of Dhar District Iron (as fe)
(Pre- Monsoon)
N
Legend
Desirable
Non-potable
Dhar Boundery
0 4 8 16 24 32
Kilometers

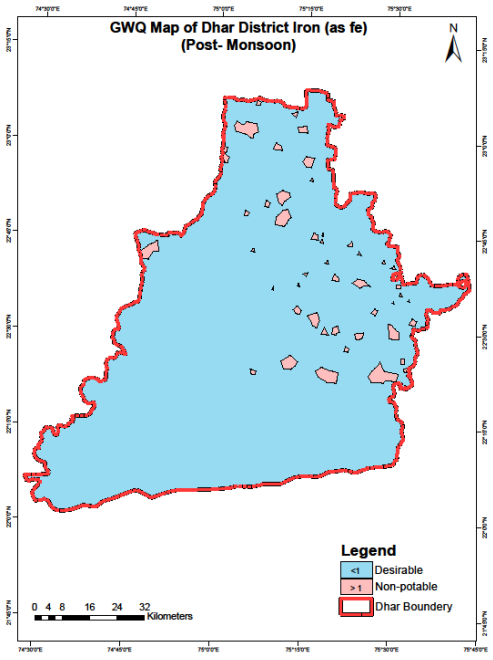
GWQ Map of Dhar District Iron (as fe)
(Post- Monsoon)
N
Legend
Desirable
Non-potable
Dhar Boundery
0 4 8 16 24 32
Kilometers

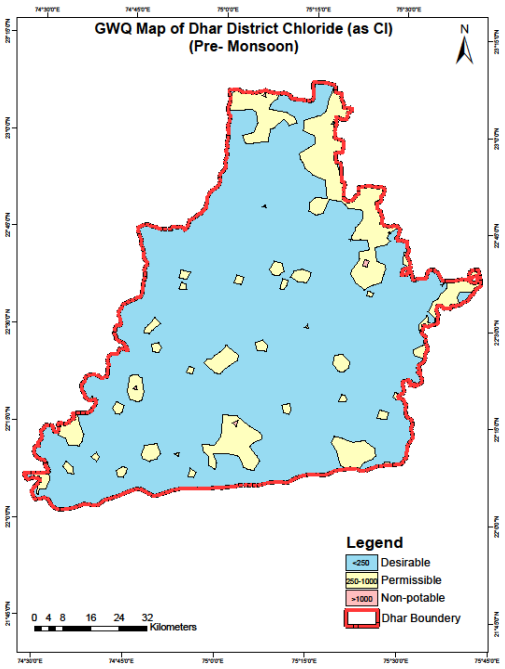
GWQ Map of Dhar District Chloride (as Cl)
(Pre- Monsoon)
N
Legend
<250 Desirable
250-1000 Permissible
>1000 Non-potable
Dhar Boundery
0 4 8 16 24 32
Kilometers

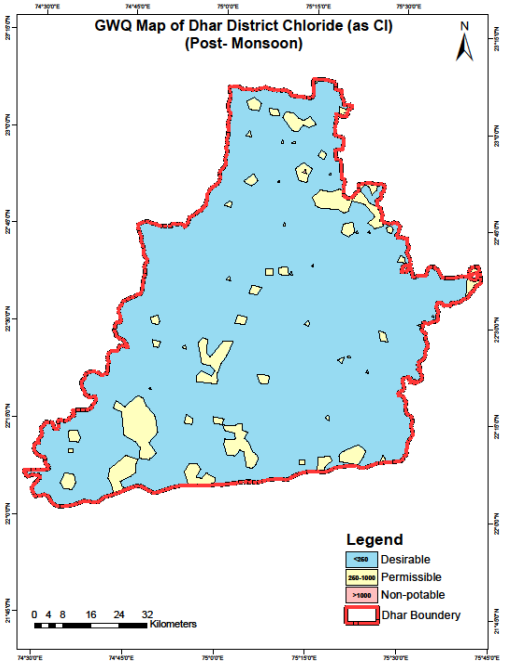
GWQ Map of Dhar District Chloride (as Cl)
(Post- Monsoon)
N
Legend
<250 Desirable
250-1000 Permissible
>1000 Non-potable
Dhar Boundery
0 4 8 16 24 32
Kilometers

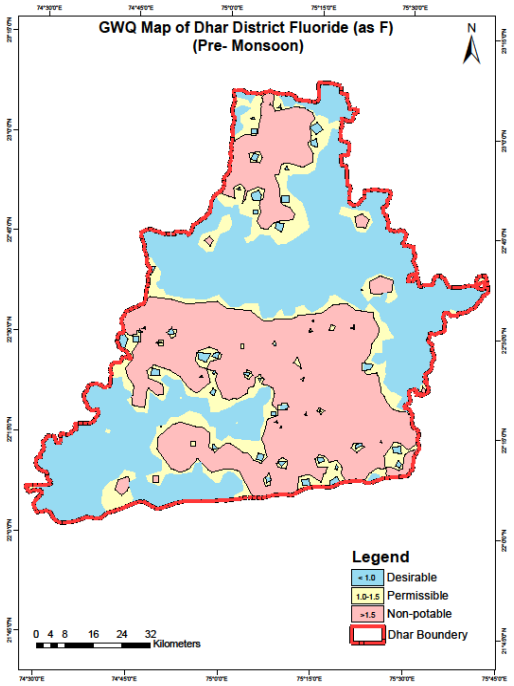
GWQ Map of Dhar District Fluoride (as F)
(Pre- Monsoon)
N
Legend
< 1.0 Desirable
1.0-1.5 Permissible
>1.5 Non-potable
Dhar Boundery
0 4 8 16 24 32
Kilometers

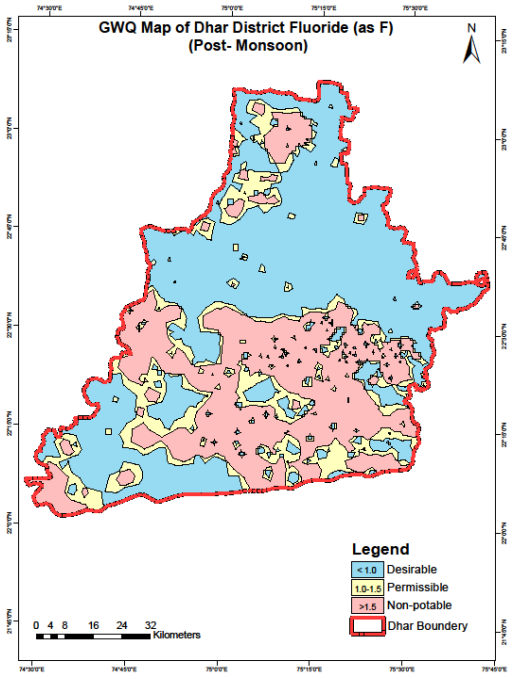
GWQ Map of Dhar District Fluoride (as F)
(Post- Monsoon)
N
Legend
< 1.0 Desirable
1.0-1.5 Permissible
>1.5 Non-potable
Dhar Boundery
0 4 8 16 24 32
Kilometers

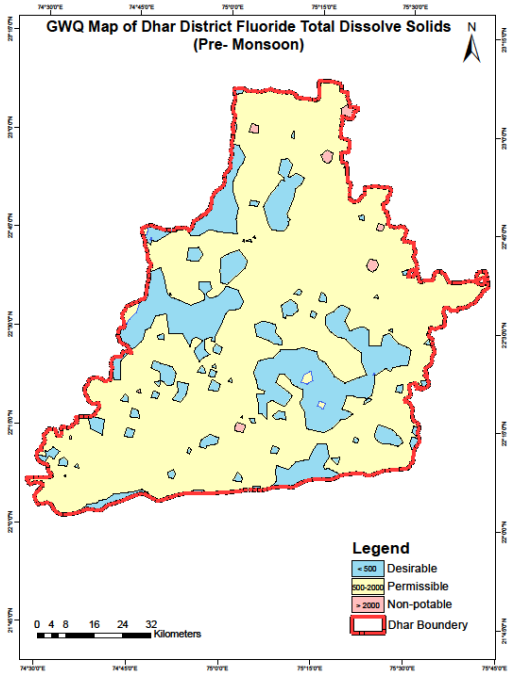
GWQ Map of Dhar District Fluoride Total Dissolve Solids
(Pre- Monsoon)
N
Legend
< 500 Desirable
500-2000 Permissible
> 2000 Non-potable
Dhar Boundery
0 4 8 16 24 32
Kilometers

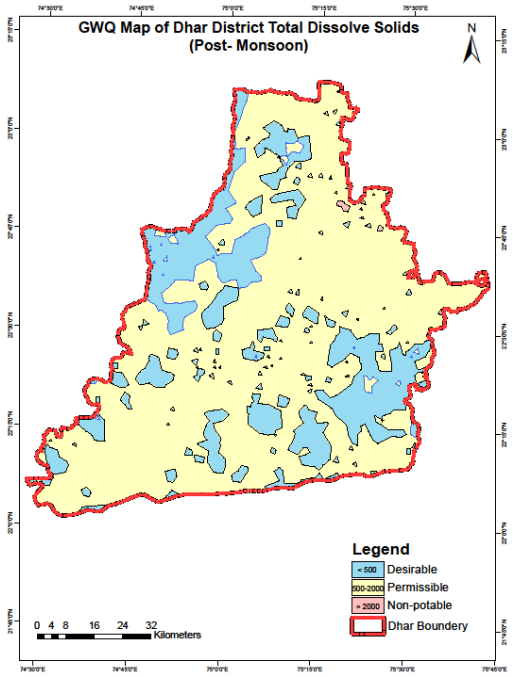
GWQ Map of Dhar District Total Dissolve Solids
(Post- Monsoon)
N
Legend
< 500 Desirable
500-2000 Permissible
> 2000 Non-potable
Dhar Boundery
0 4 8 16 24 32
Kilometers

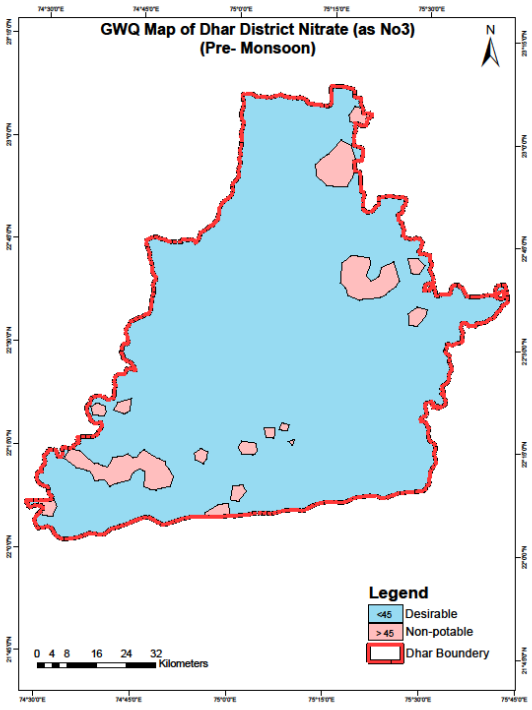
GWQ Map of Dhar District Nitrate (as No3)
(Pre- Monsoon)
N
Legend
<45 Desirable
> 45 Non-potable
Dhar Boundery
0 4 8 16 24 32
Kilometers

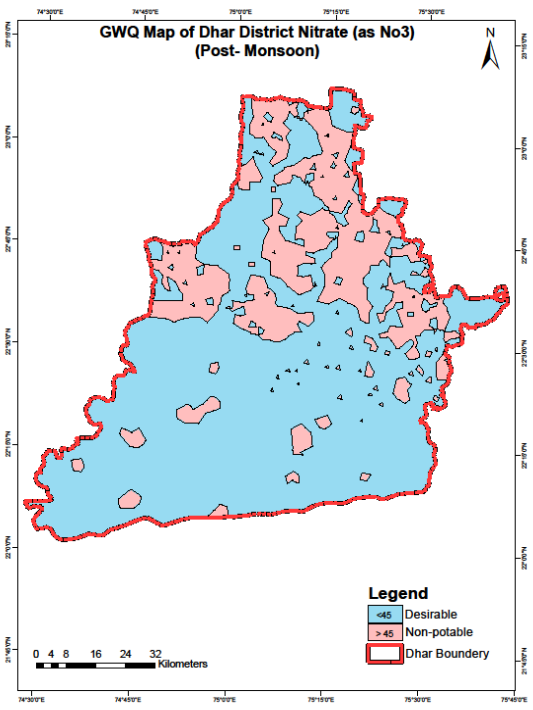
GWQ Map of Dhar District Nitrate (as No3)
(Post- Monsoon)
N
Legend
<45 Desirable
> 45 Non-potable
Dhar Boundery
0 4 8 16 24 32
Kilometers

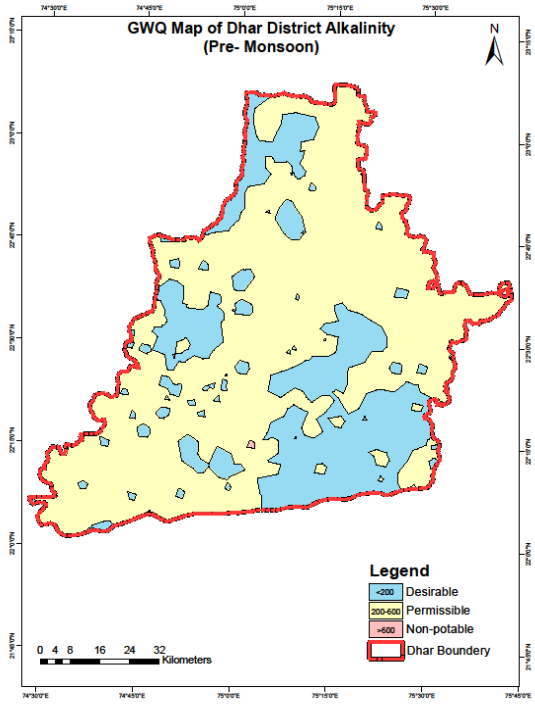
GWQ Map of Dhar District Alkalinity
(Pre- Monsoon)
N
Legend
<200 Desirable
200-600 Permissible
>600 Non-potable
Dhar Boundery
0 4 8 16 24 32
Kilometers

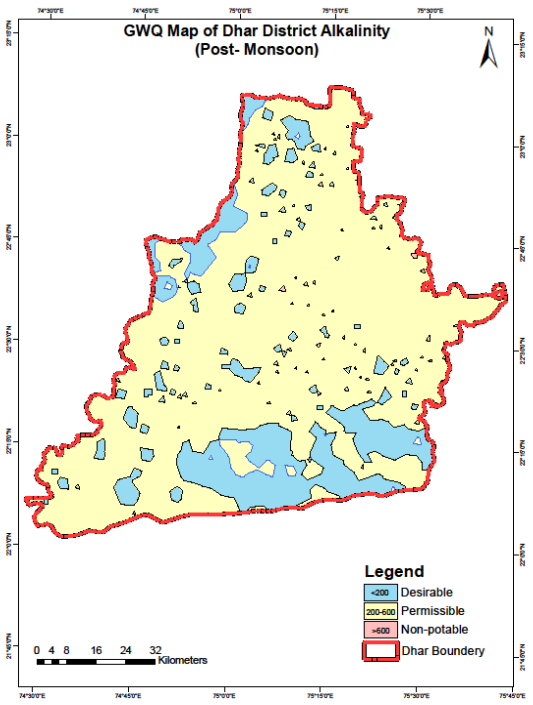
GWQ Map of Dhar District Alkalinity
(Post- Monsoon)
N
Legend
<200 Desirable
200-600 Permissible
>600 Non-potable
Dhar Boundery
0 4 8 16 24 32
Kilometers

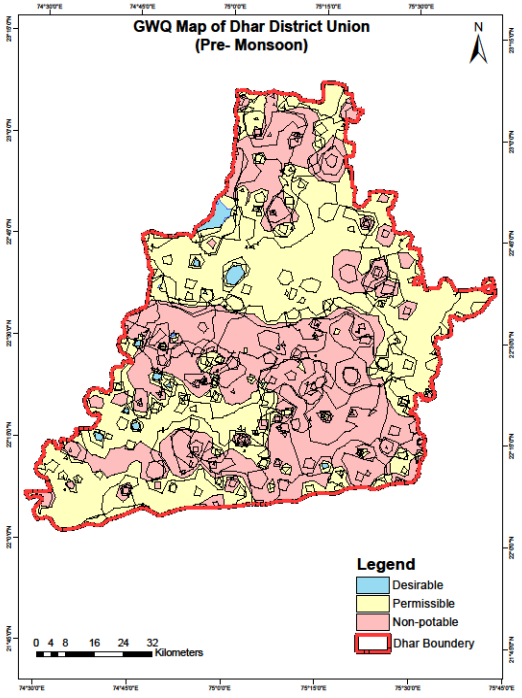

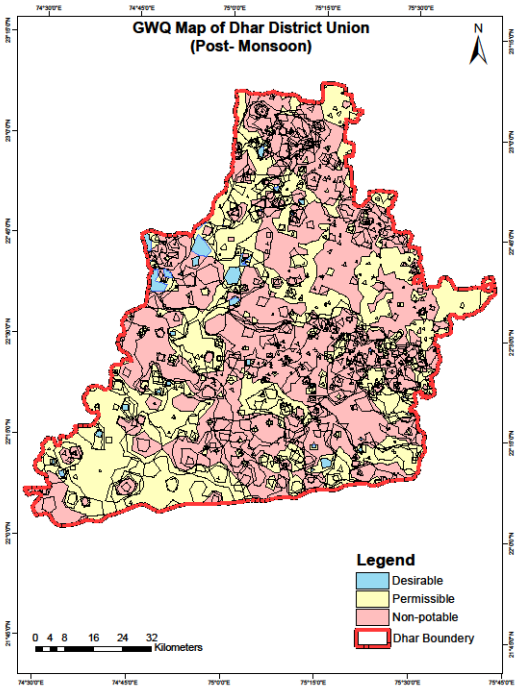

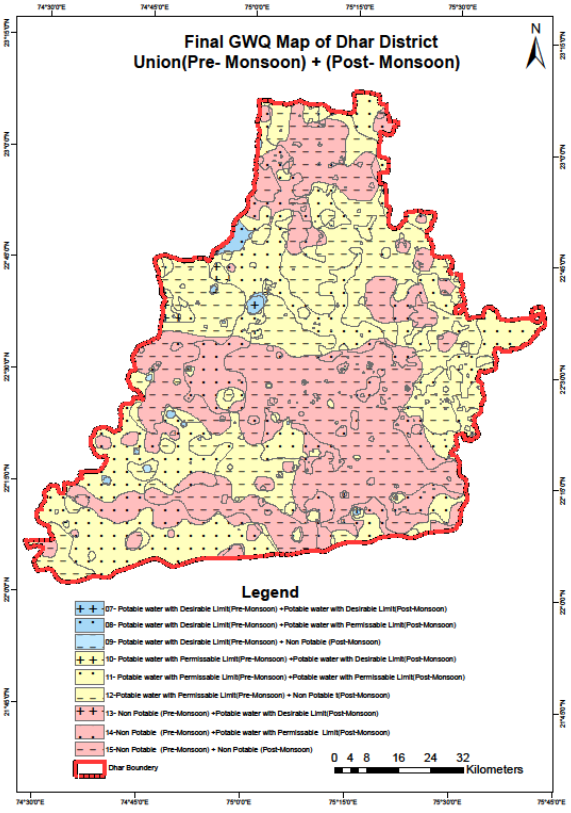

3. Results and Discussion

In the present study attempt has been made to generate the ground water quality class map by integration of Pre-monsoon ground water quality class map and Post-monsoon ground water quality class map. In the final ground water quality class map the following 9 classes have been identified.

1) **Non-Potable water (Pre-Monsoon) +Non-Potable water (Post-Monsoon)..... Class-15;**

This class covers an area of **2534.58 Sq.km** which is **31.11 %** of the total study area (**8145.31 sq.km)** and Out of **1824** total Habitation, **584** Habitation which is **32.01%** are lying in this class. This area is mainly lies in the Northern & Southern & south eastern part of the study area lying mainly in the Basaltic region. This class is Non-Potable in both Pre & Post monsoon season due to the concentration of the following elements - (1) **pH**- is ranging from 6.7 to 9.6 mg/l (2) **Total Hardness** is ranging from - 16 to 1510 mg/l (3) **Iron** is ranging from - 0.01 to 3.38 mg/l (4) **Chloride** is ranging from - 23 to 1261 mg/l (5) **TDS** is ranging from - 60 to 3300 mg/l (6) **Nitrate** is ranging from - 0.09 to 317.37 mg/l(7) **Fluoride** is ranging from - 0.1 to 14 mg/l (8) **Alkalinity** is ranging from - 42 to 824 mg/l

2) **Non-Potable water (Pre-Monsoon) + Potable water with Permissible limits (Post-Monsoon)..... Class – 14;**

This class covers an area of **1164.01 Sq.km** which is **14.29%** of the total study area (**8145.31 sq.km)** and Out of **1824** total Habitation, **306** Habitation which is **16.77%** are lying in this class. This area is mainly lies in the western & south eastern part of the study area lying in the basaltic region and this class is Non-Potable water in Pre Monsoon due to the concentration of the following elements ranging from (1) **Total Hardness**- 68 to 2260 mg/l (2) **Iron**- 0.05 to 1.19 mg/l (3) **Chloride**- 6.04 to 1373 mg/l (4) **TDS**- 320 to 3700 mg/l (5) **Nitrate**- 02 to 220 mg/l (6) **Fluoride**- 0.21 to 8.3 mg/l.

3) **Non-Potable water(Pre-Monsoon) + Potable water with desirable limits(Post-Monsoon).....Class-13;**

This class covers an area of **10.54 Sq.km** which is **0.129 %** of the total study area and **09** Habitation which is **0.49%** are lying in this class. This class is Non-Potable in Pre-monsoon due to the concentration of the following elements ranging from -(1) **pH**- 7.68 to 8.78 mg/l (2) **Fluoride**- 2.82 to 5.11 mg/l.

4) **Potable water with Permissible limits (Pre-Monsoon) +Non-Potable water (Post-Monsoon).....Class-12;**

This class covers an area of **2027.07 Sq.km** which is **24.88%** of the total study area and **369** Habitation which is **20.23%** are lying in this class. This area is mainly lies in the Northern & central part of the study area lying in the basaltic region and this class is Non-Potable water in Post-monsoon season due to the concentration of the following elements ranging from - (1)) **Total Hardness**- 72 to 780 mg/l (2) **Iron**- 0.03 to 1.65 mg/l (3) **Nitrate**- 4.72 to 157.17 mg/l (4) **Fluoride**- 0.19 to 4.34 mg/l.

5) **Potable water with Permissible limits (Pre-Monsoon) + Potable water with Permissible limits (Post-Monsoon)..... Class-11;**

This class covers an area of **2254.01 Sq.km** which IS **27.64 %** of the total study area and **502** Habitation which is **27.52%** lying in this class.

6) **Potable water with Permissible limits (Pre-Monsoon) + Potable water with desirable limits (Post-Monsoon)..... Class-10;**

This class covers an area of **73.85 Sq.km** which is **0.905 %** of the total study area. **28** habitation which is **1.53%** are lying in this class.

7) **Potable water with desirable limits (Pre-Monsoon) + Non-Potable water (Post-Monsoon)……Class-9;**

This class covers an area of **8.83 Sq.km** which is **0.108 %** of the total study area and **03** Habitation which is **0.16%** are lying in this class. This class is Non-Potable water (Post-Monsoon) season due to the concentration of the following elements. (1) **Total Hardness**- 196 to 796 mg/l (2) **Nitrate**- 13 to 133 mg/l (3) **Fluoride**- 0.75 to 2.59 mg/l.

8) **Potable water with desirable limits (Pre-Monsoon) + Potable water with Permissible limits (Post-Monsoon)..... Class- 8;**

This class covers an area of **45.37 Sq.km** which is **0.55%** of the total study area and covers **15** Habitation which is **0.82%** are lying in this class.

9) **Potable water with desirable limits (Pre-Monsoon)+Potable water with desirable limits(Post-Monsoon)..... Class- 7;**

This class covers an area of **27.02 Sq.km** which is **0.33%** of the total study area and it has only **08** Habitation which is **0.43%** are lying in this class.

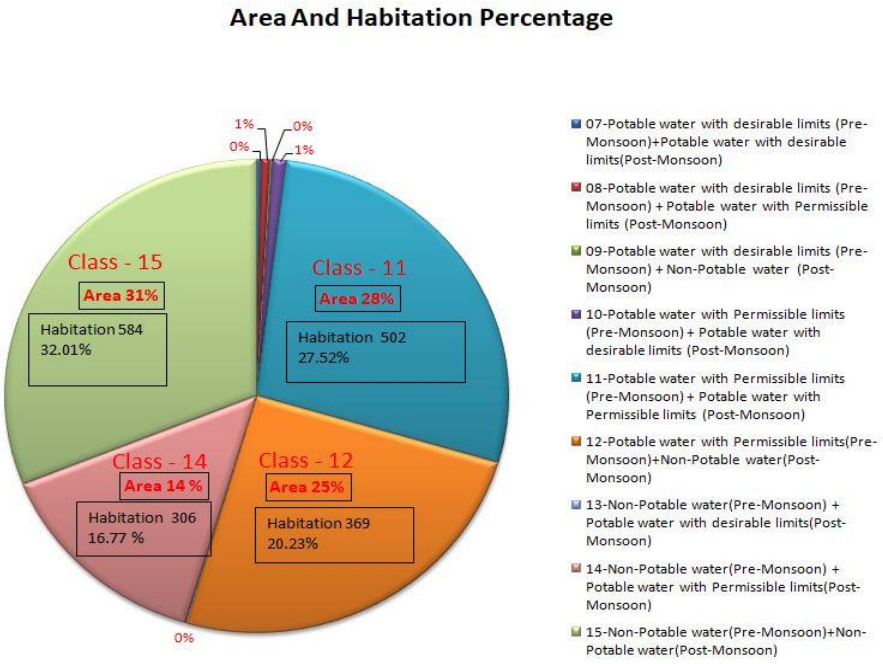

Figure 1. Area and habitation percentage

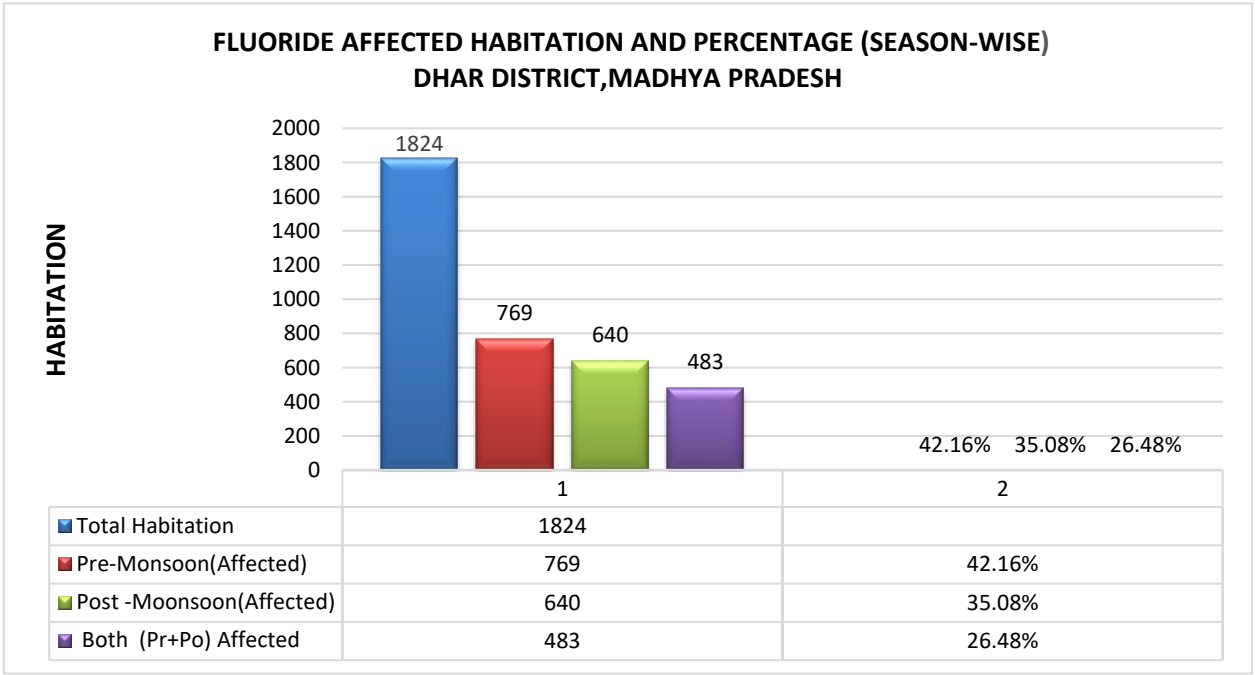

Figure 2. Fluoride affected habitation and percentage (season-wise) Dhar district, Madhya Pradesh

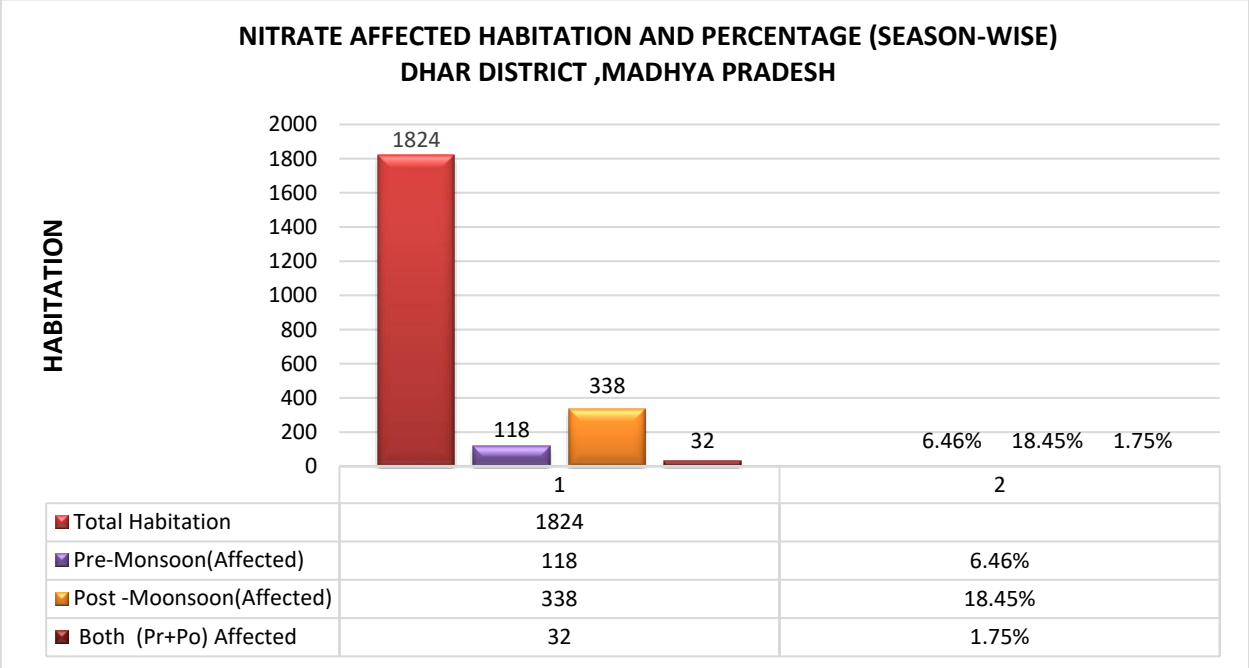

Figure 3. Nitrate affected habitation and percentage (season-wise) Dhar district, Madhya Pradesh

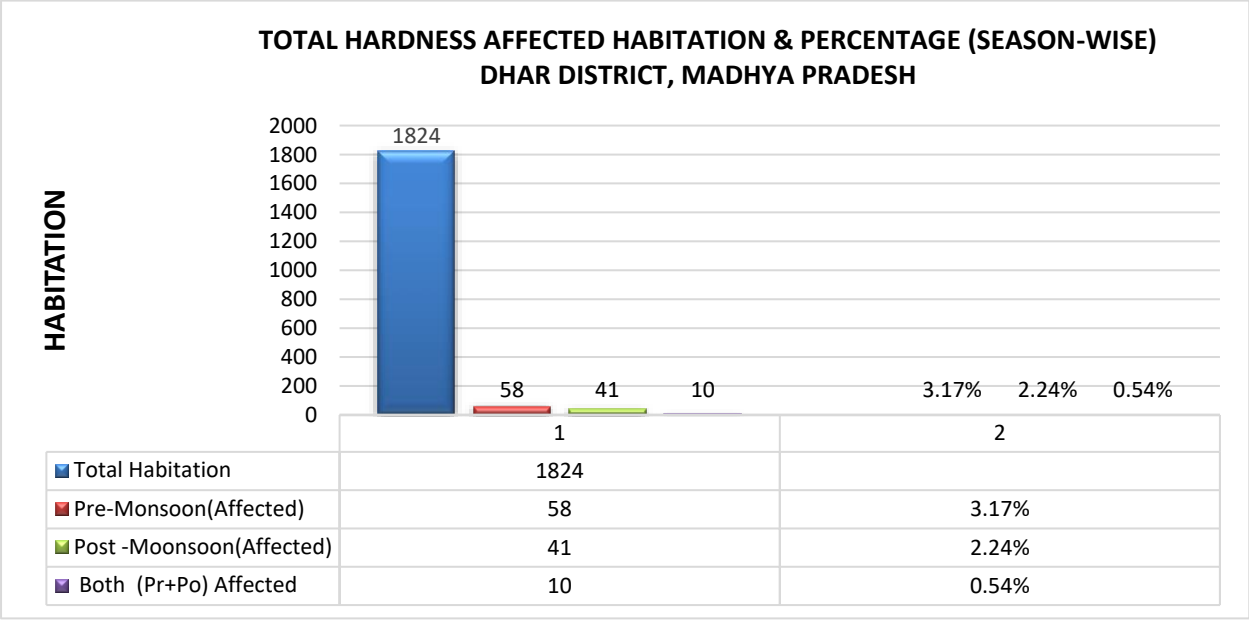

Figure 4. Total hardness affected habitation and percentage (season-wise) Dhar district, Madhya Pradesh

The **Fluoride** is the main element which is being found beyond permissible limit in the Dhar district. In Dhar district out of the total 1824 Habitations, In **pre- Monsoon** season **769 Habitation** which is **42.16%,** while in **post-Monsoon** season **640 Habitations** which is **35.08 %** are affected by excess of Fluoride, while in Both **pre and post - Monsoon** seasons (Union), **483 Habitations** which is **26.48 %** of the total Habitations are affected by excess of Fluoride which is non-potable.

Nitrate is the second element which is being found beyond permissible limit in the Dhar district. In Dhar district out of the total 1824 Habitations, In **pre-Monsoon** season **118 Habitation** which is **6.46 %,** while in **post-Monsoon** season **338 Habitations** which is **18.45 %** are affected by excess of Nitrate, while in Both **pre and post Monsoon** seasons (Union), **32 Habitations** which is **1.75%,** of the total Habitations are affected by excess of Nitrate which is non-potable.

Total Hardness is the third element which is being found beyond permissible limit in the Dhar district. In

pre-Monsoon season **58 Habitation** which is **3.17 %,** while in **post-Monsoon** season **41 Habitations** which is **2.24 %** are affected by excess of total Hardness while in Both **pre and post Monsoon** seasons (Union), **32 Habitations** which is **0.54 %** of the total Habitations are affected by excess of total Hardness which is non-potable.

pH is the Fourth element which is being found beyond permissible limit in the Dhar district. In **pre-Monsoon** season **27 Habitation** which is **1.48%**, while in **post-Monsoon** season **15 Habitations** which is **0.82 %** are affected by excess of pH , while in Both **pre and post- Monsoon** seasons (Union), **10 Habitations** which is **0.54%** of the total Habitations are affected by excess of pH which is non-potable.

Iron(fe) is the fifth element which is being found beyond permissible limit in the Dhar district. In **pre-Monsoon** season **8 Habitation** which is **0.43%,** while in **post-Monsoon** season **60 Habitations** which **3.28 %** are affected by excess of Iron(fe), while in Both **pre and post Monsoon** seasons (Union), **1 Habitation** which is **0.054%** of the total Habitations are affected by excess of Iron(fe) which is non-potable.

4. Conclusion

Based on the correlation between water quality and the existing geological formation, the problematic areas were identified. The results indicate that certain parameters mainly Fluorides, Nitrates, Total Hardness, pH and TDS were beyond the permissible limits in Dhar district.

The analysis of the results drawn at various stages of the work revealed that integration of Remote Sensing and GIS are effective tools for the preparation of various digital thematic layers and maps showing spatial distribution of various water quality parameters. Monitoring of pollution patterns and its trends with respect to urbanization is an important task for achieving sustainable management of groundwater. Spatial distribution maps of various pollution parameters are used to demarcate the locational distribution of water pollutants in a comprehensive manner and help in suggesting groundwater pollution control and remedial measures in a holistic way.

The continued consumption of fluoride in excess to 1.5 mg/l either through water, air or food items for a long time may cause dental, non- skeletal and skeletal fluorosis (Chand Dinesh, 2001). Fluoride > 1.5 mg/l Fluoride in excess can cause several ailments viz. Neurological, Muscular, Allergic, gastrointestinal effects, urinary problem, headache. Fluoride > 3 mg/l can result skeletal fluorosis and skeletal abnormalities. Fluoride >10 mg/l over a long period can result in crippling fluorosis.

References

Chand, D. (2001). Fluoride in Drinking Water: A Challenge of the millennium, International workshop on Fluoride in Drinking Water: Strategies. *Management & Mitigation*.

District Resource Map Dhar District, (2000). Published by Geological Survey of India.

Ground Water Quality Mapping, Rajiv Gandhi National Drinking Water Mission (RGNDWM), (2011). Methodology Manual, Hydrogeology Group, NRSA, National Remote Sensing Centre, Indian Space Research Organisation, Dept. of Space, Govt. of India, Hyderabad.

Jain, R. (2013). Ground Water Quality Mappping around Keolari in Seoni District of M.P. using Remote Sensing and GIS Techniques, Project Report for M.Tech. degree at NIT Warangal.

Jalali, M. (2005). Nitrates leaching from agricultural land in Hamadan, Western Iran. *Agriculture, Ecosystems and Environment, 110,* 210-218. https://doi.org/10.1016/j.agee.2005.04.011

National Geomorphological and Lineament Mapping on 1:50,000 scale, (2010). Manual, Geological Survey of India Ministry of Mines Government of India and Indian Space Research Organisation Department of Space Government of India.

Olajire, A. A., & Imeokparia F. E. (2001). Water quality assessment of Osun River: Studies on inorganic nutrients. *Environ. Monitor. Assess., 69*(1), 17-28. https://doi.org/10.1023/A:1010796410829

Saha, D., Dhar, Y. R., & Sikdar, P. K. (2008). Geochemical Evolution of Groundwater in the Pleistocene Aquifers of South Ganga Plain, Bihar. *Jour. Geol. Soc., 71*, 473-482.

Sarala, C., & Ravi, B. P. (2012). Assessment of Groundwater Quality Parameters in and around Jawaharnagar, Hyderabad. *International Journal of Scientific and Research Publications, 2*(10), October 2012 1 ISSN 2250-3153.

Copyrights

International Journal of Chemistry; Vol. 14, No. 1; 2022
ISSN 1916-9698 E-ISSN 1916-9701
Published by Canadian Center of Science and Education

Catalysis Mechanism and Application of Carbon Gasification Reaction-A Comparison of Two Heterogeneous Catalysis Mechanisms

Jia Min Jin

Correspondence: Jia Min Jin, Shanghai Research Institute of Materials, Shanghai, China.

Received: March 8, 2022 Accepted: April 13, 2022 Online Published: April 17, 2022

doi:10.5539/ijc.v14n1p23 URL: https://doi.org/10.5539/ijc.v14n1p23

Abstract

This article is a brief summary article of research. The results of the three times experiments are reviewed. two heterogeneous catalysis mechanisms are introduced, namely: Chemical Reaction Mode Cyclic Catalysis Mechanism-CRM and Electron Cyclic Donate-Accept Catalysis Mechanism-ECDAM or Electron Orbital Deformation-Recovery Cyclic Catalysis Mechanism -EODRM. Some difficulties encountered by CRM are listed. The author clearly points out that the CRM is not credible。This false theory has misled us for more than 100 years.

About ECDAM, the article also gives a brief description. The main point of ECDAM is that the catalysis phenomenon are physical rather than chemical phenomenon. The catalysts do not participate in chemical reactions. It's just contact, electron cyclic donate-accept or electron orbital deformation-recovery cycle. The theory contains three viewpoints:

1. There is a boundary between the catalyst and the poison.

2. The active of the catalyst or the degree of toxicity of the poison is closely related to ihe electronegative value of the catalyst or poison.

3. The active of catalyst is closely related to the chemical state of the catalyst

The selectivity of catalyst is also related to electronegative or energy level

According to ECDAM, the author considers that there are several problems worth studying in production and scientific research. such as: alumina is a poison in the Fe ammonia synthesis catalyst. The Cordierite ($2MgO{\cdot}2Al_2O_3{\cdot}5SiO_2$) ceramic honeycomb support is also a poison in automotive exhaust purification catalyst. The Cordierite ceramic honeycomb is retardant in wall flow filter for diesel vehicles. Activated carbon is a poison in the Ruthenium catalyst for ammonia synthesis. Alumina and activated carbon all are a poison to noble metal catalysts, and so on.

Keywords: heterogeneous catalysis, catalysis Mechanism, CRM, EODRM

1. Introduction

Because the chemical and physical properties of solid catalysts affect the catalytic active of catalysts at the same time. The result is that the catalysis phenomena are very complicated and were regarded as mysterious and not amenable to rational interpretation. For a long time, the selection study of catalysts is always in the skill stage of the laboratory. The author thinks that the basic reason is lack of correct theoretical guidance.

At present, it can be seen from literature that there are two heterogeneous catalysis mechanisms. One is the CRM widely adopted, and it is raised to the height of the “principle” by the scholars, this CRM is also instilled in high school textbooks. It can be said that CRM is deeply rooted in catalytic academia. Another catalysis mechanism is the EODRM or ECDAM proposed by author. The EODRM is completely different from CRM, which consider that catalytic phenomena are physical rather than chemical phenomena, and that catalysts do not participate in chemical reactions. It's just contact, electron cyclic donate-accept, electron orbital cyclic deformation-recovery. The electrocatalytic, photocatalytic, microwave catalysis, laser catalysis are all physical phenomena, only different energy levels.

2. About the CRM

In the Catalyst Handbook（Catalyst Handbook 1982), the expression for the CRM is as follows;

$$R+M \rightarrow X$$

$$X \rightarrow P+M$$

Where R is reactant, P is product, M is catalyst, X is intermediate. The catalyst M takes part in a chemical reaction and regenerates the same catalyst as original after reaction. From reactant to product, R→P, it does not generate, Instead, the

intermediate is generated by catalyst with reactant, and then the product is generated by the intermediate. The reason is that such a reaction way requires lower energy.

In the high school textbooks in China on the catalytic mechanism of biocatalyst enzyme, it is also based on CRM.

Reactant +enzyme→ intermediate→ product+enzyme

Enzymes take part in chemical reactions, produce intermediate compounds, and finally release the same enzymes as original. The Enzymes are constantly decomposed and generated.

About the CRM, the most obvious way to put it should be “Sabatier principle” (in 1902) and “Boubart principle”(in 1992).

In 2009, Deutschmann, O, et al had wrote a book, [*Heterogeneous catalysis and solid catalysts*] (Deutschmann.,O,2009). In this book, two “principles” advocated by the catalysis academia are repeatedly mentioned. One is the “Sabatier principle”, and the other is the” Boudart principle”, which author call as the “S-B principle”.

The Sabatier principle proposes the existence of an unstable intermediate compound formed between the catalyst surface and at least one of the reactants. The intermediate must be stable enough to be formed in sufficient quanitities and labile enough to decompose to yield the final product or products.

The Boudant principle is that the most fundamantal principle in catalysis is that of the catalytic cycle, which may be based on a redefinition of a catalyst by Boudart “A catalyst is a substance that transforms reactants into products, through an uninterrupted and repeated cycle of elementary steps in which the catajyst is changed through a sequence of reactive intermediates, until the last step in the cycle regenerats the catalyst in its original form”. “The activity of the catalyst is defined by the number of cycles per unit time or turnovers or turnover frequency(TOF;unit:S^{-1}),The life of the catalyst is defined by the number of cycles before it dies.”

1981 year, Mckee. D.W. (Mckee., D,W,1981) has studied the catalysis of the alkali metal oxides and their salts, alkaline earth metal oxides and their salts, transition group metals and their oxides, noble metals and other catalysts on $C+O_2$, $C+CO_2$, $C+ H_2O$ and $C+H_2$ reactions with advanced instrument(CAEM-Controlled Atmosphere Electron Microscope) . He has done a lot of experimental studies, wrote more than 100 pages of lengthy articles. Finally, he considers that on balance “specific oxidation-reduction cycles” have been conspicuously successful in interpreting the effects of these compounds in the various types of carbon gasification reactions. But the writer feelings that the "specific" word is nowhere to be seen. Although the author shows that the complex catalysis remains unclear and needs to be better studied afterward.

A senior American scholar has studied the catalysis of the noble metal Pt on the $C+CO_2=2CO$ and $C+H_2O=H_2+CO$ reaction, they also adopted CRM to account for the catalysis mechanism. They believed that Pt is continuously reduced and oxidized by H_2,CO and H_2O,CO_2 in the catalyze process. This is also Oxgen Transfer Mechanism-OTM. Even though the paper says " proposed mechanism".

In 2016, Chen ping, a young scientist from Chinese Academy of Sciences, and other researchers published a high-level paper in the international top academic Journal (Nature Chemistry). They have proposed the design theory of "dual-activation center" ammonia synthesis catalyst. Two activation centers such as TM (transition group metal) and LiH are continuously decomposed and regenerated in the catalyzing process of ammonia synthesis. In fact, they also follow the “S-B principle” or the traditional ancient CRM principle. It can be seen that the younger generation also inherited the idea of CRM.

Based on the above, CRM has been widely adopted in the catalytic community for more than 100 years and it is deeply rooted in catalystic field.

3. Three Times Experimental Studies

The most main idear of the CRM is that the catalyst must take part in the chemical reaction, and it has to be a cyclic reaction. In order to explore whether CRM can be trusted, the author has conducted three times experimental studies.

3.1 $BaCO_3$ Catalysis in Carburizing Box (the 1960s)

The $BaCO_3$ is commonly used as catalyst in solid carburizing agent of surface of steel parts. At the beginning, the mechanism of carbonate decomposition to release CO_2 which reacts with carbon to produce carbon monoxide and thus increasing the rate of carburization was used to account for the reason for accelerating carburizing rate. Later, it was found that $CaCO_3$, which can release a large amount of carbon dioxide, but it has no catalytic activity, while barium carbonate, which does not decompose at the carburizing temperature, has carburizing activity. Therefore, the mechanism of carbon dioxide release was abandoned and the Oxygen Transfer Mechanism, namely OTM, was adopted.

Namely:

$$BaCO_3+C=BaO+2CO \quad (1)$$

$$2CO=CO_2+[C] \quad (2)$$

$$CO_2+BaO=BaCO_3 \quad (3)$$

The OTM is also CRM.This is a typical CRM. BaO is an intermediate compound, and the $BaCO_3$ is constantly decomposed and generated in the carburizing process.

The mechanism was first proposed by R.A.Ragaz & L.O.Kowalke at 1931 (R,A,Ragaz & L,O.Kowalke 1931).

The equilibrium pressure of reaction (1) was measured by author (Jin,J,M., 1963). At the carburizing temperature 946^0C, the equilibrium pressure is 0.226 atm., which is much lower than the1atm.of carbon monoxide pressure in the carburizing box. It indicates that the $BaCO_3$ cannot be decomposed by carbon, that is, the $BaCO_3$ does not take part in chemical reaction and the cyclic reaction of "decomposition-generation" cannot at all occur.

3.2 The catalysis of Fe, Co, Ni, Cu, Ag and SiO_2,S on the Reducton Reaction Rate (Jin, J,M.1982) (the 1970s)

The authors have done a few times verification experiments refer to the CRM and EODRM. These have included the active of catalyst and poisonousness of poison, such as Fe, Co, Ni, Cu, Ag, SiO_2, S. The experimental results show that Fe etc. appear catalytic active on carbon gasification reaction. Iron appears the greatest catalytic active. They relative actives are Fe > Cu, Fe>Ni, Cu>Ni, Ag>Cu and Co>Ni. The SiO_2 and S are poison. The poisonousness of SiO_2 appears to be more poisonousness than S. The experimental results agree well with EODRM, At the same time, it also strongly shows that the CRM simply cannot account for the results of the experiment. Because they can't take part in a chemical reaction in the reaction box. Because there's a lot of solid carbon in the reaction box, while the carbon is a powerful reducing agent at 1000^0C. Thermochemical data can justify perfectly that Fe, Co, Ni, Cu and Ag can only take the form of metallic state. The oxidation-reduction cyclic reaction cannot at all occur in the reduction reaction box.

3.3 The Catalysis of Alloy Elements and the Mechanism of Carbon Dissolving Into Fe in Iron-Graphite Powder Metallurgy Compect During Sintering (T,Hong 1986).(the 1980s)

Sintered steel parts are made of iron powder, graphite powder, alloy powder after mixing and pressing sintering. How graphite is dissolved into iron and the effect of alloying elements are naturally the subject of research

The experiment result shows that:

1. Temperature, compects density, atmosphere, alloy elements, vacuum degree all affect the rate of carbon dissolute into Fe

2. The dissoluting rate of carbon into iron depends entirely on the carbon gasification reaction. The solid-solid reaction between Fe-C is almost zero. Carbon gasification reaction is the control step of carbon dissoluting rate,

3. Alloying elements W and K_2CO_3 appear catalytic active to accelerate carbon dissoluting rate, and the SiO_2 and S is poison. In particular great significance, the experimental result shows that the hydrogen appears catalytic active on the carbon gasiphication. Because the hydrogen is less electronegative than carbon. But it is a poisoner on the Fe catalyst. Because the it`s electronegativity is higher than Fe.

The results of the above three times experiments for long 30 years are in complete agreement with the ECDAM judgment. But the CRM was unable to explain the results of three times experiment study.

The CRM can neither illustrates that a catalyst, such as Fe, appears catalytic active in a wide temperature range, such as 600^0-1000^0c, on the FeO reduction, nor that many elements or compounds all appear catalytic active at the same temperature, such as 1000^0c. Because the cyclic generation-decomposition or oxidation-reduction chemical reaction equilibrium requires a strict reaction condition and the reaction equilibrium condition is all different.

If according to CRM, the catalyst must participate in chemical reactions, the result will appear many chemical reactions and intermediate compounds, and each said his own, it is dazzling, the research of catalysis mechanism will be leaded to bottomless abyss.

A familiar example is that housewives know that salt (NaCl) appears catalyze active for coal combustion, and CRM cannot explains the reason at all, because it is impossible for NaCl to decompose- generate repeatedly cyclic reactions in coal furnaces. Owing to NaCl is a very stable compound.

The author can cite many examples to illustrate that CRM is uncredible Because it's too cumbersome, Thus, I don't want to say any more.

Therefore, the author considers that the catalytic academia to improve CRM to "principle" is incredible. Using "TOF" to define catalyst activity and service life is obviously out of thin air. It is to fool people.

4. The ECDAM or EODRM`s Viewpoint

Back in the 1960s, based on the experimental results and theoretical analysis, the author points out that the CRM is not credible. Unfortunately, it didn't get attention.

The ECDAM were proposed in the 1970s. The ECDAM or EODRM contains three viewpoint.

4.1 There Are a Boundary Between the Catalyst and Poison

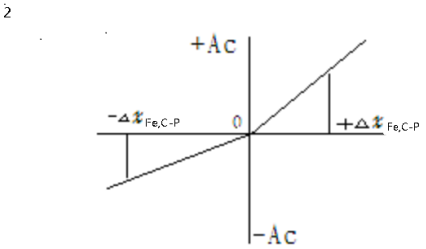

Fig. 1. Relationship between electronegativity differences and catalytic activities.

In figure 1, +Ac shows catalytic active, -Ac shows poisonousness, $+\Delta\chi_{Fe,C-P}$ shows the electronegativity difference, Footnotes Fe,C shows iron or carbon, P shows the catalyst, promoter, poison or support . For example;$+\Delta\chi_{Fe-P}$ Shows the difference between Fe-promoter,such as Al_2O_3,LiH etc.,. $+\Delta\chi_{C-P}$ shows the difference between C and catalyst, such as $BaCO_3$,Fe,Ni etc.cayalyst.

From Fig.1, the coordinate "0" point of the $\Delta\chi=0$ is a demarcation between the catalyst and the poison or inhibitor. For the carbon gasification reaction, this demarcation is the electronegativity value of the carbon, $\chi_c=2.55$. Any elements or compounds with electronegativities value greater than 2.55 should be a poison, such as P, S,Cl. Any elements or compounds less than 2.55 should be a catalyst, such as Fe, Co, Ni, Cu, Pt etc.. For iron - based ammonia synthesis catalyst, the demarcation is the electronegativity value of iron, $\chi_{Fe}=1.83$. Any elements or compounds with electronegativities greater than 1.83 should be a poison, such as C, N, P, S, Cl, Ni, Cu, etc .and any elements or compounds less than 1.83 should be a catalyst, such as alkali metal, alkaline earth metal. For the noble metal catalysts, the demarcation is the electronegativity value of noble metal, $\chi_{Pt}=2.28$.

On the element periodic table, for carbon gasification reaction,these elements at the right of carbon ,such as Alkali metal, Alkaline earth metal ,Transition group metal and Noble metal should be catalyst and those elements at the left of carbon ,such as P, S, Cl, F should be poison,

For iron - based ammonia synthesis catalyst, these elements at the right of Fe, such as Alkali metal, Alkaline earth metal should be catalyst and those elements at the left of Fe, such as, Cu, NI, C, P, S, Cl, F should be poison,

SiO_2, Al_2O_3, cordierite($2MgO\cdot 2Al_2O_3\cdot 5SiO_2$.) are all acidic materials, their electronegativity is greater than carbon, iron and Pt, Pd, Ru. Therefore, they are poison to iron Ni, nolbe metal catalyst and carbon.

A very interesting is that the Cu is a catalyst for carbon gasification reaction, but it becomes a poison in iron based ammonia synthesis catalyst, which had been proved to be true in production practice. Because the Cu is between iron and carbon on the element periodic table, its electronegative is less than carbon and more than iron. This result strongest proofs that ECDAM or EODRM is credible.

4.2 The Active Size of Catalyst Is Closely Related to the Electronegativity Value of Catalyst

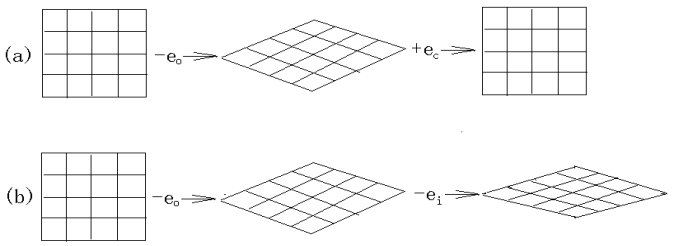

Scheme 1. The imaginative catalyzing and poisoning model.
(a). catalyzing. (b). poisoning.
$-e_o$, $-e_i$ ---electron is seized by oxygen or inhibitor.
$+e_c$ ---electron is donated by catalyst or promotor.

The scheme 1 (a) is a imagine figure of catalyzing .The scheme (b) is a imagine figure of poisoning.

From scheme 1(a), because the oxygen is more electronegative than carbon, $\chi_o > \chi_c$, the suspend electrons on the surface of the carbon must be snatched by the adsorbed oxygen, there was a contest for electrons between oxygen and carbon. the result is a deformation of electron orbitals in the carbon crystal or matrix, the crystal structure changes from square to diamond. If you are using chemical or physical methods to donate electrons to the carbon matrix, the contest electron situation is eased. The carbon bond breaking energy is reduced, CO is easy to generate. Therefore, the function of a catalyst, promotor or accelerator is to donate electrons to carbon or iron matrix, to revert a deformed electron orbital or crystal structure from a diamond to a square. Thus, catalysis is only an electron donate-accept cycle or electron orbital deformation-recovery cycle, without chemical reactions, let alone intermediate compounds. Therefore, any element or compound that can give electrons to carbon(or Fe) has catalyze active; otherwise, it is poison. the catalyze phenomenon is a physical phenomenon, not a chemical one, the catalyst does not participate in the chemical reaction, it is just contact, electron donate-accept, or electron orbital deformation- recovery.

From scheme 1（b), these elements or compounds that are higher electronegative than carbon will further take away the electrons of carbon, the electron orbits in carbon matrix is further deformation, the result is that the carbon bond breaking energy is elevated, the CO desorption is more difficult and therefore the reaction rate is slow down.

From Fig.1, The $+\Delta\chi$value higher is, the higher the catalytic active is. The-$\Delta\chi$ value higher is, the higher the poisonousness is. Therefore, whether carbon gasification reaction, iron based ammonia synthesis reaction or noble metal catalytic reaction, alkali metals and their salts are always the most active catalysts or promoters, while P, S and C are always poisons. Long-term production practice has proved this rule beyond doubt.

4.3 The Catalytic Actives of the Catalysts Are Closely Related to the Chemical States of the Catalyst

The catalytic activity of a catalyst is closely related to its chemical state. When the chemical states have changed, the electronegativity is different, and the catalytic activity is different.

The most compelling example is iron. The Iron has three chemical states, namely Fe, FeO and Fe_2O_3. For carbon gasification reaction, the experimental study proves that the Fe has catalytic active, but the FeO has no catalytic active, while the Fe_2O_3 becomes a poison at high temperature.

For salt catalysts, the catalytic activity varies with the cation and anion in salt.

When the anion is constant in the salt, the molecular electronegativity of salt increases with the increase of the electronegativity of cations in salt. Similarly, when the cation is constant, the molecular electronegativity of salts increases as the electronegativity of anions increases its catalytic activity changes with the increase of the electronegativity of the anion.

For carbon gasification reaction, for alkali metal carbonates, their relative catalytic active is $Cs_2CO_3 > K_2CO_3 > Na_2CO_3$. For alkaline earth metal carbonates, the their relation catalytic active is $BaCO_3 > SrCO_3 > CaCO_3 > MgCO_3$. For sodium ealts catalyst, the catalytic activity of Na_2CO_3 is greater than $NaNO_3$.Na_2SO_4, NaCl, Na_3PO_4. All these have been confirmed by experiments and production practice.

The research results of Chen Ping's team found that using LiH as a promotor for iron-based ammonia synthesis catalyst can greatly improve the catalytic activity of iron catalyst. According to EODRM, this is inevitable Because LiH is less electronegative than carbonate.

Different chemical states, there are different electronegativity, so there are different catalytic activity.

The core idea of EODRM is that the catalyst does not participate in chemical reactions, it's just “contact”, electron donate-accept cycle or electron obital deformation- recovery cycle, there is no intermediate. There are no generation-decomposition and oxidation-reduction cycles. Adsorption of the reactants results in the electron movement and distortion of electron orbitals. Desorption of the product results in electron orbital recovery. The electronegativity difference is what drives electrons to move. A continuous cycle of adsorption and desorption completes the production proces. The activity and selectivity of the catalyst depend on the energy level of the catalyst.

In modern times, electrocatalysis, photocatalysis, microwave catalysis and laser catalysis all are physical phenomena, which coincide with EODRM.

5. Using the EODRM to Judge Some Probrems Existing in Industrial Production

According to EODRM, it is found that there are many problems worthy of study in the field of research and production.

5.1 Alumina Poisoning in the Iron-Based Ammonia Synthesis Catalyst

Iron-based ammonia synthesis catalyst is considered by the academic community to be a classic catalyst. It is also the most studied catalyst. It has been used for more than 100 years. The chemical composition of the catalysts produced in

different countries is almost the same. It contains 2,5-3,0% Al_2O_3 which is called structural promoter. However, the experimental study of Aika.K (Aika, K., 1985) and H. G. Du (H, G, Du., 2002) have proved that alumina appears poison to carbon gasification reaction. The electronegativity of alumina is greater than that of carbon and iron, and it is poison to both carbon and iron catalysts. The production practice shows that C, P and S are poison to iron - based ammonia synthesis catalyst The greater the poison, the lower the permissible content. The permissible content of sulfur in ferro-based catalysts is <0.003%. The content of alumina is 1000 times that of sulfur, which is seriously poisons the catalytic activity of iron. The author considers that there are three high situations, such as high temperature, high pressure and high energy consumption, in synthetic ammonia production, which may be caused by improper use of alumina.

The physical and chemical properties of the catalyst simultaneously affect the catalytic activity of the catalyst, lead to the catalystic phenomenon is very complex. The advantages of alumina are high melting point, high strength, and especially high specific surface area, The favourable side of the physical properties covered up the unfavorable side of the chemical properties. It disturbs people's sight. In terms of chemistry property, Alumina should be a poison. Both adsorption and desorption increase energy consumption. Therefore, author considers that it is not appropriate to use alumina as a promotor for the synthesis of iron - based ammonia.

5.2 Carbon Support Poisoning in the Ruthenium Ammonia Synthesis Catalyst

The Ruthenium-based ammonia synthesis catalyst has been developed by British-American two companies cooperative study after for more than 10 years. The support material of the catalyst Ruthenium is the activated carbon after with high temperature graphitization.

According to EODRM, $\Delta\chi_{Ru\text{-}C}$=2.2-2.55=-0.35, The active carbon is poison to Ruthenium catalyst. The use of this support, must use more noble metals, the result is that the catalyst is very expensive.

5.3 Catalyst Support for Automobile Exhaust Purification

The most frequent type of catalytic converter in automobiles is the three-way catalyst (TWC) for stoichiometrically operated gasoline engines with an annual production of over 60x106units. The TWC systems contain Pt, Pd and Rh. The catalytic components are supported by a cordierite honeycomb monolith coated with high surface area γ-Al_2O_3. According to EODRM, the cordierite ($2MgO\text{-}2Al_2O_3\text{-}5SiO_2$) is acid material, it is poison to noble metal catalyst. In order to meet emission standards, more catalysts must be used.

In order to meet higher emission standards, The Germans have developed the Fe-Cr-Al metal coil honeycomb support. Compared with cordierite ceramic honeycomb carriers, At the same emission standard, noble metals loaded with metal coil honeycomb support are approximately 1/2 of the ceramic support. This clear indication that inappropriate support materials can waste a lot of noble metals catalyst. It is estimated that about 100 tons of noble metals are wasted each year.

The second support, i.e.γ-Al_2O_3 plating layer is also poison to noble metal catalyst. Fortunately, rare earth oxides are gradually replacing alumina.

The automobile catalyst is developing in a reasonable direction, which is in perfect agreement with EODRM's expectation.

The author believes that the powder metallurgy porous metal honeycomb support should be the most rational support.It's much better than the metal coil honeycomb. Large specific surface area and the plating layer is not easy to peel off, we did it and got good experimental results.Due to the lack of funds and other reasons, it is give up at halfway.

5.4 Diesel Exhaust Wall Flow Soot Filter

Diesel exhaust soot filter, at present, it still use the cordierite ceramic honeycomb wall flow filter. The cordierite is a poison to carbon gasification. The filter is too slow to regenerate, it cannot be used continuously. As a result, the americans used two filters, one job and the other to regenerate, with the result that prices are too expensive to promote.

The author suggests that the powder metallurgy honeycomb filter should be used in diesel soot filter, because the catalytic active of iron on carbon gasification reaction is much greater than that of noble metal.

5.5 Support Materials

Alumina and active carbon are mass produced as noble metal catalyst support in many factories around the world. High strength, high melting point, high specific surface area, high chemical stability, abundant resources and so on are the advantages of alumina, active carbon. However, according to EODRM, both are poison to Fe, Ni, Pt, Pd, Ru and so on catalysts, Unreasonable support will consume more noble metals. As far as automotive TWC catalysts are concerned, because of the use of unreasonable support materials. About 100 tons of noble metals are wasted every year.

From the internet, the support of fuel cell Platinum catalyst is made by carbon black or graphite at early stage. Later, the carbon nanotube is developed. The catalyst support of denitrification in power plant has adopted the cordierite ceramic honeycomb or stainless steel mesh. The author thinks that all are unreasonable.

6. Conclusion

1. Experimental and theoretical analysis show that the decomposition - generation, oxidation - reduction cyclic reaction does not exist, so it is unthinkable to improve CRM to “principle”, using “TOF” to represent catalyst active and service life is obviously out of nothing.

2. Catalysis is a physical phenomenon rather than a chemical one. The catalyst does not participate in the chemical reaction. It is only contact, electron cyclic donate-accept and electron orbital cyclic deformation- recovery. EODRM or ECDAM's three viewpoints are confirmed by experiment and production practice. The active and selectivity of the catalyst are closely related to the electronegativity or energy level of the catalyst.

3. According to EODRM, author considers that there are several unreasonable measures in industrial production. It is lead to serious economic losses.

References

Aika, K., Ohya, A., Ozaki, A., Inoue, Y., & Yasumoli, I. (1985). Support and promoter effect of Ruthenium catalyst, *Journal of Catalysis, 92*, 305-311. https://doi.org/10.1016/0021-9517(85)90265-9

Catalyst Handbook (*1982*). Beijing Chemical Industry Press, p.964.

Deutschmann, O., Knozinger, H., Kochloefl, K., & Turex, T. (2009). *Heteroegeneous Catalysis and Solid Catalysts*. Wiley-VCH Verlag GmhH & Co. KGaA, Weinheim.

Du, H. G., & Yang, J. H. (2002). Catalytic effect of mineral impurities on dissolution loss reaction of coke in blast furnace. *iron smelting, 21*(4), 22-24.

Hong, T., Jin, J. M., & Wu, J. Q. (1986). *Study on the dissolution mechanism of carbon in the Fe-C compect at sintering.* Masters thesis. Shanghai Research Institute of Materials.

Jin, J. M. (1966). *Carburizing effect of carbonate in solid carburizer, proceedings of the first national annual conference on heat treatment*, Chinese society of mechanical engineering, 1963, Beijing machine press, 389.

Jin, J. M., Jia, G. Y., Reng, J. Y., & Zhu, Z. Z. (1982). *Mechanism of catalysis and poison of mineral impurities in carbon on carbon reduced ferric oxide,* National Conference on Metallic Powders.

Mckee D. W. (1981). Catalyzed Gasification Reactions (*in Chemistry and Physics of Carbon*). Marcel Dekker. New York.

Ragatz, R. A., & Kowalke, L. O. (1931). *Metal & Alloy*, *2*, 343.

International Journal of Chemistry; Vol. 14, No. 1; 2022
ISSN 1916-9698 E-ISSN 1916-9701
Published by Canadian Center of Science and Education

Steady State Heat Transport by Microbubble Dispersions Mediating Convection With Phase Change Dynamics

William B Zimmerman

Correspondence: William B Zimmerman, Mappin Street, Shefield S1 3JD, UK.

Received: November 7, 2021 Accepted: March 25, 2022 Online Published: April 14, 2022

doi:10.5539/ijc.v14n1p30 URL: https://doi.org/10.5539/ijc.v14n1p30

Abstract

A new theory for additional heat transfer convected by a dispersed phase of microbubbles was posited recently. An additional convection term in the heat transport equation reflects the latent heat of vapor of the liquid carried by the microbubbles from hot zones that vaporize more liquid to cold zones where condensation releases the latent heat. This theory was shown to be consistent with analysis of observations of freezing times measured by in the original Mpemba effect study, by inferring heat transfer coefficients fitted by Newton's law of cooling. In this paper, the scaling analysis, leading to the proposition that the additional heat flux is proportional to the phase fraction of microbubbles, is tested by steady state solutions of the canonical hot wall / cold wall buoyant convection problem. For phase fractions 0.02 and 0.1, the maximum ratio of additional Nusselt number emergent is five, occurring in the microfluidic regime. Increasing the characteristic length of the domain maintains the monotonicity of the increase in additional Nusselt number ratio over the case of no microbubbles present. The additional heat transfer due to the microbubble dispersion, ranging from 5-50%, is found to be nearly proportional to the microbubble phase fraction for the range of 0.02 to 0.2. However, larger characteristic lengths introduce insufficient heat flux from the hot wall to maintain a "driven cavity" flow structure, so that the steady state structure that emerges is a stable stratification with thin boundary layers near the hot and cold walls, with weak shear flow convection. The stable stratification resultant at higher characteristic lengths suppresses the additional heat flux due to microbubble mediation, but only moderately deviating from proportionality.

Keywords: phase change energy storage, microbubbles, direct contact heat transfer, evaporators, condensers.

1. Introduction

Microbubbles are famous for increasing mass transfer, especially useful in fermentation processes (see Gilmour and Zimmerman (2020)), yet do not have the same efficacy at heat transfer due to a complication. Generally, the solvents that are utilized where heat transfer is desirable are volatile. This additional heat transferred by hot microbubbles is partitioned between sensible heat transfer to the liquid or to provide the latent heat for evaporation of the solvent. Zimmerman et al. (2013) exploited this possibility by observing that microbubbles achieve internal homogeneity and equilibration with their gas-liquid interface within a few milliseconds of contact time from injection. By arranging that the liquid layer height limits the contact time to within that regime of maximum vaporization, without any time for sensible heat transfer, thermal *non-equilibrium* can be maintained with much higher vaporization rates than conventional boiling.

Isothermal distillation is possible, which is important for thermally unstable chemical composition of the solvent or suspended materials, such as microbes, that are thermally sensitive. Many other uses in chemical and biological processing are reviewed in Gilmour and Zimmerman (2020). The target in this paper is direct contact heaters / condensers such as those reviewed by Ribeiro and Lage (2004,2005), but with the novel introduction of microbubbles replacing conventional fine bubbles.

However, Zimmerman (2021) posited that most contacting configurations for microbubbles would achieve vapor-liquid equilibria as the contact time would naturally exceed those few milliseconds. The direct contact condenser has potential for exploitation of heat transfer by microbubbles. That paper posited an additional benefit to the obvious high gas-liquid interfacial area (therefore potential high interfacial heat transfer) and the high bubble flux (potentially hectares per cubic meter per second). Microbubbles that pass through a hot zone or near a heated surface will quickly vaporize, within milliseconds, to the saturation pressure, while absorbing the latent heat. Similarly, as they approach a cold surface or pass through a cold zone, they will condense the vapor, and release the associate latent heat. Zimmerman (2021) derived, from control volume analysis, an additional convection term for the heat transport equation.

Using scaling analysis, it was deduced that the additional convective term would introduce an additional heat flux that is proportional to the microbubble phase fraction, as well as an estimate of the constant of proportionality. The hypothesis

was supported by analyzing the time to freezing transient experiments of Mpemba and Osborne (1969) with boiled water. The heating rates were found to correlate linearly with the inverse solubility of oxygen at the initial temperature, reflecting that the microbubble phase had equilibrated with the dissolved gas composition in the liquid. The purpose of this paper is to test, for steady state solutions to the canonical hot wall/cold wall problem, called heat transfer in a slot with differential side wall heating, detailed in the classic book of Turner (1979), whether the scaling analysis of the modified heat transport equation holds, i.e. the additional heat flux is proportional to the microbubble phase fraction. Of course, the classical hot wall / cold wall problem is treated here with a microbubble dispersion in water, rather than a simple fluid.

Microbubbles have only been used in heat transfer dynamics since the seminal study of Zimmerman (2013), with the intention of minimizing heat transfer effects and maximizing solvent evaporation or binary distillation in sequels. In this paper, the intention is to characterize the level of additional heat transfer in water due to dispersions of air microbubbles, by exploiting phase change—evaporation in hot liquid near the hot wall, condensation in cold liquid near the cold wall.

The paper is organized as follows. In Section 2, the modifications to the hot wall / cold wall canonical problem are set out in the governing equations, following Zimmerman (2021), and subsequently simulated using Galerkin finite element methods with a spatially resolved mesh, for a wide range of domain sizes in the laminar flow regime. In Section 3, the results are represented and discussed. In Section 4, the conclusions are drawn.

2. Methodology: Buoyant Convection Modelling

Coupling momentum transport and heat transport is a well studied area of transport phenomena. The governing equations are

$$\rho\frac{\partial \mathbf{u}}{\partial t}+\mathbf{u}\cdot\nabla\mathbf{u}=-\nabla p+\mu\nabla^2\mathbf{u}+\rho\boldsymbol{g}$$
$$\frac{\partial \rho}{\partial t}+\nabla\cdot\rho\mathbf{u}=0 \qquad \rho c_p\left(\frac{\partial T}{\partial t}+\mathbf{u}\cdot\nabla T\right)=\kappa\nabla^2 T \tag{1}$$

Here, the dependent variables are described as follows: $\boldsymbol{u}$ is the velocity vector, p is the pressure, and T is the temperature. The independent variables are spatial coordinates (implied in the differential operators) and time t. Everything else is a parameter (μ, $\rho(T)$, c_p, κ, $\boldsymbol{g}$) with fixed value once the fluid and venue are selected. If there is no imposed moving boundary or pressure gradient, then the motion is created by temperature gradients. Zimmerman (2021) proposed, from control volume analysis of cycling the evaporation and condensation dynamics, a modified heat transport equation for a dispersed microbubble phase in volatile liquid:

$$\rho c_p\frac{DT}{Dt}=\kappa\nabla^2 T-\phi\nabla\cdot\mathbf{u}F=\kappa\nabla^2 T-\phi F\nabla\cdot\mathbf{u}-\phi\mathbf{u}\cdot\left(F'\nabla T\right) \tag{2}$$

There are two additional terms once the extra divergence term is expanded. ϕ is the volume or phase fraction of microbubbles. $F(T)$ is a state function which has the connotation of the additional energy potential that is convected by the flow representing the latent heat of vaporization for the amount of vapor (of the volatile liquid) in the dispersed microbubble phase, per unit volume:

$$F\left(T\right)=c^*\left(T\right)\Delta H_V\left(T\right)=\frac{p^*\left(T\right)}{RT}\Delta H_V\left(T\right) \tag{3}$$

$p^*\left(T\right)$ is the saturation pressure of the liquid at the absolute temperature T. For simple volatile liquids, the saturation pressure is tabulated and well correlated by the Antoine equation. R is the gas constant.{ XE "buoyant convection" } $\Delta H_V\left(T\right)$ is the latent heat of vaporization, also commonly tabulated for volatile liquids, and commonly correlated by polynomial fit.

Equations (1) and (2) are commonly simplified by the Boussinesq approximation for buoyant convection, and non-dimensionalized by adopting scalings for length (h, the characteristic length scale), time ($\frac{\rho_0 c_{p,0} h^2}{\kappa}$), and velocity ($\frac{\mu_0}{\rho_0 h}$). With these scalings, the system of equations (1) modified by (2) becomes:

$$\frac{\partial \mathbf{u}}{\partial t} + \mathbf{u}\cdot\nabla\mathbf{u} = -\nabla p + \mathrm{Pr}(T)\nabla^2\mathbf{u} - \mathrm{Gr}\hat{\rho}(T)\hat{\boldsymbol{k}}$$
$$\nabla\cdot\mathbf{u} = 0$$
$$\frac{DT}{Dt} = \nabla^2 T - \phi \mathrm{N}_{\mathrm{Mpemba}}(T)\mathbf{u}\cdot\nabla T \qquad (4)$$

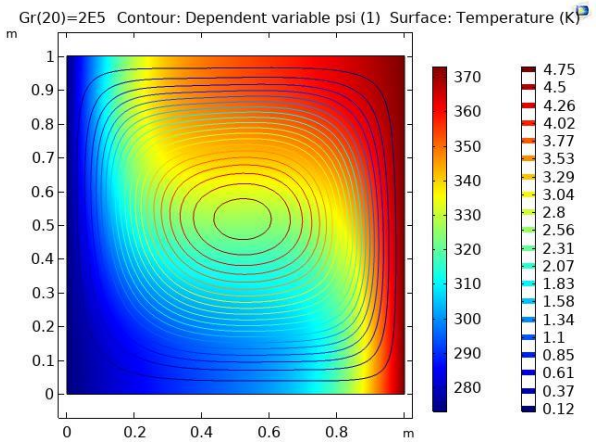

Figure 1. Streamfunction and temperature profile for the steady state solution to (4) for water with Gr=2□10^5 (h=1.43mm) in the hot wall-cold wall problem on a unit square. No microbubble phase, i.e. f = 0

The PDE engine used is Comsol Multiphysics v. 5.6. An exemplar solution for Gr=2□10^5 with grid convergence found by using an extremely fine mesh with 26254 elements (236064 degrees of freedom) is shown in Figure 1. A mesh resolution study showed convergence to the at least three significant figures in the Nusselt number – the emergent global feature characterizing heat flux across either the hot or cold walls.

As illustrated in Zimmerman (2006), such steady state buoyant convection problems must be solved by parametric continuation in the nonlinearity parameter Gr. For a fixed liquid, such as water, Gr has the interpretation of being controllable by changing the size of the square. For instance, with water, Gr=10^{13} corresponds to a side of h = 52.7cm for the square domain. Typically, the parametric continuation for (4)-(5) takes 200~300 logarithmic steps to achieve Gr~10^{13}. Because of the cubic dependence on h in Gr, for most of the parametric continuation, the hot wall-cold wall domain is very small, achieving microfluidic scales around Gr~$10^{4\text{-}6}$. Figure 1 is representative of this range.

The Prandtl number for water can be found from the NIST database of liquid properties and represented as a cubic spline interpolation function. The steady state of the model equations (4) and (5) are solved by the Galerkin finite element method for the hot wall-cold wall problem, where the hot wall is held at fixed temperature $T_1 = 373K$ and cold wall $T_1 = 273K$, on the unit square with upper and lower boundaries as no flux surfaces. This is described in section 3.2 of Zimmerman (2006) for the simpler convection situation with constant Prandtl number for water and vanishing N_{Mpemba}.

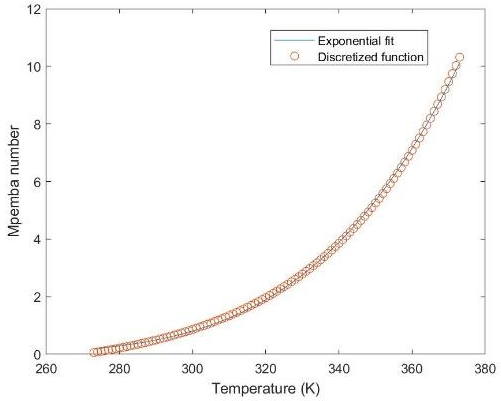

Figure 2. $N_{Mpemba} = \dfrac{F'(T)}{\rho_0 c_{p,0}}$ plotted against absolute temperature for water, along with the exponential fit, where the "0" reference state are the properties of water at 20°C. Right: Streamfunction and temperature profile for the steady state solution to (4) for water with *Gr*=2□10^5 (h=1.43mm) in the hot wall-cold wall problem on a unit square. No microbubble phase, i.e. $\phi = 0$

$\hat{\boldsymbol{k}}$ is the unit vector in the positive (antiparallel gravity) direction. $\hat{\rho}(T)$ is the specific gravity of water, taken from Zimmerman (2006) as an interpolation function via cubic splines. There are three dimensionless functions / parameters governing the dynamic similarity**{** XE "dynamical similarity" **}** of the problem: (i) the Mpemba number is defined in the caption of Figure 1, expressing the novel component of this buoyant convection analysis due to transport of the latent heat via the microbubble phase; (ii) the Prandtl number**{** XE "Prandtl number" **}** that is a function of the fluid and temperature; (iii) the buoyancy group **{** XE "Rayleigh number" **}**that gives the relative importance of gravitation to dissipative mechanisms:

$$\mathrm{Pr}(T) = \frac{\mu(T) c_p(T)}{\kappa(T)}; \quad \mathrm{Gr} = \frac{\rho_0^2 c_{p,0} g h^3}{\mu_0 \kappa_0} = \frac{g h^3}{\nu_0 \alpha_0} \tag{5}$$

3. Results and Discussion

Figure 1 and Figure 3 present a set of steady state solutions for streamlines and temperature profiles for parametric series of gravity group Gr = (2□10^6, 2□10^6, 2□10^9, 2□10^{11}, 2□10^{13}) which span the equivalent side length of millimeter to half meter scale. This parametric series is a subset of the 200-300 solutions swept so that convergence is found for each subsequent value via parametric continuation. Of course, the reason parametric continuation is necessary is that gravity group Gr is a proxy for the level of nonlinearity in the dynamics. Highly nonlinear solutions are difficult to find without starting nearby in the basin of attraction for the solution via the multidimensional Newton's method employed for iterative convergence by the PDE engine.

Figure 1 has the "bullseye" shaped streamlines consistent with the canonical lid driven cavity problem (see Zimmerman, 1998) and a temperature profile moderately different from the linear temperature gradient of pure conduction. The hot (red) regime has started to extend over the top, while the cold (blue) regime is spreading over the bottom of the domain. On average, the vertical profile is now density stably stratified, i.e. hot less dense water over cold more dense water. Figure 3(top) continues this development with further spreading of the hot zone at the top and the cold zone at the bottom, as the streamlines become asymmetric. Figure 3(second frame) shows that as Gr increases, the development of the stable stratification becomes dominant. The hot wall has a very thin boundary layer that is hot liquid, practically partitioned from the main stratified shear flow by an interposed cold layer. That interposed cold layer (and the squashed hot, near wall liquid layer) become thinner and thinner at the higher Gr group values in the bottom panels of Figure 3. By Gr ~ 10^{13}, the stratification seems nearly total, with barely visible boundary layers near the hot and cold walls. Simulation

above Gr ~ 10^{13}, requires refining the mesh further, especially near the hot and cold walls to resolve the thinning boundary layers, and re-starting parametric continuation from very low Gr values – computationally expensive. Although these four simulations were conducted with $\phi = 0.02$, it should be noted that all four microbubble phase fractions, including $\phi = 0$, result in visually indistinguishable flow and temperature profiles.

To distinguish among the heat transfer dynamics for variation of microbubble phase fraction, some other metric than the steady state temperature profile is necessary. The common metric is the Nusselt number, which has the interpretation of the total heat transfer across a boundary relative to the conductive heat transfer. At steady state, since there is no accumulation of heat in the domain, the total heat transfer across all boundaries nets to zero. As the upper and lower boundaries are no flux boundaries, the choice to compute the Nusselt number is arbitrary between the hot and the cold wall. For convenience we take the cold wall. The Nusselt number is then defined, as applied to this geometry, is

$$Nu = \frac{\int_{\partial B} q_{tot} dS}{\int_{\partial B} q_{cond} dS} = \frac{\int_0^1 \hat{n} \cdot \nabla T dy}{\int_0^1 \Delta T dy} = \frac{1}{T_1 - T_0} \int_0^1 \frac{\partial T}{\partial x} dy \tag{6}$$

Figure 4 is the log-log plot of Nusselt number Nu against the gravity group Gr for four different values microbubble phase fraction $\phi = 0$, 0.02, 0.1, and 0.2. It is clear that the heat transfer rate monotonically increases with microbubble phase fraction, as the curves are parallel, but too close to discern the variation with ϕ. This is better achieved by a relative comparison, which uses the ratio of the Nusselt number in the presence of microbubbles to the Nusselt number in absence of microbubbles, Figure 5.

Figure 5 clarifies that the predicted scaling of the additional microbubble mediated heat flux is nearly proportional to the microbubble phase fraction for the maximum increase, which occurs in the microfluidic regime with Gr~10^6. Thereafter, it is clear from the temperature / streamfunction profiles in Figure 3 that the fluid becomes density stratified, with the strength of stratification increasing as Gr~10^{11}. It is not clear from the profiles whether or not the stratification strength continues to rise above this level, as the profiles are only modestly different. The monotonic response to ϕ is apparent as the curves are non-intersecting and parallel in behavior. The maximum increases are ~ 5%, 25%, and 45% which are close to linearly related to ϕ.

Of course, there is a rationale for why the stratification forms and then grows stronger. It is well known that in microfluidic transport, the surface area to volume of the fluid duct is very large. Zimmerman (1999) analyzed the formation of stable stratification in solutions where the density is a strong function of solute concentration, including ideal solutions as well as non-ideal, even non-monotonic mixing rules. In scenarios where stirring is introduced, if the stirring is sufficiently weak, then stable stratifications form that minimize the integrated density within the domain.

(a)

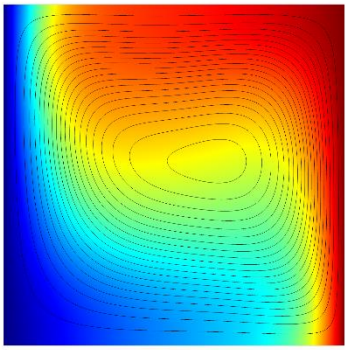

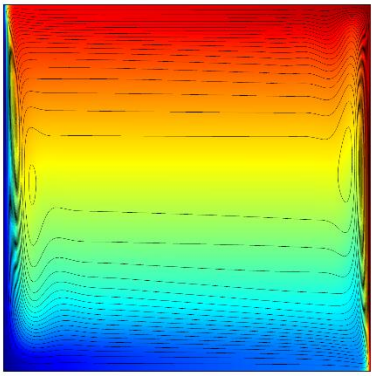

(b)

(c)

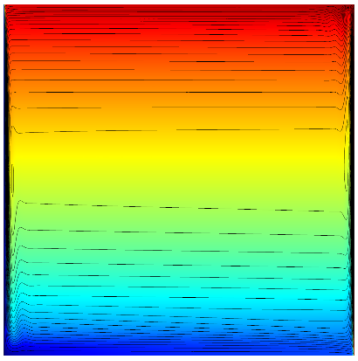

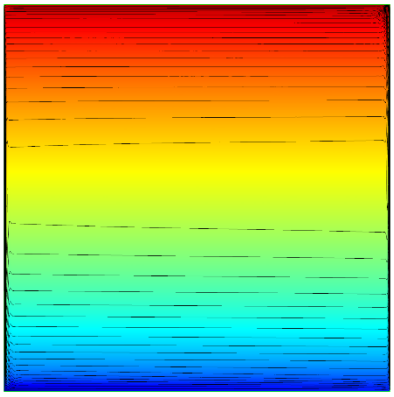

(d)

Figure 3. Steady state solutions with a parametric series in gravity group (a) – (d) (Gr =2□10^6, 2□10^9, 2□10^{11}, 2□10^{13}) which can be thought of as simply changing the length of the side to (h = 3.1mm, 3.1cm, 14.3cm, 52.7cm) with $\phi = 0.02$. All four values of $\phi = 0$, 0.02, 0.1, and 0.2 that were trialled have visually identical temperature and streamfunction profiles. Red represents T=373K and dark blue T=273K. The streamlines are twenty uniformly spaced level sets of streamfunction from zero (the walls) to the maximum value (different in each case).

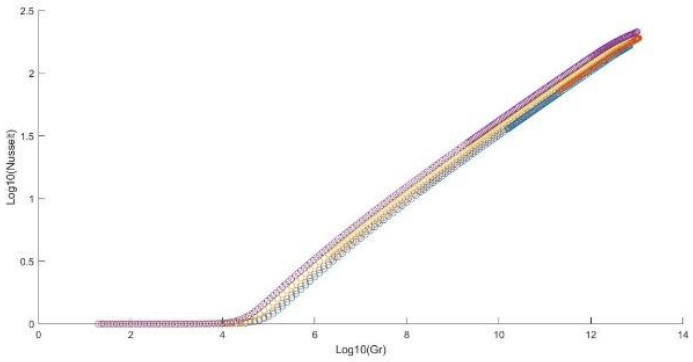

Figure 4. Common logarithm of the Nusselt number plotted against the common logarithm of the gravity group Gr for four different values microbubble phase fraction $\phi = 0$, 0.02, 0.1, and 0.2. The lowest curve is $\phi = 0$, with Nusselt number monotonically increasing with ϕ. Because the log-log plot diminishes the distinguishability of small percentage differences in values, only this monotonic increase is a discernible trend. It should be noted that grid dependency becomes an issue for Gr>10^{12}, as the boundary layers near the hot and cold wall become very thin.

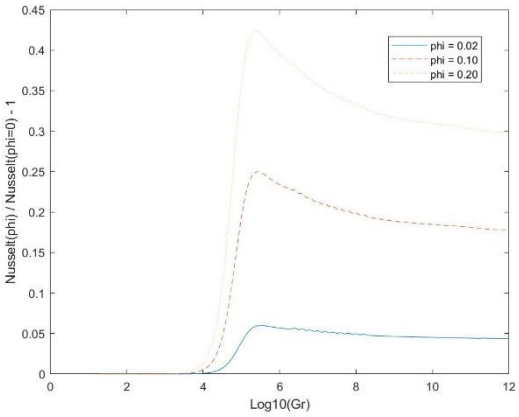

Figure 5. Fractional change in the ratio of Nusselt numbers for ϕ relative to $\phi = 0$, plotted against the common logarithm of the gravity group Gr for three different values microbubble phase fraction $\phi = 0.02$, 0.1, and 0.2. The lowest curve is $\phi = 0.02$, with Nusselt number monotonically increasing with ϕ. From the microfluidic scale of Gr>~10^4, the additional convective flux due to the microbubble phase rises rapidly, peaking in the millimeter scale Gr>~10^6, before plateauing with a minor decay over the next six decades, before grid dependency becomes an issue.

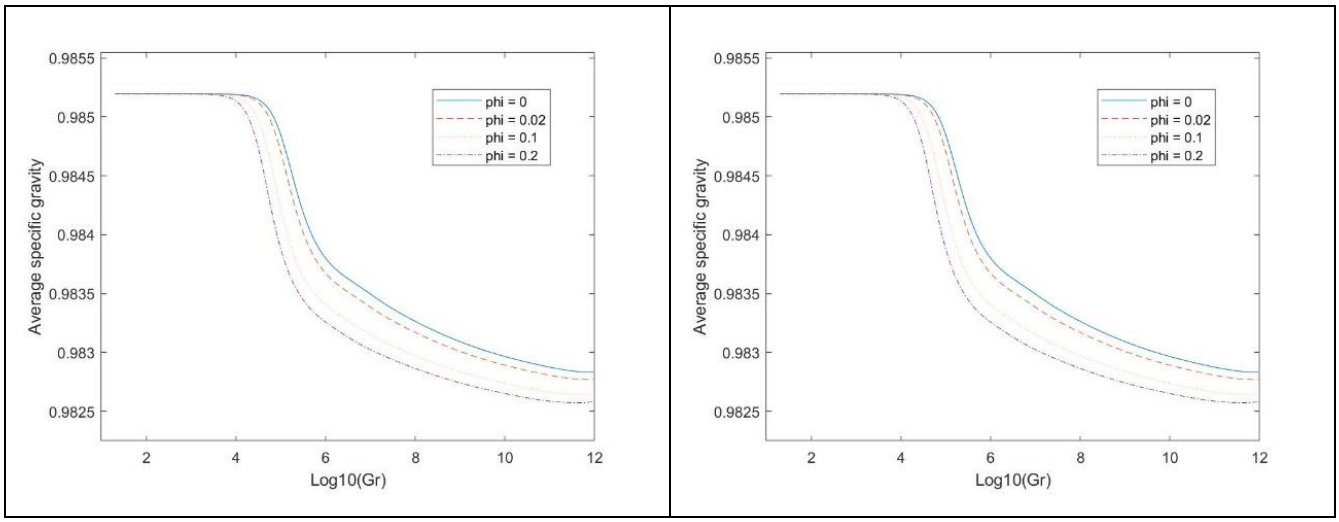

Figure 6. (top) Volume-averaged specific density with Gr variation for selected ϕ values. (bottom) Volume-averaged temperature with Gr variation for selected ϕ values

As the stirring rate increases, the kinetic energy can lift the solute so that a steady solution achieves greater than the minimum integrated density. In this heat transfer analogue, the stirring kinetic energy is injected proportional to the surface area of the hold wall, hence why the Nusselt number rises with increasing Gr. However, the total mass rises proportional to the volume of the duct. So eventually, the stirring force is insufficient to lift the mass to higher potential energy as Gr rises, so the temperature field (solute) is arranged to minimize the energy integral, i.e. the stable stratification suppresses convective mixing / heat transport.

Figure 6 makes clear that increasing ϕ increases the strength of the stable stratification as it achieves lower average specific gravity – starts the formation of the stable stratification at lower Gr values and accelerates the stabilization with increasing ϕ and Gr. This is a direct consequence of better heat transfer, as the bottom frame of Figure 6 illustrates. Average temperature also rises with increasing ϕ and Gr. The microfluidic range, Gr ~$10^{4\text{-}6}$, shows exponential increase in strength of the stable stratification / average temperature, before both

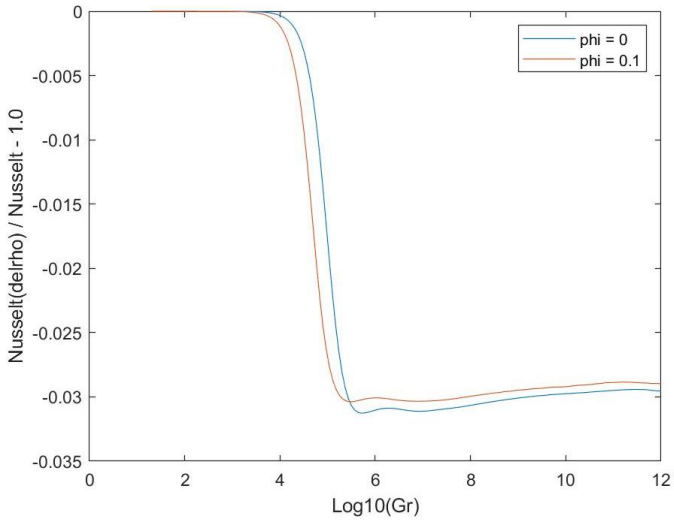

Figure 7. Modifying the specific gravity for the air saturation of water influence according to the correlation of Watanabe and Iizuka (1985). Fractional change in the ratio of Nusselt numbers for fixed ϕ , plotted against the common logarithm of the gravity group Gr for three different values microbubble phase fraction $\phi = 0.0$, and 0.1. The lower curve is $\phi = 0$.

level off in the millimeter scale, with a constant plateau achieved in the meter scale. Zimmerman and Rees (2007) studied the double diffusion problem with initial stable stratification, but strong sidewall heating. In the transient situation, the stable stratification can be overturned by sufficiently strong heating, as the stratification strength depends on solute distribution.

One area of speculation is the role of the change in specific gravity of water due to air saturation. Watanabe and Iizuka (1985) carefully measured the change in specific gravity of water with saturated, dissolved air, as a function of water temperature. Their cubic polynomial correlation was used to modify $\hat{\rho}(T)$ for temperatures below 53°C, the neutral change temperature (they measured between 0 and 45°C). Oxygen and nitrogen solubility fall off dramatically above 53°C, so there is negligible contribution above this level. This translates into a piecewise cubic polynomial modifying equations (4).

$$\Delta\hat{\rho}(T) = \begin{cases} -5.252\times10^{-3} + 1.474\times10^{-4}\mathrm{T} \\ -3.0689\times10^{-6}\mathrm{T}^2 \\ +4.0688\times10^{-8}\mathrm{T}^3, \quad \mathrm{T} < 326\mathrm{K} \\ 0, \qquad\qquad\qquad\quad \mathrm{T} > 326\mathrm{K} \end{cases} \tag{7}$$

As the average temperature in the domain typically varies between 323K and 332K (cf. Figure 6) with increasing Gr in the range explored, the average effect of air saturation on changing density is typically around -6□10^{-4}. However, it is the spatially distributed effect that is of concern in the free convection dynamics explored here. Figure 7 illustrates that the maximum change in Nusselt number due to the density change from air-saturation is approximately a 3% decrease, which plateaus above Gr~10^6. However, as found for all ϕ values, the change with Nusselt number is indistinguishable visually. Compare Figure 8 with Figure 5 to see that there is no discernible *relative* difference to the effect of microbubble phase fraction ϕ. Zimmerman (2021) argues that the thermal diffusivity increases with uniformly dispersed ϕ according to common mixing rules, but as in all length scales of interest, convection dominates the contribution to the Nusselt number, negligible effect will arise from considering the thermal diffusivity dependence on microbubble phase fraction.

This is perhaps the largest buoyancy effect that is unaccounted for in this model – the effect of the two phase density on the phase fraction of microbubbles. However, the assumption underpinning the treatment in this paper is that microbubble phase fraction is uniformly distributed spatially. Undoubtedly, for any real steady state convection with dispersed microbubbles, the volume increases in warm zones and decreases in cold zones due to the vaporization and condensation, respectively. Treating these two contributions to density variation would require adding the heat transport (and consequential changes to mass transport) effects of (4) to the bubbly flow and mass transport model of Al-Mashhadani et

al. (2015) – beyond the scope of this paper.

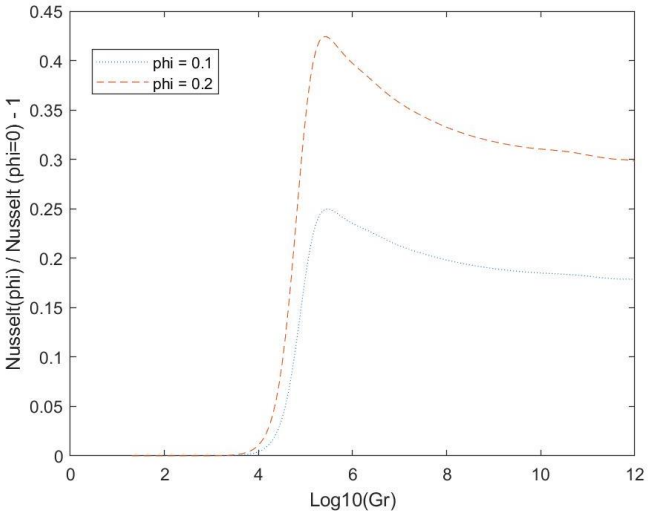

Figure 8. Modifying the specific gravity for the air saturation of water influence according to the correlation of Watanabe and Iizuka (1985). Fractional change in the ratio of Nusselt numbers for ϕ relative to $\phi = 0$, plotted against the common logarithm of the gravity group Gr for three different values microbubble phase fraction $\phi = 0.1$, and 0.2. The lower curve is $\phi = 0.1$.

4. Conclusions

The hypothesis of proportionality between the additional heat transfer and the microbubble phase fraction holds within the microfluidic range of flow cells, where convection dominates is proposed in Zimmerman (2021) as due to scaling analysis. The prediction is found to hold only closely in the microfluidic regime of steady state buoyant convection. Monotonic increase but less than proportionality holds with larger flow cell characteristic lengths where stable stratification forms under steady state conditions. The formation of the stable stratification dominates the heat transfer dynamics, which could be alleviated by continuous microbubble injection and removal, such as in the airlift loop open system, frequently adopted for bioreactors (Al-Mashhadani et al. (2015)).

Nonetheless, the predicted levels of additional heat transfer with the presence of a microbubble dispersion of air in water vary from 5-50% with the phase fraction of 0.02 to 0.2. These additional heat transfer rate are consistent with the decreases in the time to freezing observed by Mpemba and Osborne (1969). If they hold in other common heat transfer configurations such as bioreactors, heat pumps, and direct contact evaporators and condensers, substantial efficiency increases can be achieved with slight increase in processing costs due to injection of long lived microbubble dispersions.

NOMENCLATURE

c_p	[J/kgK]	Heat capacity at constant pressure
c^*	[mol/m^3]	Saturation concentration
F	[J/m^3]	Latent heat density within dispersed microbubbles
g,$\boldsymbol{g}$	[m/s^2]	Gravitational acceleration constant/vector
h	[m]	Side length for 2-D square domain
Gr	[-]	Non-dimensional gravity group parameter
N_{Mpemba}	[-]	Dimensionless function of temperature
Nu	[-]	Non-dimensional ratio of total to conductive heat flux
p	[N/m^2]	Pressure scalar – dimensional or dimensionless (context)
P^*	[N/m^2]	Saturation pressure
Pr	[-]	Prandtl number (temperature dependent)
q	[W/m^2]	Heat flux
R	[J/molK]	Gas constant
T	[K]	Temperature – dimensional or dimensionless (context)
t	[s]	Time coordinate
$\mathbf{u}$	[m/s]	Velocity – dimensional or dimensionless (context)
x	[m]	Coordinate – dimensional or dimensionless (context)
z	[m]	Coordinate – dimensional or dimensionless (context)
Special characters		
α	[m^2/s]	Thermal diffusivity
ϕ	[-]	Microbubble phase fraction
κ	[W/mK]	Thermal conductivity
$\hat{\boldsymbol{k}}$	[-]	Unit vector anti-parallel to gravity
$\hat{\boldsymbol{n}}$	[-]	Outward pointing unit normal to the domain
ρ	[kg/m^3]	Density
$\hat{\rho}$	[-]	Specific gravity (temperature dependent)
μ	[Pa·s]	Dynamic viscosity
Subscripts		
0		Ambient or reference state

Acknowledgments

The author acknowledges the Engineering and Physical Sciences Research Council (EPSRC) for supporting this work financially (Grant no. EP/K001329/1, EP/N011511/1 and EP/S031421/1). This work was presented as part of a keynote address at the 15th International Conference on Heat Transfer, Fluid Mechanics, and Thermodynamics (HEFAT-15). A version was published as part of the conference proceedings.

References

Al-Mashhadani, M. K. H., Wilkinson, S. J., & Zimmerman, W. B. (2015). Airlift bioreactor for biological applications with microbubble mediated transport processes. *Chem. Eng. Science, 137*, 243-253. https://doi.org/10.1016/j.ces.2015.06.032

Gilmour, D. J., & Zimmerman, W. B. (2020). Microbubble Intensification of Bioprocessing. *Advances in Microbial Physiology*, *77*, 1-35. https://doi.org/10.1016/bs.ampbs.2020.07.001

Mpemba, E. B., & Osborne, D. G. (1969). Cool? *Phys. Educ., 4,*172-175. https://doi.org/10.1088/0031-9120/4/3/312

Ribeiro, C. P., & Lage, L. P. C. (2004). Experimental study on bubble size distributions in a direct-contact evaporator. *Braz. J. Chem. Eng., 21*(1), 69-81. https://doi.org/10.1590/S0104-66322004000100008

Ribeiro, C. P., & Lage, L. P. C. (2005). Gas-Liquid Direct-Contact Evaporation: A Review. *Chemical Engineering and Technology*, *28*(10), 1081-1107. https://doi.org/10.1002/ceat.200500169

Turner, J. S. (1979). Buoyancy effects in fluids. Cambridge University Press, Cambridge.

Watanabe, H., & Iizuka, K. (1985). The Influence of Dissolved Gases on the Density of Water. *Metrologia, 21*, 19. https://doi.org/10.1088/0026-1394/21/1/005

Zimmerman, W. B. J. (2006). Multiphysics Modelling with Finite Element Methods, World Scientific Series on Stability. *Vibration and Control of Systems, 18*, Singapore. https://doi.org/10.1142/6141

Zimmerman, W. B. (1998). The effect of chemical equilibrium on the formation of stable stratification. *Appl. Sci. Res., 59,* 298-298. https://doi.org/10.1023/A:1001147808516

Zimmerman, W. B., & Rees J.M. (2007). Rollover instability due to double diffusion in a stably stratified cylindrical tank. *Physics of Fluids, 19,* 123604. https://doi.org/10.1063/1.2827488

Zimmerman, W. B., Al-Mashhadani, M. K. H., & Bandulasena, H. C. H. (2013). Evaporation dynamics of microbubbles. *Chemical Engineering Science*, *101*, 865-877. https://doi.org/10.1016/j.ces.2013.05.026

Zimmerman, W. B. (2021). Towards a microbubble condenser: Dispersed microbubble mediation of additional heat transfer in aqueous solutions due to phase change dynamics in airlift vessels. *Chemical Engineering Science, 238,* 116618. https://doi.org/10.1016/j.ces.2021.116618

International Journal of Chemistry; Vol. 14, No. 1; 2022
ISSN 1916-9698 E-ISSN 1916-9701
Published by Canadian Center of Science and Education

Levels of Heavy Metals Contamination (As, Cd, Hg, Pb) in Some Human Consumption Water Sources in Agbangnizoun and Za-Kpota Town Halls, Southern Benin

Emmanuel Azokpota[1,2], Alassane Youssao Abdou Karim[1,2], Alphonse Sako Avocefohoun[2], Abdoul Kader Alassane Moussa[2], Constant Adandedjan[3], Virgile Ahyi[4], Jean Christian Alowanou[2] , Julien Adounkpe[1], Daouda Mama[1], Dominique Sohounhloue[2]

[1]Laboratory of Applied Hydrology (LHA)/University of Abomey - Calavi, Bénin

[2]Laboratory for Study and Research in Applied Chemistry (LERCA) / University of Abomey-Calavi, 01 BP 2009 Cotonou, Bénin

[3]Water and Food Quality Control Laboratory, BP 01-882 Cotonou, Bénin

[4]Inter-Regional University of Industrial Engineering, Biotechnology and Applied Sciences (IRGIB-Africa University

Correspondence: Alassane Youssao Abdou Karim, Laboratory of Applied Hydrology (LHA)/University of Abomey - Calavi, Bénin; Laboratory for Study and Research in Applied Chemistry (LERCA) / University of Abomey-Calavi, 01 BP 2009 Cotonou, Bénin.

Received: April 17, 2022 Accepted: May 20, 2022 Online Published: May 23, 2022

doi:10.5539/ijc.v14n1p41 URL: https://doi.org/10.5539/ijc.v14n1p41

Abstract

In the current decades, the increasing presence of metallic contaminants in water for human consumption has become a major public health concern. This concern is even more pronounced in rural areas such as in the Town Halls of Agbangnizoun and Za-Kpota where the majority of households use surface water, wells and tanks to satisfy their daily drinking water needs, without any prior treatment, due to the low level of access to drinking water supplied by the State. This study aims at assessing the levels of contamination of these resources in mercury (Hg), cadmium (Cd), lead (Pb) and arsenic (As). The mercury was determined using the cold vapor technique by the Direct Mercury Analyzer (DMA-80) while lead and cadmium were analyzed by molecular absorption spectrophotometry by the DR 3900. The Arsenic was extracted by distillation using the silver diethyldithiocarbamate method then measured by molecular spectrophotometry technique. The results show that surface waters contain great quantities of metals than well and cistern waters. Lead (220.97 ±9.45 µg/L) and cadmium (20.13 ±0.17 µg/L) in surface waters have levels above WHO guidelines and Bénin standards. On the other hand, there is no significant difference between the metal concentrations of well and cistern waters at the 5% threshold. Significant correlations are established between toxic metals (Pb and Cd) and physical parameters (turbidity and suspended matters) at the threshold of 1 %. As for mercury (Hg) and arsenic (As), the concentrations are very lower than these of Cd and Pb and below the quantification limit of the device. These results confirm that the surface waters consumed by the populations of the Town Halls of Agbangnizoun and Za-Kpota do not respect drinking water standards.

Keywords: metals, drinking water, Agbangnizoun, Za-Kpota

1. Introduction

Heavy metals are naturally present in the environment in trace amounts. Their toxicity is much greater in the event of chronic or acute contamination, generally resulting in serious physiological and neurological effects (Grandjean, 1984; Fergusson, 1990; Plumlee and Ziegler, 2003).

Regarding lead for example, sensitivity to toxic effects is more marked in young children. This is related to the permeability of their blood-brain barrier. These are exposed to lead poisoning which results in clinical disorders, biological abnormalities and various histopathological alterations, cognitive and neurobehavioural damage; this pathology is manifested by anorexia, vomiting, irritability, behavioral problems, abdominal pain, coma, and death (INSPQ, 2003; Degbey et al., 2010; Laurent et al., 2013 Beauchamp, 2003).

Mercury poisoning in humans can also cause hydrargyria or hydrargyrism, which is characterized by damage to the nerve center. It is also a nephrotoxic toxic element.

The toxicity of arsenic depends on its degree of oxidation: As (O) > As (III) > As(V) (Callender, 2003). Toxicity increases with the degree of arsenic methylation (Fergusson, 1990; Alloway and Ayres, 1997; Chung et al., 2002). Arsenious oxide, or white arsenic (improperly called arsenic), As2O3 is a violent poison.

Cadmium is also very toxic in all its forms (metal, vapour, salts, and organic compounds); it is one of the few elements with no known function in the human body or in animals. In humans, it causes kidney problems in particular; this can result in irreversible nephropathy, which can lead to renal failure with renal tubular functional impairment from certain concentrations in the renal cortex and to increased blood pressure (Plumlee and Ziegler, 2003). The digestive system is the first to be affected following cadmium poisoning. The symptoms observed are gastroenteritis, vomiting, diarrhea and myalgia (striated skeletal muscle pain).Among the nine (09) Town Halls in the Zou Region the Town Halls of Agbangnizoun and Za-Kpota are the two with a low drinking water coverage rate. 25.2% of households have access to drinking water in the Town Hall of Agbangnizoun and 21.5% of households have access to it in the Town Hall of Za-kpota (INSAE, 2016) against an average Zou Region coverage of 53.4 %. The majority of households, therefore often use rainwater collected in tanks, wells and surface water without any prior treatment to satisfy their daily drinking water needs. Surface water and traditional wells are, for the most part, unfit for consumption because of their level of contamination and may contain toxic pollutants for humans (WHO, 2003, Babadjidé, 2011). In these two Town Halls, agriculture holds an important place with the use of pesticides and chemical fertilizers. The water consumed is therefore exposed to pollutants originating from agricultural sources because the contamination of surface or underground water by toxic substances is closely linked to that of the soil and to the use of pesticides, in this case fungicides which contain heavy metals (Coats, 1991; Deluisa et al., 1996; Bourrelier and Berthelin, 1998). This situation of degradation of water resources is exasperated by poor management of household waste in the two Town Halls where 94.8% of households in Agbangnizoun and 91.6% of households in Za-Kpota discharge waste directly into nature (INSAE, 2016). Indeed, urban wastes contain sources of heavy metals such as batteries (Hg, Zn, Pb, Cd), paints (Cr, Cd, Pb), plastics (Cd, Ni), cardboard paper (Pb) (De Miquel, 2001; Aloueimine, 2006). This study aims to assess the level of contamination in toxic metals (Hg, Pb, Cd and As) of surface water, wells and cisterns consumed by the populations of the concerned areas.

2. Material and Methods

2.1 Study Framework

The Town Halls of Agbangnizoun and Za-kpota are located in southern Bénin (Figure 1), in the Region of Zou. There are two rainy seasons, from March to July for the high season, from August to October for the low one and two dry seasons, December to March for the high season, July to August for the low one. The average annual rainfall varies between 900 mm and 1200 mm of water.

Table 1. Geographical coordinates of the water sampling villages

Town Halls	***Districts***	***Villages***	***Geographical coordinates***
AGBANGNIZOUN	SAHE	SAHETO	7°03'42.2"N 1°56'51.0"E
		COUFFONOU	7°02'21.4" N 1°55'28.0" E
		ADJAHA	7°06'51.5" N 1°54'17.7" E
ZA-KPOTA	KPAKPAME	YABA	7°18'23.5"N 2°06'11.8"E
		TOGA	7°20'29.3"N 2°09'38.2"E
	ZA-KPOTA	OUMGBEDIHO	7°13'30.7"N 2°14'00.9"E

Limited to the north and west by the Town Hall of Abomey, to the south by the Couffo River, to the east by the Town Halls of Bohicon and Zogbodomey, the Town Hall of Agbangnizoun has an area of 244 km² and a density of 1,116 inhabitants/Km^2.

According to the General Census of Population and Housing carried out by the National Institute of Statistics and Economic Analysis in 2013 (RGPH, INSAE, 2013), its population is 72,549 inhabitants, of which 34,782 are male and 37,767 females distributed in 16,763 households including. Administratively, the Town Hall is divided into ten (10) Dstricts and fifty-one (51) villages.

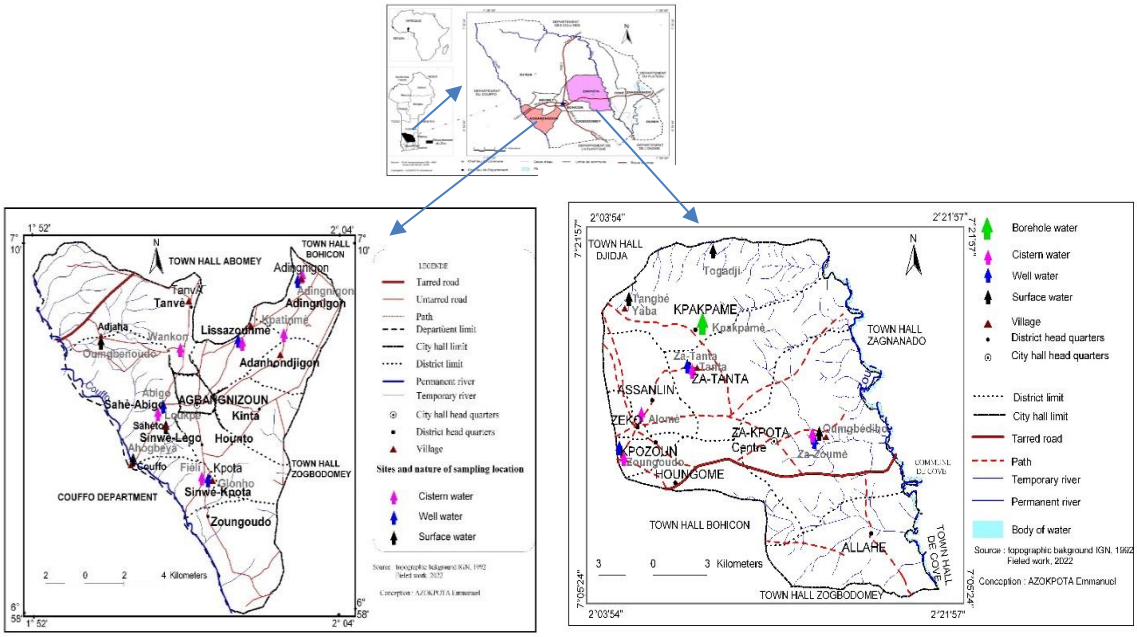

Figure 1. Maps of Zou Region, Agbangnizoun (to the left) and Zakpota (to the right) Town Halls showing the water sampling sites

As for the Town Hall of Za-Kpota, it is limited to the northwest by the Town Hall of Djidja, to the northeast by the Town Hall of Zagnanando, to the southwest by the Town Hall of Bohicon, to the east by the Town Hall of Covè and to the south-east by the Town Hall of Zogbodomey. It covers an area of approximately 600 km2 on which live 132,818 inhabitants, including 61,945 males and 70,873 females, distributed in 29,240 households, of which 15,199 are agricultural (RGPH4, 2013). According to the same source, the Town Hall of Za-Kpota is made up of 56 villages grouped into eight (8) districts from which we have choice six villages for this study (Table 1).

2.2 Water Sampling

The sampling method used for the campaigns is consistent with that used by the same authors in the previous article (Azokpota et al., 2022). The water from a borehole serves as a control sample because its composition is assumed to be close to that of natural water (low concentration of contaminants). The water samples were taken from plastic bottles previously washed and rinsed in the laboratory using the so-called "ultra-clean" method, then dried in an oven at 105°C. This protocol consists of: cleaning with nitic acid (HNO_3) 15%, HCI 1% (ACS reactive grade, J. T. Baker, Phillipsburg, U.S.A.) followed by seven rinses with ultra-pure water (Milli-Q system; > 18 MΩ.cm). These flasks were also rinsed with the water to be sampled in the field. The water sample was taken about 5 cm from the surface. Then, these samples were acidified by adding concentrated nitric acid (HNO_3) (v/v). These bottles were half filled before adding 2ml of HNO_3 (65%) then completely filled before being hermetically sealed to prevent any gas leaks. These samples were then labeled before being placed in a cooler containing cold packs.

2.3 Analysis Method

The determination of lead and cadmium is done in three stages: mineralization (Digestion according to HACH), extraction with pure chloroform recta and molecular absorption spectrophotometer (DR 3900). As for mercury, the dosage was carried out by the MILESTONE Direct Mercury Analyzer (DMA-80) using the cold vapor technique.

Digestion according to HACH

The stages of mineralization are for Cd and lead are:

- measure 40 mL of liquid sample in a 100 mL digesdahl flask.

Add 3 mL of concentrated sulfuric acid and bring to 440°C on the mineralizer;

- let it char for 3 to 5 minutes;

- add 10 mL of hydrogen peroxide 30 to 50% volume using a capillary funnel. If the sample is not completely clear, continue adding 5mL fractions;

- let the hydrogen peroxide evaporate completely and remove the vial from the mineralizer;

- after cooling (approximately 15 min), top up with distilled water up to the 100 mL line.

Filtering

Filtration is done using a GF/C membrane, with a porosity of 0.45 µm for dissolved metals analyses.

Prior treatment for mercury determination

The water samples did not undergo any treatment before the Hg analysis phase.

Prior treatment for arsenic determination

Finally, the arsenic was extracted by distillation using ISO 2590: 1973 (the silver diethyldithiocarbamate method) and then quantified by molecular spectrophotometry with DR 3900 device.

2.4 Statistical Processing of Analysis Results

All statistical analyses were performed in the R statistical software package, version 4.0.0 (R Core Team, 2020). We calculated descriptive statistics on the data and used barplot to explore the variation in water parameters (lead concentrations, cadmium concentrations, mercury concentrations and arsenic concentrations) among the water sources and campaigns. We then tested for significant effects of water parameters on water sources and collection campaigns using separate Kruskall-Wallis test since assumptions for Multivariate Analysis Of Variance were violated. When the null hypothesis is rejected in a validation, Wilcoxon multiple comparisons test is performed using multicomp package. When the influence is significant from the analysis of variance, the separation of the two metals averages has been made with the Student - Newman Keuls test. The relationship between the different water parameters was evaluated with the Pearson correlation test. The one-sample t-test was used to compare the three water sources. The concentration of each type of water have been compared with Beninese standards and those of the World Health Organization for drinking water. For all statistical analyses, the significance threshold used is 5%.

3. Results and Discussion

Spatial evolutions of median values of metal concentrations

The Kruskal Wallis test was carried out to study the evolution of the median values of the concentrations. The results show the p-value is less than 0.05 (P-value =0.0001). So there is a difference in significance at the 5% threshold between the median values of the concentrations of metals in the waters of the different localities studied. The multivariate analysis of variances (Figure 2) made it possible to see that the concentrations of mercury (Hg) and arsenic (As) are very lower than these of cadmium (Cd) and lead (Pb) and below the quantification limit of the device for the arsenic.

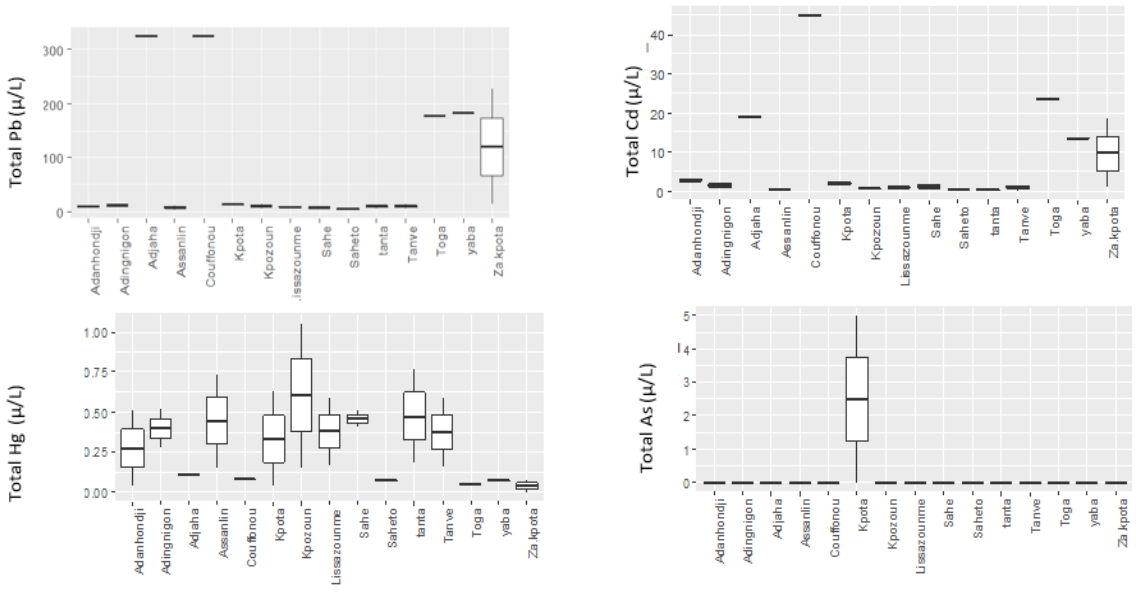

Figure 2. Comparison of median values of metal concentrations according to localities for the first campaign; Pr(>F)=0.0001

These results show two trends of variations of metals concentrations in water samples. Cadmium and lead concentrations are in the order of micrograms per liter to a few tens and hundreds micrograms per liter. While mercury and arsenic concentrations are in the order of a few tenths of micrograms per liter or in the state of traces (below the quantification limit).

Influence of water sources on Pb, Cd and As concentrations variations between the two campaigns

Lead, Cd and As concentrations did not vary significantly ($p<0.05$) in cistern, surface and well water between the two sampling campaigns despite a slight upward trend (Figure 3). On the other hand, surface waters have concentrations of Pb and Cd higher than those of cisterns at the 5% threshold. While cistern water is more contaminated with arsenic compared to surface and well water.

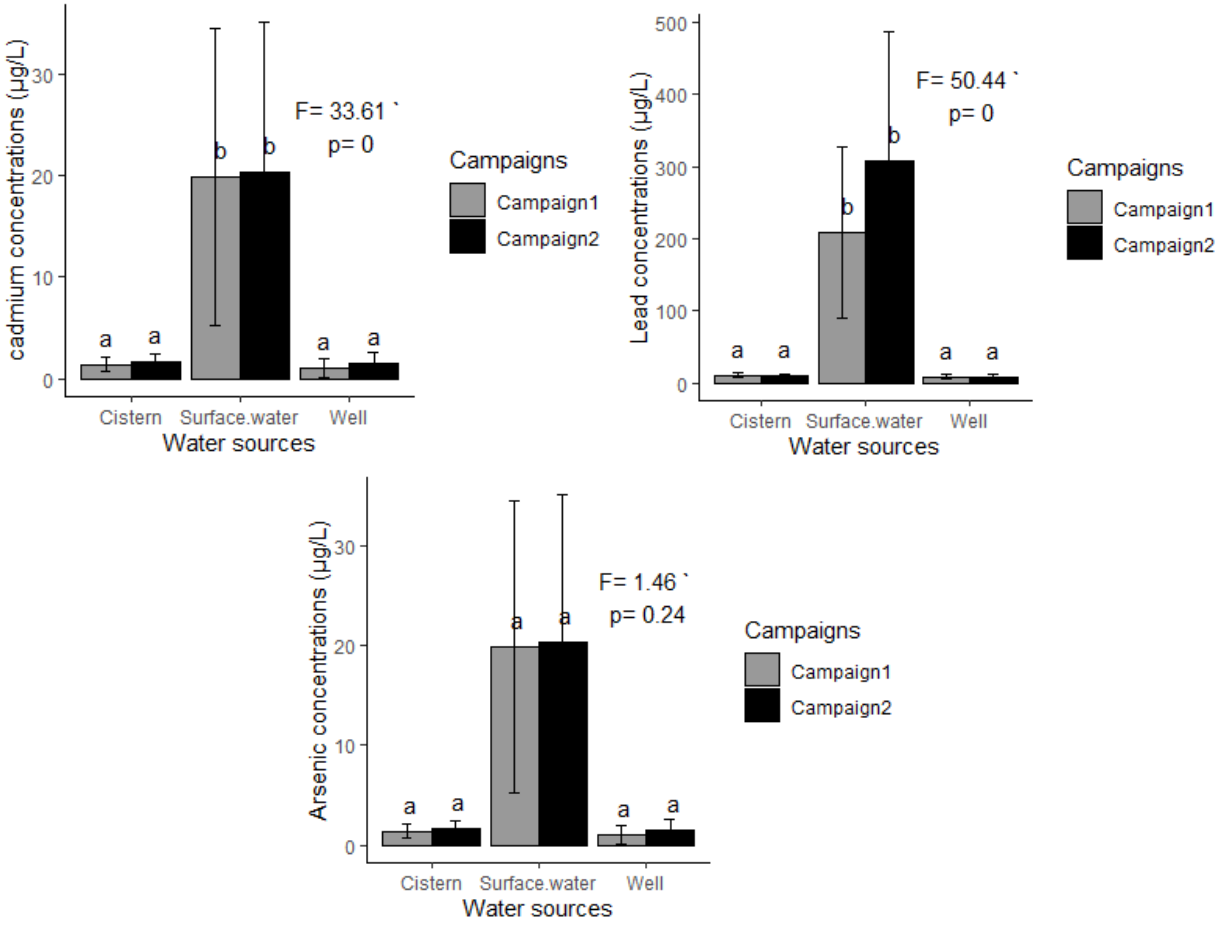

Figure 3. Variations in the concentrations of Pb, Cd and As according to the water sources between the two sampling campaigns

Variations of mercury residues

As for mercury (Hg) residues, the highest concentration of Hg was recorded in Kpozoun (1,060 µg/L) and the lowest in Za-Kpota with a concentration below the detection threshold in cistern water samples. Indeed, the cisterns are left open and exposed to bad weather throughout the rainy period while waiting for the drought period. The average concentrations recorded are 0.580; 0.077 and 0.186 µg/L in cistern, surface and well water, respectively. After cistern water, well water is the most contaminated with Hg. This indicates a local source like from using material as the thermometer, cosmetics products and pomades for women, etc. Indeed, the populations are frequently in contact with these waters for their daily needs by plunging all kinds of containers into them. These wells are also left open; which also exposes them to the weather.

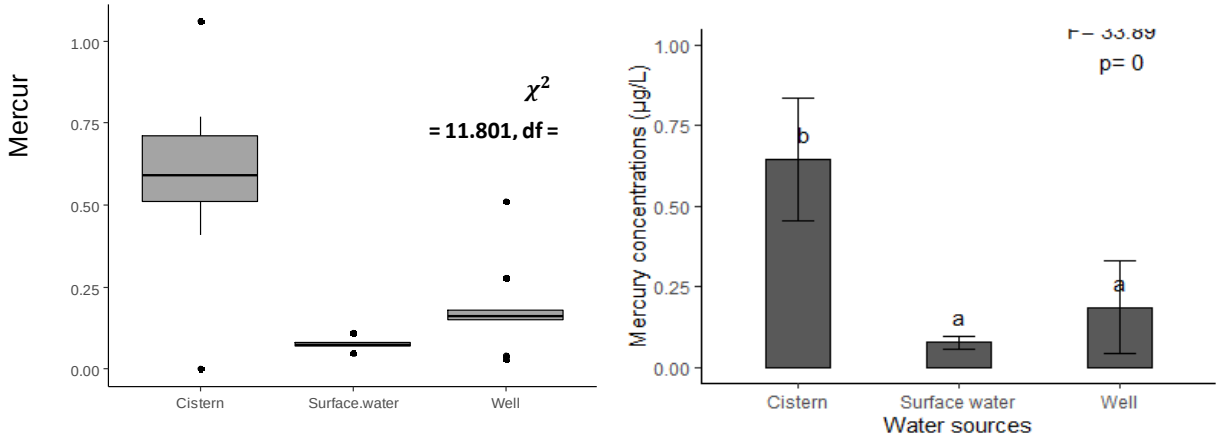

Figure 4. Comparison of median values (at the left) and means (at the right) of Hg concentrations according to water sources

The Kruskal Wallis test was carried out to study the evolution of median values of mercury concentrations (Figure 4). The results show the p-value is less than 0.05 (P-value =0.003). So there is a difference in significance at the 5% threshold between the median values of the concentrations of cistern, surface and well water.

Variations in concentrations of arsenic (As) residues

Most of the results obtained for arsenic residues are below the detection limit. Only the water samples taken from Kpota (5.00 µg/L) during the first sampling campaign and from Adingnigon (10 µg/L) in cistern water and Assanlin (3 µg/L) during the second sampling campaign in well water have showed concentrations above quantification limit (Table 2).

Evolution of the concentrations of Pb and Cd

The results of the analyses carried out for the metals are presented in Table 2.

Lead residues are mainly represented in the surface water collected during the first sampling campaign on the sites of Adjaha (in Agbangnizoun), Couffonou (in Agbangnizoun) and Za-kpota (in Za-kpota) then in Toga and Yaba (in Za-Kpota). The Sahèto (in Agbangnizoun) site has the lowest lead concentration among the surface waters studied. The highest lead concentrations are obtained during the second sampling campaign with a value of 611 µg/L in Yaba, 296.25 µg/L in Za kpota and 261 µg/L in Adjaha.

As for rainwater stored in cisterns and water from traditional wells, the trends in lead residue variations are similar with concentration values ranging from 5.82 µg/L at Sahe to 13.77 µg/L at Kpozoun (in Za-kpota) for cistern water and 3.53 µg/L at Assanlin (in Za-kpota) to 12.70 µg/L at Adingnigon (in Agbangnizoun) for the first sampling campaign.

Correlations between the parameters studied

From the analysis of tables 3 and 4, it appears that:

- The concentration of suspended solids in the water is very strongly correlated with the concentration of lead (r = 0.98 with $p < 0{,}0001$) on the one hand, and very strongly correlated with the concentration of cadmium (r = 0.99 with $p < 0{,}0001$) on the other hand ;

- The colour of the water is very strongly correlated with lead concentrations (r = 0.96 with $p < 0{,}0001$) on the one hand and strongly correlated with cadmium concentrations (r = 0.93 with $p < 0{,}0001$) on the other hand;

- Water turbidity is correlated with cadmium concentrations (r = 0.74 with $p < 0{,}0001$).

From these significant correlations, it can be deduced that the large part of lead and cadmium (in particulate phase) is kept by suspended solids in the water, as shown by the results of the phase speciation of said metals (Table 3). The turbidity of the water depends on the suspended solids which are at the origin of the water colour. This justifies the strong correlations observed between lead and cadmium fixed on suspended matter and the colour of the water. The correlation between suspended solids and metals also explains that established between turbidity, lead and cadmium.

Legend

Cond	TDS	Turbo	SM	NO2-	NO3-	PO43-	bp	CD	Col	ammo	Sulp
Conductivity	TDS	Turbidity	Suspended Matter	Nitrites	Nitrates	Orthophosphate	Lead	Cadmium	Colour	Ammonium	Sulphates

Table 2. Correlation matrix (Pearson)

Variables	pH	Temp	Cond	TDS	Turbo	SM	NO2-	NO3-	PO43-	Pb	Cd	Colo	ammo	Sulp
pH	1													
Temp	**-0.5320**	1												
Cond	**-0.6039**	**0.5608**	1											
TDS	-0.4112	0.3955	**0.8878**	1										
Turbo	-0.0149	0.1410	-0.1753	-0.1439	1									
MY	-0.0395	-0.2443	0.2941	**0.4608**	**0.7763**	1								
NO2-	-0.0080	-0.1039	0.3466	**0.5038**	**0.5775**	**0.9112**	1							
NO3-	**-0.4315**	**0.6381**	**0.6577**	**0.4292**	-0.0963	-0.2183	-0.2261	1						
PO43-	-0.2562	0.3606	0.1774	0.0937	0.0545	-0.0367	-0.0907	**0.6227**	1					
Pb	-0.0329	-0.2320	0.2874	**0.4621**	**0.6843**	**0.9801**	**0.9244**	-0.2273	0.1997	1				
Cd	0.0288	-0.2643	0.2604	**0.4327**	**0.7478**	**0.9904**	**0.9274**	-0.2581	-0.0803	**0.9642**	1			
Colo	-0.0383	-0.2031	0.2659	**0.4475**	**0.5949**	**0.9512**	**0.9207**	-0.2355	**0.5790**	**0.9650**	**0.9380**	1		
ammo	0.1386	-0.1831	0.2729	**0.4723**	**0.5115**	**0.8274**	**0.9447**	-0.2187	**0.7342**	**0.8638**	**0.8441**	**0.8383**	1	
Sulp	-0.1130	0.0722	0.0534	0.0155	0.1573	0.3728	**0.4538**	-0.1433	-0.2123	0.3771	0.3981	0.4038	0.0250	1

Values in bold are different from 0 at significance level alpha=0.05

Table 3. Probability values associated with the correlation between water parameters

Variables	pH	Temp	Cond	TDS	Turbo	MY	NO2-	NO3-	PO43-	Pb	Cd	Color	ammo	Sulf
pH														
Temp	**0.0090**													
Cond	**0.0023**	**0.0054**												
TDS	0.0513	0.0618	**< 0.0001**											
Turbo	0.9501	0.5532	0.4599	0.5450										
SM	0.8581	0.2614	0.1732	**0.0269**	**< 0.0001**									
NO2-	0.9711	0.6370	0.1051	**0.0143**	**0.0039**	**< 0.0001**								
NO3-	**0.0398**	**0.0011**	**0.0006**	**0.0410**	0.6621	0.3170	0.2995							
PO43-	0.2379	0.0909	0.4180	0.6705	0.8051	0.8680	0.6806	**0.0015**						
Pb	0.8817	0.2868	0.1837	**0.0264**	**0.0003**	**< 0.0001**	**< 0.0001**	0.2969	0.3987					
Cd	0.8962	0.2229	0.2300	**0.0392**	**< 0.0001**	**< 0.0001**	**< 0.0001**	0.2344	0.7366	**< 0.0001**				
Color	0.8623	0.3526	0.2201	**0.0323**	**0.0028**	**< 0.0001**	**< 0.0001**	0.2794	**0.0075**	**< 0.0001**	**< 0.0001**			
ammo	0.5281	0.4031	0.2077	**0.0229**	**0.0126**	**< 0.0001**	**< 0.0001**	0.3161	**0.0002**	**< 0.0001**	**< 0.0001**	**< 0.0001**		
Sulf	0.6076	0.7432	0.8088	0.9439	0.4735	0.0798	**0.0296**	0.5141	0.3689	0.0761	0.0599	0.0560	0.9167	

Values in bold are different from 0 at significance level alpha=0.05

Lead concentration's variations

The Student - Newman Keuls test of the results shows that the concentration of total lead in water varies significantly ($p<0.05$) depending on the alternative water sources (Table 4). On average for the two targeted campaigns, the total lead in surface water is significantly higher (220.97µg/L) than in cistern waters (10.90µg/L), wells (10.37µg/ L) and drillings (8.22µg/L) (witness). There is a significant difference between the lead concentration obtained in the sampled surface waters and the guidelines regulated by the WHO and the Bénin standards. The lead concentration in the well and cistern waters is significantly lower than Beninese standards. On the other hand, surface waters have a high concentration which significantly exceeds the guideline values set by the WHO and the standards of Bénin.

Table 4. Variation of metals according to water sources

Parameters	***Water sources***			
	Cisterns	***Wells***	***Surface waters***	***Drilling (witness)***
Cadmium (µg/L)	2.42± 0.19[b]	1.28± 0.17[b]	20.13± 1.46[a]	0.82± 0.17[c]
Lead (µg/L)	10.90 ± 0.61[b]	10.37 ± 0.10[b]	220.97± 9.45[a]	8.22± 0.66[b]

Legend: The same letters (a or b) mean that there is no significant difference between the values.

Cadmium concentration's variations

Regarding cadmium, the statistical analysis has showed that the results obtained are similar to those of lead. The average total cadmium, for the two years, is the lowest (0.82 µg/L) in the drilling waters (witness) compared to surface waters which have a total cadmium concentration of 20.13 µg/L, an increase of more than 95%. Moreover, the total cadmium concentrations vary significantly ($p<0.05$) from one alternative water source to another. The cistern and well waters concentrations in cadmium are significantly lower than the WHO guideline values and the Bénin standard. On the other hand, surface waters contain a cadmium concentration significantly higher than the reference values.

The concentrations represent the average values of the waters of the different sources. the same letters (a or b) mean that there is no significant difference between the values.

The presence of metal concentrations (Pb and Cd) in the water consumed above the witnesses and standards indicates a contribution of anthropogenic activities (agriculture, solid and liquid wastes). The results obtained are in agreement with those of African researchers (Table 5) who have devoted research to the metallic contamination of waters where the values of lead vary from 0.02 to 70.4 mg/L in surface waters (Kakulu et al., 1992; Chitou et al., 2010; Youssao et al., 2011; Blinda et al., 2013; Kabunga et al., 2013; Onivogui et al., 2013; Yapi et al., 2014; Fouad et al., 2014; Traore et al., 2015; Wanga et al., 2015; Greichus et al., 2015; Mohiuddin et al., 2015; Fahssi et al., 2016; Edward et al., 2017; Kadriua et al., 2017; Agbandou et al., 2018). On the other hand, our results are in disagreement with those obtained by researchers where the values of Cadmium vary from 0.1 to 20.49 mg/L in surface waters (Chitou et al., 2010; Yapi et al., 2014; Fouad et al., 2014; Wanga et al., 2015; Greichus et al., 2015; Mohiuddin et al., 2015). For the well waters, the cadmium values obtained (0.0010 mg/L) are contrary to those obtained by researchers and which are in the range of 0.02 mg/l to 0.23 mg/l exceeding the standards for cadmium (Tanouayi et al., 2015; Yapi et al., 2014; Gbamele et al., 2020); those of lead (0.010 mg/L) are lower than the values (0.03 mg/l to 4.8 mg/l) obtained by other researchers (Peliba et al., 1991; Creppy et al., 2003; Tanouayi et al., 2015; Chaïeb et al. , 2016; Gbamele et al., 2020 ; Yapi et al., 2014). As for the cistern waters, the average values obtained for lead (0.010 mg/L) and cadmium (0.002 mg/L) are lower than the values obtained respectively by Legret et al.,1994 and Hebabaze et al., 2015 in rainwaters collected in cisterns for lead (0.078 mg/L and 0.016 mg/L) and cadmium (0.017 mg/L and 0.011 mg/L).

Health effects linked to the presence of these toxic metals in drinking water are known. Mention may be made, for lead, of lead poisoning, which results in clinical troubles, biological anomalies and various histopathological alterations, cognitive and neurobehavioural damage, increased sensitivity to the toxic effects of lead in young children linked to blood-brain barrier permeability, anorexia, vomiting, irritability, behavioral disturbances, abdominal pain, coma, and death; in pregnant women, there is harm to the development of the central nervous system of the fetus (INSPQ, 2003; Degbey et al., 2010; Laurent et al., 2013). The health effects linked to cadmium are: kidney pains, bone alterations and arterial hypertension; " Itai Itai " characterized by bone decalcification, proteinuria and glucosuria (Botta and Bellon, 2004; Rodier et al., 2009).

Table 5. Calculation of contamination indexes (CI) of lead and cadmium residues

No,	Water sources	Localities	Sample name	Campaign_1_Concentrations in µg/L				Campaign_2_Concentrations in µg/L			
				Pb_tot	CI $_{Pb}$	Cd_tot	CI $_{Cd}$	Pb_tot	CI $_{Pb}$	cd_tot	CI $_{Cd}$
20	Drilling (Reference)	Kpakpame	BF/AEV(Reference)	10.35	0.00	3.01	0.00	10.35	0.00	3.01	0.00
16	Cistern	Sahe	Cistern 1	5.82	-0.28	1.88	-0.23	6.81	-0.21	1.96	-0.21
17		Adingnigon	Cistern 2	9.7	-0.03	2.13	-0.17	10.2	-0.01	2.25	-0.14
18		Adanhondji	Cistern 3	10.84	0.02	2.15	-0.17	10.75	0.02	2.25	-0.14
19		Kpota	Cistern 4	12.04	0.08	2.29	-0.14	11.97	0.07	1.85	-0.24
20		Tanve	Cistern 5	13.47	0.13	1.75	-0.26	11.32	0.04	0.94	-0.52
21		Lissazounme	Cistern 6	9.28	-0.05	1.37	-0.37	9.88	-0.02	3.26	0.04
22		Kpozoun	Cistern 7	13.77	0.14	0.6	-0.67	9.89	-0.02	1.1	-0.46
23		Assanlin	Cistern 8	10.83	0.02	0.29	-0.82	11.02	0.03	0.5	-0.72
24		tanta	Cistern 9	12.36	0.09	0.71	-0.62	12.63	0.10	0.89	-0.54
25		Za kpota	Cistern 10	13.22	0.12	0.96	-0.52	12.23	0.08	1.52	-0.33
1	Surface water (SW)	Adjaha	SW Adjaha	325.63	0.94	18.75	0.72	261	0.92	13.21	0.63
2		couffonou	SW Couffo	324.38	0.94	45	0.87	325	0.94	46	0.88
3		Za kpota	SW Oung	227.81	0.91	18.44	0.72	296.25	0.93	20.51	0.74
4		saheto	SW Saheto	5.35	-0.32	0.41	-0.76	49.25	0.65	2.11	-0.18
5		Toga	SW Toga	178.44	0.89	23.44	0.77	297	0.93	25.2	0.79
6		yaba	SW Yaba	183.13	0.89	13.44	0.63	611	0.97	15.02	0.67
7	Well (W)	Adanhondji	W Adan	9.92	-0.02	3.46	0.07	8.02	-0.13	3.5	0.08
8		Adingnigon	W Adin	12.7	0.10	0.9	-0.54	12.84	0.11	1.02	-0.49
9		Assanlin	W ASS	3.53	-0.49	0.7	-0.62	2.06	-0.67	2.69	-0.06
12		Kpota	W Kpota	13.44	0.13	1.67	-0.29	5.95	-0.27	1.09	-0.47
10		Kpozoun	W Kpozoun	6.17	-0.25	0.94	-0.52	14.2	0.16	2.1	-0.18
11		Lissazounme	W Lissazou	7.85	-0.14	0.76	-0.60	7.61	-0.15	0.85	-0.56
14		Sahe	W Sahe	7.98	-0.13	0.4	-0.77	7.65	-0.15	1.01	-0.50
15		tanta	W Tanta	6.49	-0.23	0.24	-0.85	6.94	-0.20	51	0.89
13		Tanve	W Tanve	5.96	-0.27	0.36	-0.79	6.01	-0.27	0.34	-0.80

Table 6. Phase speciation of Cadmium and Lead in surface waters

Surface water	***Lead (µg/L)***			***Cadmium (µg/L)***		
	Dissolved(D)	***Particulate(P) (P)***	***P/D [1]***	***Dissolved(D)***	***Particulate(P)***	***P/D***
Adjaha	15.29	245.71	16	2.1	11.11	5
Couffonou	13.75	311.25	23	3.6	42.4	12
Oumgbediho	26.61	269.64	10	1.96	18.55	9
Saheto	27.71	21.54	1	0.5	1.61	3
Toga	13.51	283.49	21	2.91	22.29	8
Yaba	17.54	593.46	34	1.58	13.44	9

P/D represents the particulate Pb / dissolved Pb and the particulate Cd / dissolved Cd ratios

The phase speciation results show that the P/D ratio varies from 1 to 34 for lead and from 3 to 12 for cadmium (Table 6). This relatively high ratio shows that the total lead and cadmium present in the water are found in high proportion in the particulate form retained by suspended matter. This means that most of the lead and cadmium inputs are essentially in the particulate form and there is little mineralization of the organic matter contained in the water. The total lead and cadmium in water are therefore mainly found in the form of particles. These lead and cadmium particles can have as, among other sources, aerial fallout that is drained to surface waters by runoff. Under certain environmental conditions, the mineralization of organic matter having fixed the particulate lead and cadmium could increase the dissolved lead and cadmium which would merge with the total lead and cadmium, as in the case of water sources where suspended matter are low or even non-existent. This is the case of cistern and well waters where the total lead and cadmium practically merge with the dissolved lead and cadmium.

Spatial evolution of total lead levels

Analysis of variance of total lead levels according to Town Hall

Total lead is the only pollution parameter that differs significantly from one Town Hall to another; the highest concentration (78.50 µ/L) has been recorded in the waters of Za-kpota Town Hall (Figure 5).

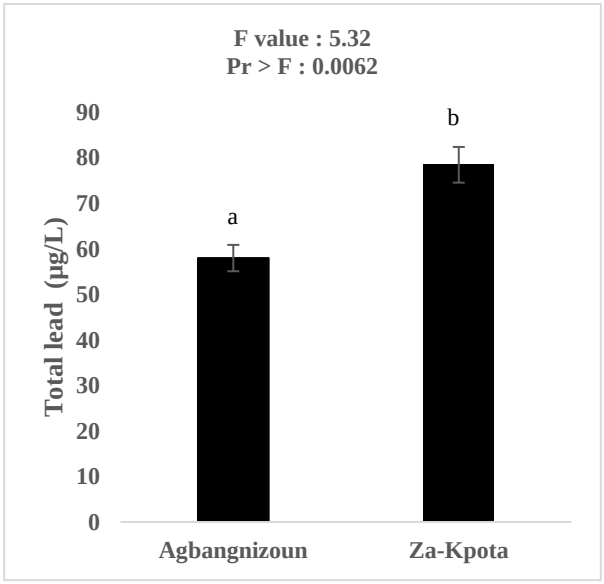

Figure 5. Variation in the average concentration of lead in the Town Halls studied

Analysis of variance of total Pb and Cd concentrations according to the concerned localities

The water samples collected in Adjaha and Couffonou are more polluted in lead (293.32 µg/L and 324.69 µg/L respectively). The lead concentration is lower in the threshold of 0.05 (Figure 6), in the waters of Adanhondjigon Adingningon , Assanlin , Kpota , Kpozoun , Lissazounmè , Tanta and Tanvè. As far as the cadmium is concerned, the highest concentration was recorded in Couffonou (45.50 µg /L).

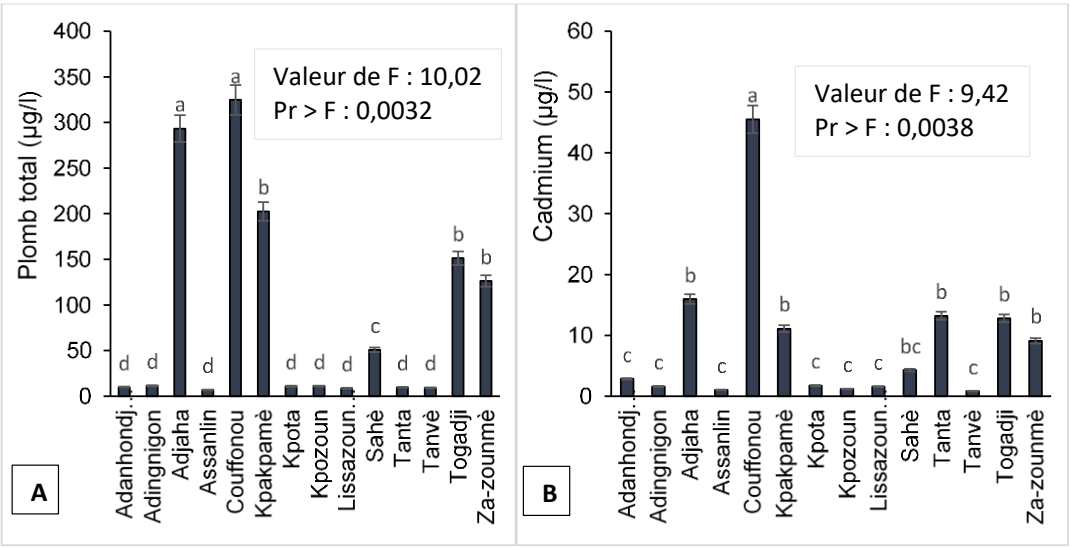

Figure 6. Variation of pollution parameters in the sampled localities

Contamination indexes (CI) of lead and cadmium residues

The contamination index is defined in relation to the reference site, representative of the natural background noise of the study area. For a metal i, it is determined by the formula:

$$IC_i = \frac{(C_i - C_{réf})}{C_i + C_{réf}},$$

Where Ci is the concentration of metal i at the sample site and $Cref$ its concentration at the control sample site which is sample BF/AEF, the drilling water. The results are presented in Table 6 where the abbreviations used are as follows: Pb_tot =Total Lead; Cd_tot = total cadmium; As_tot = Total Arsenic; Hg_tot = Total Mercury.

The analysis of the table 6 makes it possible to deduce that the contamination indexes of lead and cadmium vary from

one water source to another and from sampling campaign to another. However, we note some peculiarities within the same source.

Except of the Sahèto water, all the calculated indexes for surface waters sampled, has showed positive contamination indexes for lead and cadmium during the two campaigns.

The probable sources of contamination of these waters are the chemical fertilizers and pesticides used by agriculture in the cotton, maize and groundnut fields located in the slopes of these waters.

With regard to well and cistern water, the cadmium contamination indexes are negative during the first campaign, except for the cistern water sampled at Lissazounmè and the well water sampled at Adanhondjigon and Tanta which presented positive contamination. For the two water sampling campaigns, the lead contamination indexes are positive for water from cisterns sampled at Adanhondjigon , Tanvè , Kpota , Assanlin , Tanta and Za-Kpota. Those from wells sampled at Adingnigon , Kpota for the first campaign and in kpozoun for the second campaign are also positive. The sources of contamination of cistern water by lead would therefore be aerial and probably old sheets and dry palm leaves used to cover cisterns. On the other hand, the probable source of contamination of well water by lead would be the source rock constituting the aquifer. It is the same source which would be at the origin of the presence of cadmium in the water of wells taken from Adanhondjigon and Tanta.

4. Conclusion

The study of metallic contamination of surface, traditional well and cistern waters used for drinking by human populations in Agbangnizoun and Za-kpota Town Halls, southern Bénin, shows that these waters are not suitable for consumption. The heavy metals recorded in surface waters whose average values are higher than the standards accepted for drinking water are:

- Lead with an average value of 220.97 ±9.45 µg/L;

- Cadmium with an average value of 20.13 ±0.17 µg/L.

These metals are found to a large extent, retained by suspended solids in the water. These results reflect the evidence of the poor quality of these surface waters. The influence of human activities and poor sanitation of the study area on water quality has also been picked up.

The populations who consume these waters for drinking are therefore exposed to health risks. However, the consumption of water from cisterns and traditional wells presents less danger for vulnerable populations than that of surface water. We suggest a primary treatment by water filtration before any human consumption to eliminate the particulate phase which is the most abundant.

References

Abboudi, A., Tabyaoui, H., & EL Hamichi, F. (2014). Etude de la qualité physico-chimique et contamination métallique des eaux de surface du bassin versant de Guigou. *Maroc European Scientific Journal*, August 2014 édition vol.10, N°23 ISSN: 1857-7881.

Ayad, W. (2017). *Evaluation de la qualité physico-chimique et bactériologique des eaux souterraines: cas des puits de la région d'El-Harrouch (Wilaya de Skikda). Thèse de doctorat, Université Badji Mokhtar-Annaba-Algérie. 156p*.

Botta, A., & Bellon, L. (2004). *Pollution chimique de l'eau et santé humaine.* Service de médecine et santé au travail. Laboratoire de biogénotoxicologie et mutagenèse environnementale (EA 1784, IFR PMSE 112), p. 23

Boubakar, H. A. (2010). *Aquifères superficiels et profonds et pollution urbaine en Afrique: Cas de la communauté urbaine de Niamey (NIGER), Thèse de l'Univ. Abdou Moumouni de Niamey (Niger), 198 p*p.

Bouchemal, F., & Achour, S. (2015). Qualité physico-chimique et paramètres de pollution des eaux souterraines de la région de Biskra. *Larhyss Journal,* ISSN 1112-3680, n°22, June 2015, pp. 197-212 ©2015 All rights reserved, Legal Deposit 1266-2002.

Chaïeb, A., & Khattach, D. (2016). Evaluation de la qualité physico-chimique des eaux souterraines dans le voisinage de la décharge contrôlée de Berkane (Maroc). *J. Mater. Environ. Sci., 7*(11), 3973-3983. ISSN: 2028-2508.

Chouti, W., Mama, D., Alassane, A., Ahangotade, O., Alapini, F., Boukari, M., … Afouda, A. (2010). Caractérisation physico- chimique de la lagune de Porto-Novo (sud Bénin) et mise en relief de la pollution par le mercure, le cuivre et le zinc. *Journal of Applied Biosciences, 43,* 2882-2890.

Degbey, C. (2011). *Facteurs associés à la problématique de la qualité de l'eau de boisson et la santé des populations dans la commune d''Abomey-Calavi au Bénin." Thèse de doctorat en Sciences de la santé publique. École de santé publique. Université Libre de Bruxelles (ULB)*.

Degbey, C., Makoutode, M., Fayomi, B., & Brouwer, C. (2010). La qualité de l'eau de boisson en milieu professionnel à Godomey au Bénin. *Journal Internationale de Santé et Travaux, 1*, PP : 15-22.

Dovonou, E. F., Hounsou, B. M., Sambienou, W. G., Adandedjan, C., Houessouga, F., & Mama, D. (2020). Qualité des eaux pluviales stockées dans les citernes pour la consommation dans la commune de Toffo: cas de l'arrondissement de Damè. *Journal of Applied Biosciences, 154*, 15871-15880 ISSN 1997-5902 J. Appl. Biosci

Dovonou, F., Adjahossou, N., Alamou, E., Alassane, A., Mama, D., & Boukari, M. (2014). Pollution des eaux souterraines par les métaux lourds et leur impact sur l'environnement: cas de l'aquifère superficiel du champ de captage intensif de Godomey au sud Bénin. *Africa Geoscience Review, 21*(1 & 2), 45-55..

Emmanuel, A., Alassane, Y. A. K., Alphonse, A., Abdoulkader, A. M., Constant, A., & Daouda, M. (2022). Physico-Chemical Characterization of Surface Waters, Traditional Wells and Cisterns Waters Consumed in the Town Halls of Agbangnizoun and Za-kpota In South Bénin. *Elixir Pollution, 163*(2022), 56064-56070. Badji Mokhtar-Annaba-Algeria University. 156p.

Fouad, S., Hajjami, K., Cohen, N., & Chlaida, M. (2014). Qualité physico-chimique et contamination métallique des eaux de l'Oued Hassar: impacts des eaux usées de la localité de Mediouna (Périurbain de Casablanca, Maroc). *Afrique Science, 10*(1), 91-102, ISSN 1813-548X. http://www.afriquescience.info

Gbamele, K. S., Konan, K. S., Kouassi, K. L., Brou, L. A., Konan, K. F., & Bini, K. D. (2020). Evaluation de la Contamination Chimique des Eaux Souterraines par les Activités Anthropiques : Cas de la Zone d'Ity-Floleu Sous-Préfecture de Zouan- Hounien, Ouest de la Côte d'Ivoire. *European Scientific Journal, 16*(6), ISSN: 1857-7881 (Print) e-ISSN: 1857-7431.

Gnazou, M. D. T., Assogba, K., Sabi, B. E., & Bawa, L. M. (2015). Qualité physico-chimique et bactériologique des eaux utilisées dans les écoles de la préfecture de Zio (Togo). *Int. J. Biol. Chem. Sci., 9*(1), 504-516, February 2015 ISSN 1997-342X (Online), ISSN 1991-8631 (Print)

Greichus, Y. A., Greichus, A., Ammann, B. D., & Hopcraft, J. (1978b). Insecticides, polychlorinated biphenyls and metals in African lake ecosystems. 3. Lake Nakuru. *Kenya Bull. Environ.Contam. Toxicol., 19*, 454-461. https://doi.org/10.1007/BF01685825

Hebabaze, S., Abdelali, S., Badri, W., & Nahli, A. (2015). Diagnostic de la qualité des eaux pluviales des toitures en vue de leur réutilisation paysagère: cas d'un établissement d'enseignement public à Casablanca (Maroc). *Larhyss Journal*, ISSN 1112-3680, n°24, Décembre 2015, 143-160.

INSAE (Institut National de la Statistique et de l'Analyse Economique). 2013. Résultats du Quatrième Recensement Général de la Population et de l'Habitation (RGPH 4), Cotonou, Bénin, 40 p.

Kakulu, S. E., & Osibanjo, O. (1992). Pollution studies of Nigerian rivers: Trace metal levels of surface waters in the Niger Delta area. *Int. J. Environ. Stud., 41,* 287-292

Lagnika, M., Ibikounle, M., Montcho, C., Wotto, D. V., & Sakiti, G. N. (2014). Caractéristiques physico-chimiques de l'eau des puits dans la commune de Pobè (Bénin, Afrique de l'ouest). *Journal of Applied Biosciences, 79*, 6887-6897; ISSN 1997-5902

Lakhili, F., Benabdelhadi, M., Bouderka, N., Lahrach, H., & Lahrach, A. (2015). Etude de la qualité physico-chimique et de la contamination métallique des eaux de surface du bassin versant de BEHT (MAROC). *European Scientific Journal*, *11*(11), 132-147.

Lamizana-Diallo, M. B., Kenfach, S., & Millogo-Rasolodimby, J. (2008). Evaluation de la qualité physico-chimique de l'eau d'un cours d'eau temporaire du Burkina Faso – Le cas de Massili dans le Kadiogo. *Sud Sci. Techno, 16*, 23-28.

lourds (Hg, Cd, Pb, Co, Ni, Zn) des eaux et des sédiments de l'estuaire du fleuve Konkouré (Rep. de Guinée). *Afrique Science, 09*(3), 36-44.

Maoudombaye. T., Ndoutamia, G., Seid Ali, M., & Ngakou. A. (2015). Etude comparative de la qualité physico-chimique des eaux de puits, de forages et de rivières consommées dans le bassin pétrolier de Doba au Tchad. *Larhyss Journal,* ISSN 1112-3680, n°24, Décembre 2015, 193-208.

Mohiuddin, K. M., Ogawa, Y., Zakir, H. M., Otomo, K., & Shikazono, N. (2011). Heavy metal contamination in water and sediments of an urban river in a developing country. *Int. J. About. Science. Tech., 8*(4), 723-736, Autumn 2011 ISSN 1735-1472 © IRSEN, CEERS, IAU. https://doi.org/10.1007/BF03326257

Ngakomo, A. R. P., Aghaindum, A. G., Abou, E. Z., & Ngassam, P. (2020). Caractéristique physico-chimique et dynamique des formes environnementales des coccidies entériques dans les eaux de sources, puits et cours d'eau dans la Commune d'Akono (Cameroun, Afrique Centrale). *European Scientific Journal, 16*(3), ISSN: 1857-7881

(Print) e- ISSN 1857-7431.

Ngouala, M. M. (2020). Characterization of groundwater in Mayombe in the south-west of the Republic of the Congo by geochemical and statistical methods. *Rev. Ivory. Sci. Technol., 35*, 446-461, ISSN 1813-3290.

Onivogui, G., Balde, S., Bangoura, K., & Barry, M. K. (2013). Evaluation des risques de pollution en métaux

Rodier, J., Bazin, C., Broutin, J. P., Chambon, P., Champsaur, H., & Rodi, L. (2005). *L'analyse de l'eau, eaux naturelles, eaux résiduaires, eau de mer, chimie, physico-chimie, microbiologie, biologie, interprétation des résultats. Ed. Dunod, Paris, 1384 p*.

Rodier, J., Legube, B., & Merlet, N. (2009). *L'Analyse de l'Eau*, éd DUNOD: 749- 775

Santé et Bien-être social Canada. 1982. Recommandations pour la qualité de l'eau potable au Canada 1978. Pièces à l'appui. Approvisionnements et Services Canada, Hull

Tanouayi, G., Gnandi, K., Ahoudi, H., & Ouro-Sama, K. (2015). La contamination métallique des eaux de surface et des eaux souterraines de la zone minière d'exploitation des phosphates de Hahotoe-Kpogame (Sud-Togo): cas du cadmium, plomb, cuivre et nickel. *Larhyss Journal,* ISSN 1112-3680, n°21, March 2015, 25-40.

Wanga, B. M., Musibono, D. E., Mpiana, P. T., Mafuana, L., Kiza, N., & Diana, J. (2015). Evaluation de la qualité physico-chimique des eaux de la rivière Kalamu de Boma, R.D. Congo. *Congo Sciences Journal en Ligne de l'ACASTI et du CEDESURK ACASTI and CEDESURK Online Journal, an International Journal, 3*(1), 56-57, ISSN: 2410-4299.

WHO. (2003). Directives de qualité pour l'eau de boisson ; volume 2, critères d'hygiène et documentation à l'appui, 2ème édition, 1050 p.

Youssao, A. K. A. (2011). *Etude de la distribution des résidus de plomb dans les écosystèmes aquatiques du Chenal de Cotonou et du lac Nokoué au Bénin. Thèse. Soutenue le 1er Décembre 2011.*

International Journal of Chemistry; Vol. 14, No. 1; 2022
ISSN 1916-9698 E-ISSN 1916-9701
Published by Canadian Center of Science and Education

Reviewer Acknowledgements

International Journal of Chemistry wishes to acknowledge the following individuals for their assistance with peer review of manuscripts for this issue. Their help and contributions in maintaining the quality of the journal is greatly appreciated. Many authors, regardless of whether *International Journal of Chemistry* publishes their work, appreciate the helpful feedback provided by the reviewers.

Reviewers for Volume 14, Number 1

Abdallah El-Gharbawy, Alexandria University, Egypt

Ahmad Galadima, Usmanu Danfodiyo University, Nigeria

Amal A. M. Elgharbawy, International Institute for Halal Research and Training, Malaysia

Ayodele Temidayo Odularu, University of Fort Hare, South Africa

Fatima Tuz Johra, Kookmin University, Bangladesh

Gholam Hossain Varshouee, National Petrochemical Company, Iran

Khaldun Mohammad Al Azzam, Al-Ahlyyia Amman University, Jordan

Nejib Hussein Mekni, Al Manar University, Tunisia

Sintayehu Leshe, Debre Markos University, Ethiopia

Sitaram Acharya, Dallas College, USA

Tony Di Feo, Natural Resources Canada, Canada

Albert John

On behalf of,

The Editorial Board of *International Journal of Chemistry*

Canadian Center of Science and Education

ACADEMIC AND OPEN ACCESS

Canadian Center of Science and Education

CCSENET.ORG

➢ CALL FOR MANUSCRIPTS

International Journal of Chemistry (IJC) is a peer-reviewed journal, published by Canadian Center of Science and Education. The journal publishes research papers in all aspects of chemistry. The journal is available in electronic form in conjunction with its print edition. All articles and issues are available for free download online.

We are seeking submissions for forthcoming issues. All manuscripts should be written in English. Manuscripts from 3000-8000 words in length are preferred. All manuscripts should be prepared in MS-Word format, and submitted online, or sent to: ijc@ccsenet.org

Paper Selection and Publishing Process

a) Submission acknowledgement. If you submit manuscript online, you will receive a submission acknowledgement letter sent by the online system automatically. For email submission, the editor or editorial assistant sends an e-mail of confirmation to the submission's author within one to three working days. If you fail to receive this confirmation, please check your bulk email box or contact the editorial assistant.

b) Basic review. The editor or editorial assistant determines whether the manuscript fits the journal's focus and scope. And then check the similarity rate (CrossCheck, powered by iThenticate). Any manuscripts out of the journal's scope or containing plagiarism, including self-plagiarism are rejected.

c) Peer Review. We use a double-blind system for peer review; both reviewers' and authors' identities remain anonymous. The submitted manuscript will be reviewed by at least two experts: one editorial staff member as well as one to three external reviewers. The review process may take four to ten weeks.

d) Make the decision. The decision to accept or reject an article is based on the suggestions of reviewers. If differences of opinion occur between reviewers, the editor-in-chief will weigh all comments and arrive at a balanced decision based on all comments, or a second round of peer review may be initiated.

e) Notification of the result of review. The result of review will be sent to the corresponding author and forwarded to other authors and reviewers.

f) Pay the article processing charge. If the submission is accepted, the authors revise paper and pay the article processing charge (formatting and hosting).

g) E-journal is available. E-journal in PDF is available on the journal's webpage, free of charge for download. If you need the printed journals by post, please order at http://www.ccsenet.org/journal/index.php/ijc/store/hardCopies

h) Publication notice. The authors and readers will be notified and invited to visit our website for the newly published articles.

More Information

E-mail: ijc@ccsenet.org

Website: http://ijc.ccsenet.org

Paper Submission Guide: http:// ijc-author.ccsenet.org

Recruitment for Reviewers: http://www.ccsenet.org/journal/index.php/ijc/editor/recruitment

➢ JOURNAL STORE

To order back issues, please contact the journal editor and ask about the availability of journals. You may pay by credit card, PayPal, and bank transfer. If you have any questions regarding payment, please do not hesitate to contact the journal editor or editorial assistant.

Price: $40.00 USD/copy Shipping fee: $20.00 USD/copy

CONTACT US

1595 Sixteenth Ave, Suite 301
Richmond Hill, Ontario, L4B 3N9
Canada
Tel: 1-416-642-2606
Fax: 1-416-642-2608
E-mail: info@ccsenet.org
Website: www.ccsenet.org

The journal is peer-reviewed
The journal is open-access to the full text
The journal is included in:

Academic Journals Database
Bibliography and Index of Geology
CABI
CAS
COPAC
Elektronische Zeitschriftenbibliothek EZB
EuroPub Database
Excellence in Research for Australia (ERA)
Genamics JournalSeek
Google Scholar
Infotrieve
JournalTOCs
LOCKSS
MIAR
NewJour
Open J-Gate
PKP Open Archives Harvester
ROAD
SHERPA/RoMEO
Universe Digital Library
WorldCat

International Journal of Chemistry
Semiannually

Publisher Canadian Center of Science and Education
Address 1595 Sixteenth Ave, Suite 301, Richmond Hill, Ontario, L4B 3N9, Canada
Telephone 1-416-642-2606 ext.215
Fax 1-416-642-2608
E-mail ijc@ccsenet.org
Website http://ijc.ccsenet.org

ISSN 1916-9698